AN ABSTRACT OF THE THESIS OF

CHRISTINE PASTOREK for the degree of DOCTOR OF PHILOSOPHY

in Chemistry presented on June 6, 1980

Title: A STUDY OF THE INFRARED INTENSITIES OF SOME SMALL MOLECULAR ANIONS

Abstract approved: Redacted for Privacy

Dr. J. C. Decius

In infrared reflectance experiments with single crystals, we have measured the bands ν_2 and ν_3 for KN_3 and KHF_2, ν_2, ν_3, and ν_4 for $CaCO_3$ and $NaNO_3$ having the calcite structure. Since an oblique incidence technique was employed, several different polarizations allowed discrimination between crystal modes whose transition dipcles were parallel and perpendicular to the crystal face normal. The bands were analyzed in terms of a damped harmonic oscillator model of the anisotropic dielectric function which associates three parameters with each mode. These parameters are: ν_T, the transverse phonon frequency; S, the strength; and γ, the damping constant. For each of these anisotropic crystals, an appropriate dipole lattice sum was used to evaluate the effective internal field. This, along with the S and ν_T parameters, was used to

determine the molecular dipole derivatives, $\partial\mu/\partial q_k$, for the several modes.

In the HF_2^- ion study, it is demonstrated that the transition strength is rather insensitive to the proportion of quadratic and quartic terms in the potential function. Also, some other intermolecular coupling mechanism, besides dipole coupling, significantly perturbs the $\partial\mu/\partial q_2$ value in the E_u species. This might possibly be hydrogen bonding between the two bifluoride ions in the unit cell.

These derivatives are then transformed to derivatives with respect to internal symmetry coordinates. To accomplish this transformation for modes 3 and 4 in $CaCO_3$ and $NaNO_3$, a molecular potential function must be available: we have carefully analyzed the uncertainties in the $\partial\mu/\partial S_k$ values which arise in consequence of imprecise definition of the potential function.

Finally, the data are reduced to atomic effective charges and charge fluxes utilizing simple bonding theory to facilitate the choice of some of the indeterminate signs of the $\partial\mu/\partial q_k$ which arise because $(\partial\mu/\partial q_k)^2$ is the measurable quantity in these studies.

A Study of the Infrared Intensities of Some Small Molecular Anions

by

Christine Pastorek

A THESIS

submitted to

Oregon State University

in partial fulfillment of
the requirements for the
degree of

Doctor of Philosophy

June 1981

APPROVED:

Redacted for Privacy

Professor of Chemistry
in charge of major

Redacted for Privacy

Chairman of Department of Chemistry

Redacted for Privacy

Dean of Graduate School

Date thesis is presented June 6, 1980

Typed by Deanna L. Cramer for Christine Pastorek

ACKNOWLEDGEMENTS

Foremost, I would like to thank Professor J. C. Decius for the many patient hours he has spent advising me on this thesis project, and for his constant support throughout all the facets of my graduate career. It is an honor to have had the privilege of working with him. I would also like to thank Professor J. W. Nibler, first of all, for his encouragement during my graduate program and, of course, for the more than generous assistance in the way of equipment and supplies. A special thanks goes to Mr. Emile J. Firpo, without whose enthusiastic vote of confidence and never ending inspiration, I would not have succeeded in accomplishing this program.

In addition, I would like to thank Drs. George B. Mast, John Wilkerson and Mr. George Carman for aiding me in the construction of the computer programs used to collect and analyze the data. My appreciation goes also to Mr. David Murhammer who assisted us in the $NaNO_3$-ν_4 studies. A grant from the Oregon State Computer Center allowed the necessary data analysis for this thesis. Although some of this work was supported by the National Science Foundation, most of it was made possible by the Department of Chemistry at Oregon State University, which has faithfully supported me as a graduate teaching assistant.

TABLE OF CONTENTS

LIST OF FIGURES

List of Figures -- continued

LIST OF TABLES

A STUDY OF THE INFRARED INTENSITIES OF SOME SMALL MOLECULAR ANIONS

I. INTRODUCTION

The small molecular anions which are the subject of this infrared intensities study in the solid state are: N_3^- and HF_2^-, each linear $D_{\infty h}$ ions with sixteen valence electrons; CO_3^{2-} and NO_3^-, both planar D_{3h} anions with twenty-four valence electrons. Potassium azide and potassium bifluoride both occur as D_{4h}^{18} crystals whereas calcite and sodium nitrate grow with D_{3d}^{6} symmetry (1). Potassium bifluoride and sodium azide have been previous topics of study in this laboratory (see references (2) and (3)). Our intention was to augment the bifluoride work of Cooke by using improved data analysis which included simultaneously fitting modes 2 and 3, the bend and antisymmetric stretch, respectively. Since ν_3 is a very strong mode, its influence over ν_2 cannot be neglected, so this new analysis of KHF_2 does undoubtedly improve the values for the infrared active dipole derivatives. By studying the infrared intensities of N_3^- in the potassium salt and comparing with those determined from the sodium salt (where a similar method of measurement and analysis was used), we hoped to be able to say something about how well the effective field of the azide ion in both salts could be accounted for. We must have a reliable method for calculating the effective field

the ion experiences if our intention is to determine molecular infrared intensities for species that are not easily studied in the gas phase.

The bit of data that eludes the analysis, whether gas phase or solid state, is the sign of the dipole derivative. Luckily, this can be deduced upon further reduction of the dipole derivatives to effective atomic charges and charge fluxes within the molecule. The sign is then rationalized by considering the relative electronegativities of the atoms involved and general notions on multiply bonded resonance structures. J. C. Decius has devised the effective charge-charge flux model, or EC-CF model, to help rationalize infrared intensities (4). We have found the charges and charge fluxes for N_3^- and HF_2^-. It would be more instructive however to compare effective charges and charge fluxes for a sequence of molecules where the effect of a successive increase in electronegativity could be studied. For this purpose we have looked at BF_3, CO_3^{2-}, and NO_3^-. The infrared intensities for BF_3 were studied in the gas phase and we have extracted them from the literature (31). The frequency dependent optical constants for sodium nitrate and calcite were reported (5) and the dipole derivatives were calculated for an isotropic dielectric model (6). More recently, the frequency dependent dielectric constant was evaluated in terms of strengths, S_j, transverse frequencies, ν_{jT}, and damping constants, γ_j, for both the internal and

external modes, but no dipole derivative analysis was given (7). Since we were happy with our success in fitting azide and bifluoride spectra, we were eager to subject calcite and sodium nitrate to the same analysis and then to determine effective charges and charge fluxes in hopes of rationalizing the dipole derivatives.

To do a vibrational intensity analysis for a molecule or molecular ion in a crystal one needs a single oriented specimen, well polished, of at least 9 mm^2 surface area. The observables in a reflection experiment are then: 1) the band shape: its width, height, and placement on the frequency scale; 2) the polarization of radiation which makes possible the identification of modes active perpendicular to or in the plane of the crystal face; 3) the angle of incidence between the normal to the crystal face and the incoming radiation. We then model the reflectance with a damped harmonic oscillator response function for the directional dispersion in the dielectric constant. To accomplish this fit, one adjusts the strength, S_j, or width of the band $(\nu_L - \nu_T)$, the transverse frequency, ν_{jT}, and the damping constant, γ_j, or the height of the band, all for a specific mode j, until the theoretical response matches the experimental reflectance. Then, provided one can account for the effective field at the ion of interest induced by all the other ions in the unit cell, S_j and ν_{jT} are used to determine $\partial\mu/\partial q_j$, or the dipole derivative with respect to

the molecular normal coordinate q for mode j. The dipole derivative is the measure of the infrared intensity for a particular mode j.

The main aim of these studies is then to quantitatively determine the dipole derivatives for the azide ion in KN_3, the bifluoride ion in KHF_2, carbonate ion in calcite, and the nitrate ion in $NaNO_3$. Consequently we have tested how well the harmonic oscillator model for the dielectric constant, with frequency independent damping, accounts for reflection in single crystals. Also we have compared our values for the various anion intensities with those obtained from different salts of the same anions. This tests directly how well interactions between ions in crystals can be described using only dipole-dipole coupling. This is a sort of oriented gas model with correction for polarizability. Finally, exercising the EC-CF model we have compared signs and magnitudes for the charges and charge fluxes in certain molecules with basic trends in electronegativities and fluxes in multiply bonded resonating structures in hopes of proposing a viable scheme for choosing the sign of the dipole derivative, a term not determinable from experiment.

These analyses have in most part appeared in publications listed as references (8), (9), and (16).

II. THEORY

The process of characterizing the effective equilibrium charges and charge fluxes within molecular anions, or the quantities and qualities that are ultimately responsible for the reflection of mid infrared radiation from certain ionic crystals, will be developed in this section. Technically, this capacity to reflect energy can be described in terms of the frequency dependence of the dielectric constant, $\varepsilon(\omega)$. We wish to define this frequency dependence with certain adjustable parameters which can then be related to the molecular dipole derivatives $\partial\mu/\partial q_j$ for the infrared active modes, j. These values will then lead to the calculation of the effective equilibrium charges and allowed charge fluxes as defined in the EC-CF model.

The first thing we need is an expression for the frequency dependence of the dielectric constant. From basic physics we know that the polarization, P, or the electric dipole moment per unit volume, is related to the frequency dependence of the complex susceptibility, $\chi(\omega)$ through the dielectric field strength, E, simply as

$$P = \chi(\omega)\ E\ . \qquad (1)$$

We also know that the electric displacement is related to the polarization as

II. THEORY

The process of characterizing the effective equilibrium charges and charge fluxes within molecular anions, or the quantities and qualities that are ultimately responsible for the reflection of mid infrared radiation from certain ionic crystals, will be developed in this section. Technically, this capacity to reflect energy can be described in terms of the frequency dependence of the dielectric constant, $\varepsilon(\omega)$. We wish to define this frequency dependence with certain adjustable parameters which can then be related to the molecular dipole derivatives $\partial\mu/\partial q_j$ for the infrared active modes, j. These values will then lead to the calculation of the effective equilibrium charges and allowed charge fluxes as defined in the EC-CF model.

The first thing we need is an expression for the frequency dependence of the dielectric constant. From basic physics we know that the polarization, P, or the electric dipole moment per unit volume, is related to the frequency dependence of the complex susceptibility, $\chi(\omega)$ through the dielectric field strength, E, simply as

$$P = \chi(\omega)\ E\ . \qquad (1)$$

We also know that the electric displacement is related to the polarization as

$$D = E + 4\pi P \tag{2}$$

and empirically that

$$D = \varepsilon(\omega)\, E \ . \tag{3}$$

The frequency dependence of the dielectric constant then can be expressed as

$$\varepsilon(\omega) = 1 + 4\pi\chi(\omega) \ . \tag{4}$$

The description of the implied absorption process in crystals is innately different from that for gases or liquids. In fluids, the absorption is mediated by molecular collisions. This is physically impossible in solids. In the solid state, absorption of radiation is a consequence of the anharmonic coupling of the wave vectors for the phonons in the long wavelength limit, $\vec{k} \sim 0$. A Hamiltonian which describes the lattice, as given in the analysis by Wallis and Maradudin (10), is simply

$$H_L = H_O + H_A \ ,$$

where the harmonic contribution is given as

$$H_O = \tfrac{1}{2} \sum_{\vec{k}_j} \{\dot{Q}(\vec{k}j)\dot{Q}(-\vec{k}j) + \omega^2(\vec{k}j)Q(\vec{k}j)Q(-\vec{k}j)\} \tag{5}$$

and the anharmonic part considering only cubic terms, is represented as

$$H_A = \frac{1}{3} \sum_{\vec{k}\vec{k}'\vec{k}''} \sum_{jj'j''} V(\vec{k}j,\vec{k}'j',\vec{k}''j'')Q(\vec{k}j)Q(\vec{k}'j')Q(\vec{k}''j'') \tag{6}$$

The $\omega(\vec{k}j)$ are normal mode frequencies, $Q(\vec{k}j)$ are the normal mode coordinates, and $V(\vec{k}j,\vec{k}'j',\vec{k}''j'')$ are the anharmonic force constants for the modes j,j',j'' at wavevectors $\vec{k},\vec{k}',\vec{k}''$. In an earlier paper (11), these authors indicated that it is precisely this anharmonic character that gives rise to a band of absorption in a crystal and furthermore, that this coupling of modes is accounted for by including a damping constant in the dispersion for the susceptibility.

Born and Huang in their esteemed tome "Dynamical Theory of Crystal Lattices" (38) first addressed the problem of vibrations in an anharmonic lattice by using time dependent perturbation theory. Wallis and Maradudin (10) in their later paper, used the time correlation formalism based on the Kubo method for calculating transport coefficients to solve for an expression for the elements of the dielectric susceptibility tensor for an ionic crystal. They found that the contribution to the dielectric susceptibility from the dispersion oscillators could be expressed as

$$\chi(\omega) = \frac{1}{2v} \sum_j \frac{(\partial\mu/\partial Q_j)^2}{\omega_{oj}} \left\{ \frac{1}{\omega+\omega_{oj}+\Delta\omega_{oj}+i\Gamma_{oj}} - \frac{1}{\omega-\omega_{oj}-\Delta\omega_{oj}-i\Gamma_{oj}} \right\} \tag{7}$$

where ω_{oj} is the characteristic frequency for mode j at $\vec{k} = 0$ and v is the volume of the primitive unit cell. The frequency shift, $\Delta\omega_{oj}$, from the purely harmonic ω_{oj}, is introduced to account for the effect of anharmonic coupling and is given by these authors as

$$\Delta\omega_{oj} = (\frac{\hbar}{2}) \sum_{\vec{k}'j'\vec{k}''j''} \frac{|V(oj;\ \vec{k}'j';\ \vec{k}''j'')|^2}{\omega(oj)\,|\omega(\vec{k}'j')\,|\omega(\vec{k}''j'')}$$

$$X\ (n_{\vec{k}'j'} + \tfrac{1}{2})\ P\ \frac{1}{\omega-\omega(\vec{k}'j')-\omega(\vec{k}''j'')} \ . \qquad (8)$$

They also give the frequency dependence of the damping constant, Γ_{oj}, to be

$$\Gamma_{oj} = (\frac{\pi\hbar}{2}) \sum_{\vec{k}'j'\vec{k}''j''} \frac{|V(oj;\ \vec{k}'j';\ \vec{k}''j''|^2}{\omega_{oj}\,|\omega(\vec{k}'j')\,|\omega(\vec{k}''j'')}$$

$$X\ (n_{\vec{k}'j'} + \tfrac{1}{2})\ \delta[\omega-\omega(\vec{k}'j')-\omega(\vec{k}''j'')] \ , \qquad (9)$$

where

$$n_{\vec{k}'j'} = [e^{\beta\hbar|\omega(\vec{k}'j')|} - 1]^{-1} \ ,$$

is the Bose-Einstein distribution for the phonon model ($\beta = (kT)^{-1}$). The symbols P and δ refer respectively to the principal part and the delta function and originate in the analysis from taking

$$\lim_{\varepsilon\to 0+} (\frac{1}{x-i\varepsilon}) \Rightarrow P(\frac{1}{x}) + i\pi\delta(x) \ .$$

ε is a parameter, not to be confused with the dielectric constant, which is used to turn on the electric field at $t = 0$, since the susceptibility is a function of the history of the system.

There are several criteria to be met if the damping constant is to display frequency dependent behavior. One obvious requirement is that anharmonic coupling of modes must exist; therefore, there are modes of the correct symmetry to couple and thus contribute to the potential energy of the lattice. These can be combination, difference, or overtone modes. The other conditions for a maximum in the damping constant come from investigating equation (9). The double sum over the wavevectors $\vec{k}'$ and $\vec{k}''$ for the associated modes j' and j'' can be broken down into two main parts. One is a function of the frequencies of the modes and the other is a delta function involving the frequencies of the modes and the frequency of the exciting radiation:

$$\Gamma \alpha \sum_{\vec{k}'j'} \sum_{\vec{k}''j''} f\{\omega(\vec{k}'j'),\omega(\vec{k}''j'')\}\delta\{\omega-\omega(\vec{k}'j') -\omega(\vec{k}''j'')\}.$$

These sums can be approximated by integrating over each wavevector:

$$\Gamma \alpha \int_{\vec{k}'} \int_{\vec{k}''} f\{\omega(\vec{k}'j'),\omega(\vec{k}''j'')\}\delta\{\omega-\omega(\vec{k}'j')$$

$$-\omega(\vec{k}''j'')\}\, d\vec{k}'d\vec{k}'' \ .$$

Since infrared radiation imposes the long wavelength limit on us, the selection rule for this process is

$$\vec{k} = \vec{k}'j' + \vec{k}''j'' = 0 \ .$$

For the case of an overtone, j' equals j", and in the following example, we will specifically discuss $2\nu_4$ in $NaNO_3$. The damping constant expression then becomes

$$\Gamma \alpha \int f\{\omega(\vec{k}'4)\}\delta\{\omega-2\omega(\vec{k}'4)\}\, d\vec{k}'$$

where $\omega(-\vec{k}') = \omega(\vec{k}')$. However, we are more interested in knowing how the damping constant varies with frequency rather than wavevector, so we can modify this integral further and state

$$\Gamma \sim \int f\{\omega(\vec{k}'4)\}\delta\{\omega-2\omega(\vec{k}'4)\}\, \frac{d\vec{k}'}{d\omega(\vec{k}'4)}\, d\omega(\vec{k}'4) \ .$$

Now, when the scanning frequency is in resonance with this mode, $\omega/2 = \omega(\vec{k}'4)$, or

$$\Gamma \sim \left[f\{\omega(\vec{k}'4)\}\, \frac{d\vec{k}'}{(d\omega(\vec{k}'4)}\right]_{\omega(\vec{k}'4)=\frac{1}{2}\omega} \ .$$

We then clearly see that for a maximum in the damping constant, the density of modes, or $d\vec{k}/d\omega$, must be large. If $\omega(\vec{k}'4)$ equals ω_4, i.e. mode 4 has negligible dispersion, Γ will be large at $\omega=2\omega_4$.

As an example for the existence of a frequency dependent damping constant, let us refer to Figure 13 for the reflectance of mode 3 in $NaNO_3$. In the region extending from ν_{3T} at 1440 cm^{-1} to ν_{3LL} at about 1600 cm^{-1}, we have observed a dip at 1448 cm^{-1} in the otherwise maximum reflectance. From a calculated density of modes (12) and a second order Raman experiment (13), we know the two phonon density for mode 2 ν_4 in this region is high. If ν_4 is around 725 cm^{-1} we would expect $2\ \nu_4$ to be around 1450 cm^{-1}, in close agreement with the observed maximum in $\Gamma(\omega)$. This feature was also observed by Nichols and Frech (14) and ascribed to the same phenomenon. In this specific example one might diagram the frequency dependence in Γ roughly as

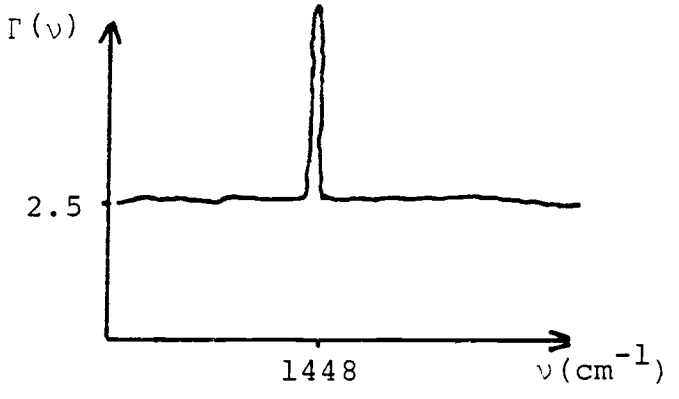

This theory seems to account for the frequency dependence of Γ in the $NaNO_3$ case. However, it is not the aim of

this present study to quantitatively determine the damping constant. We are more interested in the $\nu_L - \nu_T$ splitting, or the strength of mode j, and its transverse frequency since it is these two parameters that relate to $\partial\mu/\partial q_j$. We will neglect any dispersion in Γ and treat it as a constant over the mode j. We will see that this is usually reasonable over the frequency regions studied.

We can now revamp equation (7) into a more manageable form by making two approximations. First, we acknowledge that the $\Delta\omega_{oj}$ terms are small at room temperature and furthermore can be treated as constants. We therefore assign $\omega_{jT} \simeq \omega_{oj} + \Delta\omega_{oj}$. Second, while recognizing that there may sometimes be resonances like 1448 cm^{-1} in $NaNO_3$, we will also treat Γ_j as a constant. In light of these two approximations, equation (7) can be rewritten as

$$\chi(\omega) = \frac{1}{2v} \sum_j \left(\frac{\partial\mu}{\partial Q_j}\right)^2 \frac{1}{\omega_{jT}} \left\{\frac{1}{\omega+\omega_{jT}+i\Gamma_j} - \frac{1}{\omega-\omega_{jT}-i\Gamma_j}\right\}. \quad (10)$$

Next, we want to put this equation in a form that will lend itself to computation by combining terms and separating the real from the imaginary part. The result is that

$$\chi(\omega) = \frac{1}{v} \sum_j \left(\frac{\partial\mu}{\partial Q_j}\right)^2 \left\{\frac{\omega_{jT}^2-\omega^2+\Gamma_j^2}{D} - i\,\frac{\Gamma_j}{\omega_{jT}}\left(\frac{\omega_{jT}^2+\omega^2+\Gamma_j^2}{D}\right)\right\}, \quad (11)$$

where $D = (\omega_{jT}^2-\omega^2)^2+2\omega_{jT}^2\Gamma_j^2+2\omega^2\Gamma_j^2+\Gamma_j^4$. Furthermore, we have

found that we can simplify this expression even more by assuming the Γ_j^2 and Γ_j^4 terms can be neglected since $\Gamma_j << \omega_{jT}$. Also, in the vicinity of a mode, ω_{jT} will always be close to ω, therefore

$$\chi(\omega) = \frac{1}{v} \sum_j \left(\frac{\partial \mu}{\partial Q_j}\right)^2 \left\{\frac{\omega_{jT}^2 - \omega^2}{(\omega_{jT}^2 - \omega^2)^2 + 4\Gamma_j^2\omega^2}\right.$$

$$\left. - i \frac{2\Gamma_j\omega}{(\omega_{jT}^2 - \omega^2)^2 + 4\Gamma_j^2\omega^2}\right\}. \qquad (12)$$

So far, we have limited ourselves to the frequency dependence of χ due to the so-called dispersion oscillators. In reality, the dispersion in the infrared region is, of course, not independent of that in the electronic region. Normally the dielectric response in the high frequency region, $\varepsilon(\infty)$, is treated as a constant exemplified by the square of the index of refraction, n^2, measured at 589.3 nm. In our analysis, the high frequency dielectric constant provides a background contribution to the overall frequency dependence of ε that is added to the contribution from the infrared region:

$$\varepsilon_\sigma(\omega) = \varepsilon_\sigma(\infty) + \varepsilon_\sigma(ir) \quad (\sigma = x,y,z) \; . \qquad (13)$$

Likewise, we can express $\chi(\omega)$ as

$$\chi_\sigma(\omega) = \chi_\sigma(\infty) + \chi_\sigma(ir) \; . \qquad (14)$$

The electronic contribution to the overall susceptibility is expressed as

$$\chi_\sigma(\infty) = \left(\sum_{mm'} B_{mm'} \alpha_{m'} \right)_\sigma , \tag{15}$$

in which $\alpha_{m'}$ is the electronic polarizability of ion m' and $B_{mm'}$ is the effective field ratio that expresses the field at ion m' due to all others, m, in the unit cell. It is defined (15) as

$$\underset{\sim}{B} = [\underset{\sim}{E} - \underset{\sim}{\alpha}\underset{\sim}{D}]^{-1} . \tag{16}$$

$\underset{\sim}{E}$ is a unit matrix; $\underset{\sim}{D}$ is the field propagation tensor, a dipole wave sum. Both are $3Nx3N$ where N is the number of ions in the unit cell. These dipole wave sums are found by considering the whole lattice and in the point-dipole approximation, depend on the geometry and physical size of the unit cell. A typical form for D_z is

$$\sum_{\text{lattice}} (1/t^3)[1 - 3z^2/t^2]$$

where the coordinates of a lattice point are expressed in rhombohedral basis vectors as

$$t = \tau_1 a_1 + \tau_2 a_2 + \tau_3 a_3$$

where the τ_i are integers. It is interesting to note that $\underset{\sim}{B}$ also depends on the directional polarizability of the

distributions of electrons about the molecular ions in their unit cell.

The same effective field can be used to modify the molecular moments. In light of the above relationships and equation (4), one is led to two expressions for the dielectric constant. The high frequency dielectric constant is

$$\varepsilon_\sigma(\infty) = 1 + \frac{4\pi}{V} \sum_{mm'} B_{mm'}\alpha_{m'} \tag{17}$$

and the infrared component is

$$\varepsilon_\sigma(ir) = \frac{1}{c^2\pi V} \{\sum_j [\sum_{mm'} B_{mm'} \frac{\partial\mu(m')}{\partial Q_j}]_\sigma^2 \times [\frac{\nu_{jT}^2-\nu^2}{(\nu_{jT}^2-\nu^2)^2+\gamma_j^2\nu^2} - i\frac{\gamma_j\nu}{(\nu_{jT}^2-\nu^2)^2+\gamma_j^2\nu^2}]\} \tag{18}$$

where $\nu = \omega/(2\pi c)$, c being the speed of light, and $\gamma_j = 2\Gamma_j$. $\partial\mu(m')/\partial Q_j$ is the unit cell normal coordinate dipole derivative for ion m'

We have briefly investigated how one describes the high frequency dispersion in the dielectric constant. It has been said that the dielectric response in this region is a result of the susceptibility of the electrons to deformation by radiation. The electronic polarizability, α, is then a measure of the degree of their pliability. We also know that the polarizability is accentuated by the

existence of an induced effective field at the ion site in the unit cell of the crystal. As the incident frequency is lowered, the behavior of the atoms within the molecular framework starts to contribute to the dielectric constant. Unlike the subdued response the dielectric constant exhibits in the electronic region, the response in the infrared is one of intense absorption by molecular species in the crystal. ε is forced to become a complex quantity at the discrete frequencies of the fundamental molecular modes.

The largest contribution to the dielectric constant is expressed when the frequency of exciting radiation is lowered below the far infrared to radio frequencies. The static dielectric constant, ε_0, is usually determined by measuring the difference in capacitance between the material and a vacuum at frequencies on the order of kilohertzs. It could just as well be calculated by taking

$$\varepsilon_0 = \varepsilon_\infty + \sum_j S_j = \varepsilon_\infty + \sum_j [\sum_{mm'} B_{mm'} \frac{\partial_\mu (m')}{\partial Q_j}]^2$$

where the sum is over the strengths of the infrared modes. At low frequencies, all degrees of freedom can follow the applied field.

In this study, we intend to observe the reflection of radiation from the surface of a single crystal instead of directly measuring the dielectric constant since our aim is not to merely determine dielectric constants in the

infrared region, but rather to use the dispersion in ε to characterize the molecular dipole derivatives. The reflectance as a function of the dielectric constant, at normal incidence is known to be

$$R = \left| \frac{\varepsilon^{\frac{1}{2}} - 1}{\varepsilon^{\frac{1}{2}} + 1} \right|^2 .$$

This is the simplest expression for reflectance but the experiment it implies is the most difficult to carry out in a conventional spectrometer. Incidence angles that are near normal, around 10°, or that are oblique, greater than 15°, are preferred. In this study only oblique incidence was used with an average θ_i of about 45°. As we shall soon discover, the addition of a finite incidence angle complicates the simple formula given above, but at the same time, it opens the door for new experiments which reveal certain polarized modes that would not be observed at normal incidence ($\theta_i = 0$).

The reflection equation, according tc Decius and Hexter (15), becomes two different equations for two polarizations. If the incident electric vector is polarized perpendicular to the plane of incidence, or transverse electric (TE), we have

$$R(TE) = \left| \frac{\cos \theta_i - (\varepsilon_1 - \sin^2\theta_i)^{\frac{1}{2}}}{\cos \theta_i + (\varepsilon_1 - \sin^2\theta_i)^{\frac{1}{2}}} \right|^2 \qquad (19)$$

and if the electric vector is polarized in the plane of incidence or transverse magnetic (TM), we find

$$R(TM) = \left| \frac{\varepsilon_2^{\frac{1}{2}} \cos \theta_i - (1 - \frac{\sin^2\theta_i}{\varepsilon_3})^{\frac{1}{2}}}{\varepsilon_2^{\frac{1}{2}} \cos \theta_i + (1 - \frac{\sin^2\theta_i}{\varepsilon_3})^{\frac{1}{2}}} \right|^2 . \qquad (20)$$

The numbering used here refers to the principal axis of the frequency dependent dielectric tensors. ε_1 and ε_2 define the crystal face and ε_3 is the normal to the crystal face for all systems of at least orthorhombic symmetry. We will concern ourselves with uniaxial tetragonal and trigonal systems in which $\varepsilon_x = \varepsilon_y \neq \varepsilon_z$. This combination presents us with four different possibilities for polarized resonance of an isolated mode:

Case	Resonance in	Label	Condition
1	ε_1	TE	1 = x or y or z
2	ε_3	TM2	2 = x or y or z
3	ε_3	TM3	3 = x or y or z
4	ε_2 and ε_3	TM23	2,3 = x, y

We now have two expressions for polarized reflectance in terms of the directional energy dependence of the dielectric constant. Earlier we found an expression for the dielectric constant as a function of two mode

parameters, ν_{jT} and γ_j (see equation 18). This equation also displays the dependence of ε on the modified molecular moments, $(B\partial\mu/\partial Q_j)$. Using the operator form for $\hat{\mu} = (\partial\mu/\partial Q_j)Q$, reference (38) gives an expression involving the transition moment integral as

$$\frac{4\pi}{v}\frac{2\omega_{jT}}{\hbar}\left|B\frac{\partial\mu}{\partial Q_j}\ <0|Q|1>\right|^2 = S_j\omega_{jT}^2 , \qquad (21)$$

where S_j is a dimensionless strength parameter for mode j and $<0|Q|1>$ is the normal coordinate transition moment integral. In the limit of a purely harmonic oscillator $<0|Q|1> = (h/2\omega_{jT})^{\frac{1}{2}}$ and (21) reduces to

$$\frac{4\pi}{v}\left(\sum_{mm'} B_{mm'}\frac{\partial\mu(m')}{\partial Q_j}\right)^2 = S_j\omega_{jT}^2 . \qquad (22)$$

Otherwise, if the potential function has a strong anharmonic nature, one would need expressions for the transition moment integral. We will investigate the degree to which $\partial\mu/\partial Q$ differs for the harmonic versus quartic potential for the specific case of the ν_3 mode in bifluoride ion. It has been suggested that the mode is quartic in the potential. We have, however, found that for the ions studied here, it is reasonable to treat them in the harmonic limit and we will use the strength expression written in wavenumbers as

$$S_j^{\sigma}\nu_{jT}^2 = \frac{1}{c^2\pi v}\left(\sum_{mm'} B_{mm'}\frac{\partial\mu(m')}{\partial Q_j}\right)_{\sigma}^2 \qquad (23)$$

σ = x, y or z. Not much has been said about how to find the effective field values. This subject is covered in reference (2), and only a summary will be given below. To find $\underset{\sim}{B}$, one must know the dipole wave sum $\underset{\sim}{D}$, for the lattice and the electronic polarizabilities, $\underset{\sim}{\alpha}$. For the ions studied here these can be found in either reference (2) or (17). In the potassium azide case, we modified the values in (2) for the similarly arranged potassium bifluoride crystal, since the azide values were not previously determined.

There are two methods used to find geometrically dependent $\underset{\sim}{D}$ values: the Ewald-Kornfeld technique and the planewise summation method. Both methods are thoroughly discussed in reference (15). In either calculation, the point dipole approximation is used in that an anion is considered to be sitting at a lattice point described by the crystal structure, either D_{4h} or D_{3d} in this study.

To know the electronic polarizabilities requires that one have values for the indices of refraction for the materials being studied. The electronic polarizabilities for most group I and II cations have been determined in the halide salts of these cations where the Lorenz-Lorentz field correction valid for cubic crystals was used to fit measured indices.

We will use the polarizabilities found either by Tessman, Kahn, and Schockley (18) or those of Pirenne and Kartheuser (19). The crystalline state anion polarizabilities are more difficult to come by. One can see, however, from equation (17) that knowing the index of refraction ($\varepsilon(\infty)^2$) would lead to the polarizabilities, if $\underset{\sim}{B}$ were known! A catch-22! To get around this, one selects a value for the polarizability, calculates $\underset{\sim}{B}$ (equation (16)), then calculates an index of refraction, and compares to experiment. Repeating the procedure eventually leads to a consistent set of values for the anion polarizability and for $\underset{\sim}{B}$.

We now have enough information to find $\partial\mu/\partial Q_j$, once the reflectance band has been measured. We can write an expression for the frequency dependence of the dielectric constant in terms of three parameters which can be adjusted to fit the experiment

$$\varepsilon_\sigma(\omega) = \varepsilon_\sigma(\infty) + \sum_j \left[\frac{S_j^\sigma \nu_{jT}^2 (\nu_{jT}^2 - \nu^2)}{(\nu_{jT}^2 - \nu^2)^2 + \gamma_j^2 \nu^2} - i \frac{S_j^\sigma \nu_{jT}^2 (\gamma_j \nu)}{(\nu_{jT}^2 - \nu^2)^2 + \gamma_j^2 \nu^2}\right] . \qquad (24)$$

The parameters are: the dimensionless strength of mode j, S_j^σ, in direction σ; the transverse frequency of the mode ν_{jT} in cm^{-1}, the damping constant γ_j of the mode in cm^{-1}.

As one can see from equations (19) and (20), the reflectance will approach unity in certain limiting cases such as

$$(\varepsilon_1 - \sin^2\theta_i)^{\frac{1}{2}} = \text{pure imaginary;}$$

$$\varepsilon_2^{\frac{1}{2}} = \text{pure imaginary,}$$

$$(1 - \frac{\sin^2\theta_i}{\varepsilon_3})^{\frac{1}{2}} = \text{pure real, or vice versa.}$$

The frequency ranges over which this can happen are discussed below in the idealized limit in which γ, the damping constant, is neglected. It is instructive for us to investigate the conditions which cause the reflectance to be a maximum and those which proceed to make it a minimum since we wish to use parameters that model this behavior to calculate $\partial\mu/\partial q_j$.

The dominant behavior of the dielectric constant in the vicinity of mode j can be represented by the real part of a classical (i.e. undamped) harmonic oscillator function

$$\varepsilon^{\sigma}_{\text{REAL}}(\nu) = \varepsilon^{\sigma}_{B}(\nu) + \frac{S^{\sigma}_j \nu^2_{jT}}{\nu^2_{jT} - \nu^2} \qquad (25)$$

again σ can be x, y, or z and ε_B is the background dielectric constant. The modes that contribute to the background dielectric constant can be accounted for by expressing it as

$$\varepsilon_B^{\sigma}(\nu) = \varepsilon(\infty) + \sum_{k\neq j} \frac{S_k^{\sigma}\nu_{kT}^2}{\nu_{kT}^2-\nu_{jT}^2} \tag{26}$$

where one notes the background consists of all modes except the one being fitted. Consequently, ε_B can be larger or smaller than $\varepsilon(\infty)$. When ν equals ν_{jT}, there is a pole in the dielectric function. It swings from positive infinity through zero to negative infinity: the index of refraction becomes imaginary. As the frequency increases the dielectric constant becomes positive again and returns to its background value minus the strength from the mode it just experienced.

The conditions for maximum and minimum reflectance are listed in Table 1 for the cases 1-4 stated above, where we have also included some ballpark numbers for reference. The reader who is familiar with normal incidence experiments of this type should note that it is TM2 that most resembles a normal incidence experiment since maximum reflectance occurs between the transverse, ν_{jT}, and longitudinal, ν_{Lj}, frequencies. The reader who is unfamiliar with normal incidence behavior may wish to consult Appendix A. The longitudinal frequency is defined to be that at which the dielectric constant equals zero. It is interesting to note that TE, TM3, and TM23 experiments performed at the same θ_i drop off at the same frequency V_{jLL}. This pseudo longitudinal frequency (20) occurs at a

Table 1. Characteristic dielectric behavior for the four cases of polarized reflectance.[a]

Case	Start of Maximum R	End of Maximum R	Minimum R
TE	$\varepsilon_1 \to -\infty$ (ν_T)	$\varepsilon_1 > \sin^2\theta_i$ (ν_{LL})	$\varepsilon_1 = 1.00$
TM2	$\varepsilon_2 \to -\infty$ (ν_T)	$\varepsilon_2 > 0$ (ν_L)	$\varepsilon_2 = \frac{1-\sin^2\theta_i/\varepsilon_3}{\cos^2\theta_i}$
TM3	$\varepsilon_3 = 0$ (ν_L)	$\varepsilon_3 > \sin^2\theta_i$ (ν_{LL})	$\varepsilon_3 = \frac{\sin^2\theta_i}{1-\varepsilon_y \cos^2\theta_i}$
TM23	$\varepsilon_2 = -\infty$ (ν_T)	$\varepsilon_3 > \sin^2\theta_i$ (ν_{LL})	$\varepsilon_2 = \frac{1-\sin^2\theta_i/\varepsilon_3}{\cos^2\theta_i}$
TE	$\varepsilon_1 = -\infty$	$\varepsilon_1 > 0.50$	$\varepsilon_1 = 1.00$
TM2	$\varepsilon_2 = -\infty$	$\varepsilon_2 > 0.00$	$\varepsilon_2 = 1.50$
TM3	$\varepsilon_3 = 0$	$\varepsilon_3 > 0.50$	$\varepsilon_3 = -2.00$
TM23	$\varepsilon_2 = -\infty$	$\varepsilon_3 > 0.50$	$\varepsilon_2 = 1.50$

[a]Values given are for $\theta_i = 45°$, $\varepsilon_1 = \varepsilon_2 = 2.5$, $\varepsilon_3 = 2.0$.

higher value than ν_{jL}, which in turn is larger than ν_{jT}. From the simplified expression for the frequency dependent dielectric constant given above,

$$\nu_{jL} \simeq \nu_{jT}(1 + \frac{S_j}{\varepsilon_B})^{\frac{1}{2}} \tag{27}$$

and

$$\nu_{jLL} \simeq \nu_{jT}(1 + \frac{S_j}{\varepsilon_B - \sin^2\theta_i})^{\frac{1}{2}} \quad . \tag{28}$$

A TM3 reflection concentrates all of its intensity between ν_{jL} and ν_{jLL}. This polarization, unlike any of the other cases, selects the situation in which the electric vector in the incidence plane couples with a mode polarized perpendicular to the crystal surface. Both TE and TM23 reflectance envelop TM2 plus TM3 reflectance, except for slight differences at minimum R. One last comparison to be made between the various types of spectra is that TE, TM2, and TM23 exhibit minimum reflection after a band (at higher frequencies), whereas TM3 has a minimum reflectance before the band (at lower frequencies).

Once we have successfully modeled the reflection for mode j, the strength and transverse frequency parameter are used along with $\sum_m B_{mm'}$ in equation (23) to calculate $\partial\mu(m')/\partial q_j$. By studying the magnitudes and proposing signs for the molecular dipole derivatives for bends, stretches,

etc., one can ultimately say something about the charges on the atoms and the charge fluxes along the bonds.

Following the EC-CF analysis proposed by Decius (4), the dipole derivatives can be attributed to effective equilibrium charges, ζ_α^o, on the atoms α in the molecule and to charge fluxes, $\Delta\zeta_\alpha x_\alpha^o$ allowed during a vibration, so that

$$\Delta\mu_x = \sum_{\alpha=1}^{N} (\zeta_\alpha^o \Delta X_\alpha + \Delta\zeta_\alpha X_\alpha^o) \quad . \tag{29}$$

More completely, the contribution from the equilibrium charges can be written as

$$\Delta_1\mu_x = \sum_\alpha \zeta_\alpha^o [\sum_k \Delta x_\alpha^{(k)} S_k + \sum_{k,\ell} \Delta x_\alpha^{(k,\ell)} S_k S_\ell + \ldots] \quad . \tag{30}$$

The complete charge flux term is

$$\Delta_2\mu_x = \sum_\alpha [\sum_k \zeta_\alpha^{(k)} x_\alpha^{(o)} S_k + \sum_{k,\ell} \zeta_\alpha^{(k,\ell)} x_\alpha^o S_k S_\ell + \ldots] \quad , \tag{31}$$

where

$$\Delta x_\alpha^{(k)} = \partial \Delta x_\alpha / \partial S_k \tag{32}$$

and

$$\zeta_\alpha^{(k)} = \partial \zeta_\alpha / \partial S_k \quad . \tag{33}$$

The S_k are symmetry coordinates for mode k, and we have illustrated a mode active along the x directed molecular axis. Since we are interested in characterizing the molecular vibrations in terms of fundamental electron charges, it is more appropriate to express the dipole derivatives in terms of symmetry coordinates rather than mass weighted normal coordinates. The relationship between the two is

$$\frac{\partial \mu}{\partial S_k} = \sum_j \tilde{L}^{-1}_{kj} \frac{\partial \mu}{\partial q_j} \tag{34}$$

where $\tilde{L}^{-1}$ is the inverse of the transpose of the linear transformation matrix (21) which defines the symmetry coordinate in terms of the normal coordinates. In this study we will only consider the first order terms in the equations defining fixed charge, $\Delta_1\mu$, and charge flux, $\Delta_2\mu$ contributions to the dipole derivatives. This scheme for distributing charges in a molecular anion while conserving the overall charge and dipole is similar to but not identical with a Mulliken population analysis scheme for calculating net atomic charges in molecules (22).

For the diatomic case, we can draw some general conclusions about the importance of fixed charge versus charge flux in describing the infrared intensities from the results tabulated in (4). For very polar covalently bonded molecules, the equilibrium effective charges contribute more to the stretching intensity than the charge fluxes do. For

slightly polar or nonpolar covalently bonded systems, especially those of multiple bond character, the charge flux is responsible for most of the stretching intensity. For the nonpolar multiply bonded polyatomics this study is concerned with, we expect the stretching mode intensities to yield large charge flux values and we will see that the effective charges are determined solely by the bending mode intensities.

The procedure for dissecting the infrared intensities into charge and charge flux terms will be demonstrated for the case of the linear $D_{\infty h}$ anion. The analogous steps for the D_{3h} anion analysis can be found in Appendix B.

To find the fixed charge contribution to the dipole derivative, one is first required to write expressions for the instantaneous change in a dipole in terms of the effective equilibrium charges and the infinitesimally small cartesian changes for each atom. Next, one can write down expressions for the symmetry coordinates in terms of these same coordinate changes. Combining the two functions, one arrives at the relationship between the effective equilibrium charges and the symmetry coordinates. In addition, we must consider the conservation of linear momentum since the species is a charged ion and this will introduce mass dependence into our final expressions for the fixed charge.

For the AB_2^{-n} $D_{\infty h}$ anions, there are two active dipole derivatives: the bend, $\partial\mu/\partial S_2$, and the antisymmetric

stretch, $\partial\mu/\partial S_3$. In all our analyses, we use the convention that the positive direction for the A atom displacement corresponds to the positive dipole direction. We have also used the crystal axes to describe the molecular activities. A bending symmetry coordinate is

$$S_{2z} = r\phi = +2[\Delta z_A - \tfrac{1}{2}(\Delta z_{B1} + \Delta z_{B2})] , \tag{35}$$

and an antisymmetric stretch coordinate is

$$S_{3x} = 2^{\frac{1}{2}}[\Delta x_A - \tfrac{1}{2}(\Delta x_{B1} + \Delta x_{B2})] . \tag{36}$$

If the overall charge on the molecular anion is ζ_m then

$$\zeta_A^o + 2\zeta_B^o = \zeta_m . \tag{37}$$

We can immediately write down the expression for an instantaneous change in the dipole in terms of the effective charges and the cartesian displacements for each atom as

$$\Delta_1\mu_\sigma = \zeta_A^o \Delta\sigma_A + \zeta_{B1}^o \Delta\sigma_{B1} + \zeta_{B2}^o \Delta\sigma_{B2} , \tag{38}$$

where σ means x, y, or z. Assuming $\zeta_{B1}^o = \zeta_{B2}^o$ we can rewrite the above equation as

$$\Delta_1\mu_\sigma = \zeta_A^o \Delta\sigma_A + \tfrac{1}{2}(\zeta_m - \zeta_A^o)(\Delta\sigma_{B1} + \Delta\sigma_{B2}) . \tag{39}$$

Incorporating the conservation of linear momentum condition,

$$\frac{1}{M}[m_A \Delta\sigma_A + m_B(\Delta\sigma_{B1} + \Delta\sigma_{B2})] = 0 , \tag{40}$$

where M is the total molecular mass, into the defining equation for S_2 ($\sigma = z$) we have

$$S_2 = - \frac{M}{m_A} [\Delta z_{B1} + \Delta z_{B2}] \quad . \tag{41}$$

Rewriting equation (39) we find a more suitable form to be

$$\Delta_1 \mu_z = \zeta_A^o [\Delta z_A - \tfrac{1}{2}(\Delta z_{B1} + \Delta z_{B2})] + \tfrac{1}{2}\zeta_m [\Delta z_{B1} + \Delta z_{B2}].$$

We now have enough information to define $\Delta_1 \mu_z$ as a function of symmetry coordinates S_2

$$\Delta_1 \mu_z = \tfrac{1}{2}[\zeta_A^o - \zeta_m (\frac{m_A}{M})] S_2 \tag{42}$$

Similarly we find for the fixed charge contribution in the x direction

$$\Delta_1 \mu_x = 2^{-\frac{1}{2}} [\zeta_A^o - \zeta_m (\frac{m_A}{M})] S_3 \quad . \tag{43}$$

One parameter, namely ζ_A^o, determines the nuclear contribution to the varying dipole for both modes 2 and 3.

Next, we wish to identify the charge flux influence on the dipole derivative. If we are going to have a charge flux about an atom during a vibration, then the irreducible representation of that set of equivalent atoms must transform as the vibration. For the atoms in a $D_{\infty h}$ AB_2^{-n} molecular ion, we have only one coincidence with an active infrared mode: $S_3(\Sigma_u)$ transforms like atom $B(\Sigma_u)$. No flux occurs during the bending motion. The charge flux parameter is then

$$2^{-\frac{1}{2}} \frac{\partial(\zeta_{B1} - \zeta_{B2})}{\partial S_3} \equiv b \ . \tag{44}$$

This expression has the following meaning: as S_3 is executed, the flux of charge describes the dynamical difference between the charge on atom B1 and that on atom B2.

The complete expression for the varying dipole can now be written down. Considering equation (42) for mode 2, we have

$$\frac{\partial \mu_z}{\partial S_2} = \frac{\partial \Delta_1 \mu_z}{\partial S_2} = +\tfrac{1}{2}(\zeta_A^o - \frac{m_A}{M} \zeta_m) \ , \tag{45}$$

and consolidating equations (43) and (44) into one function for mode 3, we find

$$\frac{\partial \mu_x}{\partial S_3} = \frac{\partial \Delta_1 \mu_x}{\partial S_3} + \frac{\partial \Delta_2 \mu_x}{\partial S_3} = 2^{-\frac{1}{2}}(\zeta_A^o - \frac{m_A}{M} \zeta_m) - 2^{\frac{1}{2}} b \ r^o \tag{46}$$

where r^o is the equilibrium bond length and b has units of $e/\mathring{A}$.

The analogous relationships for the case of the D_{3h} planar molecular anions are:

$$\frac{\partial \mu_z}{\partial S_2} = 3^{-\frac{1}{2}}(\zeta_A^o - (\frac{m_A}{M}) \zeta_m) \ , \tag{47}$$

$$\frac{\partial \mu_y}{\partial S_3} = 6^{-\frac{1}{2}}(\zeta_A^o - (\frac{m_A}{m}) \zeta_m) + 3(6^{-\frac{1}{2}}) b \ r^o \ , \tag{48}$$

and

$$\frac{\partial \mu_Y}{\partial S_4} = \frac{2^{\frac{1}{2}}}{6} \left(\zeta_A^o - \left(\frac{m_A}{M}\right) \zeta_m\right) + \frac{6^{\frac{1}{2}}}{2} c\, r^o \,, \tag{49}$$

where the charge flux parameters are

$$b = 6^{-\frac{1}{2}} \frac{\partial (2\zeta_{B1} - \zeta_{B2} - \zeta_{B3})}{\partial S_3} \,, \tag{50}$$

$$c = 6^{-\frac{1}{2}} \frac{\partial (2\zeta_{B1} - \zeta_{B2} - \zeta_{B3})}{\partial S_4} \,. \tag{51}$$

For the derivations of these formulas one is directed to Appendix B.

Considering both equations (46) and (47) above, one can see that all the effective equilibrium charges can be deduced from the intensity of the bending mode S_2 in each case. This means that the effective equilibrium charges we will be finding depend on the motion of the atoms within the nonpolar molecular anions. Consequently one should not expect these effective charges to compare to those found from an LCAO-MO analysis of the atomic electron densities at equilibrium or to those charges resulting from molecular quadrupole moment experiments, since both of these investigations result in effective charges that are closer to static point charges.

III. EXPERIMENTAL

KN_3 and KHF_2 are both of D_{4h}^{18}-I4/mcm crystal structure as determined by x-ray crystallography (1) and conveniently grow with large (001) faces (x,y). As seen in Figure 1, the linear, $D_{\infty h}$, anions occupy D_{2h} sites and the cations are on D_4 sites. Since the unit cell is body centered with four molecules per unit, the dynamic primitive cell is reduced to two molecular units. These tetragonal crystals were grown by slow evaporation from saturated solutions of commercially available salts. The solutions were first filtered several times through a 0.45 μm Millipore filter and then allowed to stand loosely covered for several weeks at constant room temperature. Typical crystals were 20 x 20 x 2 mm. After afixing them to squares of Plexiglas for ease of polishing and mounting in the reflection cell, they were polished with fine carborundum paper and then wet polished with $Ce(IV)O_2$ and isopropanol on a polishing cloth. The pertinent optical constants and cell parameter units are given in Table 2.

$CaCO_3$ (calcite) and $NaNO_3$ are both of D_{3d}^{6}-$R\bar{3}c$ crystal structure (1) and have two molecules in the unit cell as shown in Figure 2. The planar D_{3h} anions are on D_3 sites and the cations occupy S_6 sites in the crystal unit cell. These crystals unfortunately do not grow with a large major face so the crystals used in this study were

Figure 1. Unit cell for tetragonal D_{4h}^{18} crystal. Filled circles = cations (D_4 sites); unfilled circles = anions (D_{2h} sites).

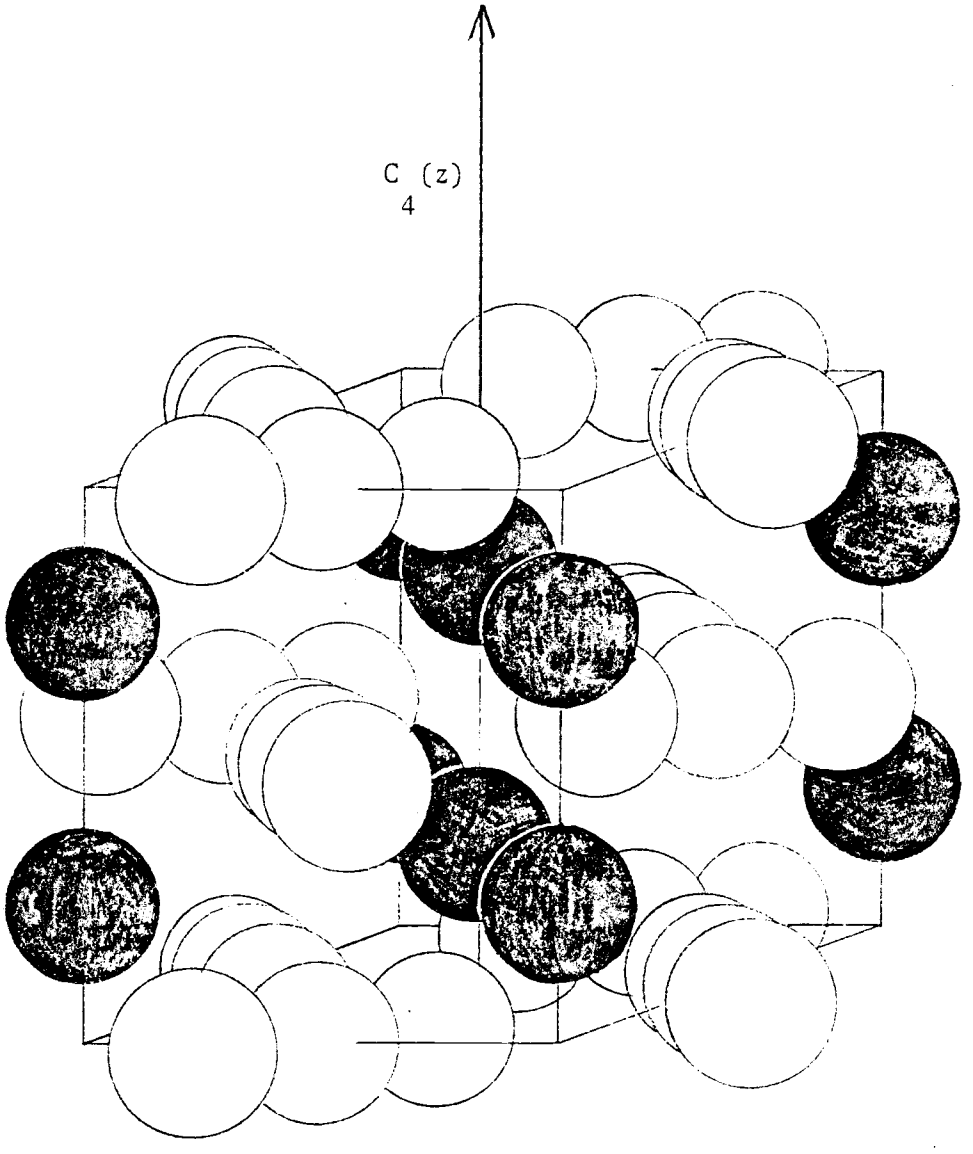
C (z)
4

Table 2. Unit cell and optical constants.

	KN_3	KHF_2	$CaCO_3$	$NaNO_3$
a(Å)	6.094[b]	5.67[b]	6.361[c]	6.325[c]
c(Å)	7.056[b]	6.81[b]	θ=46°6'[c]	θ=47°10'[c]
v(Å^3)	130.019	109.47	121.914	124.847
ε_x^a	2.749	1.833[e]	2.749[f]	2.519[f]
ε_z^a	2.016	1.772[e]	2.208[f]	1.785[f]
n_x	1.658[d]	1.354	1.658	1.587
n_z	1.420[d]	1.331	1.486	1.336
$r^{(0)}$(A-B) [Å]	1.15[b]	1.136A[c]	1.32[g]	1.218[g]
α_+ (Å^3)	1.03[e]	1.03[e]	1.1[f]	.292[f]
$\alpha_{\parallel}$ (Å^3)	7.32[h]	2.03[e]	3.18[f]	2.76[f]
$\alpha_{\perp}$ (Å^3)	2.765[h]	1.60[e]	4.21[f]	4.79[f]

[a]Measured at 589.3 nm.
[b]See reference (1).
[c]See reference (1).
[d]See reference (37).
[e]See reference (2).
[f]See reference (17).
[g]See reference (30).
[h]Present work.

Figure 2. Unit cell for trigonal D_{3d}^{6} crystal. Filled circle = cations (S_6 sites); unfilled circles = anions (D_{3d} sites).

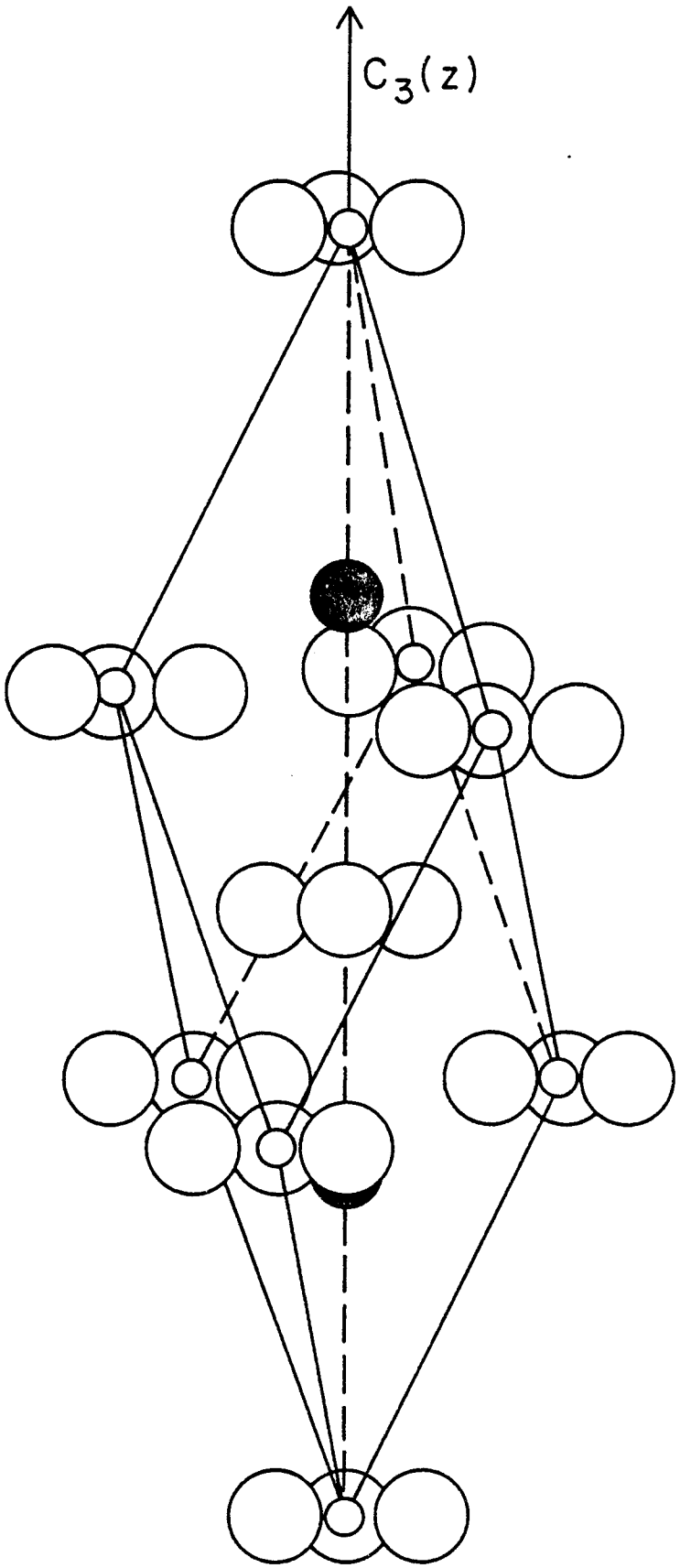
$C_3(z)$

acquired from commercial sources. The two single calcite crystals used in the study were previously cut so that the largest face (diameter about 2.5 cm, thickness 3 mm) is an xy face, perpendicular to the symmetry axis. The other crystal of similar size was cut to expose the yz face. These crystals are surplus material originally manufactured for use in anti-aircraft gun sights. The sodium nitrate crystal was purchased from the Harshaw Chemical Co. and was cut so the largest face is a yz face, on the order of 10 x 10 mm; the smallest face is an xy face of about 2.5 x 10 mm. These crystals were mounted and polished as described above, except that 100% ethanol was used to wet polish the nitrate crystal. The optical and unit cell constants are listed in Table 2.

The reflectance from these oriented single crystal specimens was recorded in the double beam transmission mode of a ratio recording Perkin Elmer 180 infrared spectrometer to minimize background absorption due to CO_2 and H_2O vapor and to eliminate any instrumental bias in the polarization studies. The mounted crystals were inserted in a modified Barnes beam condenser reflection cell which is normally used to measure transmission in very small samples (see Figure 3). This cell is equipped with three concave front surfaced metal mirrors, two of which focus the source radiation on the crystal surface and one that then sends the reflected intensity into the monochromator at a spectral

Figure 3. Perkin Elmer 180 infrared spectrometer equipped with reflection cell.

Perkin Elmer 180 Infrared Spectrometer

with Reflection Cell

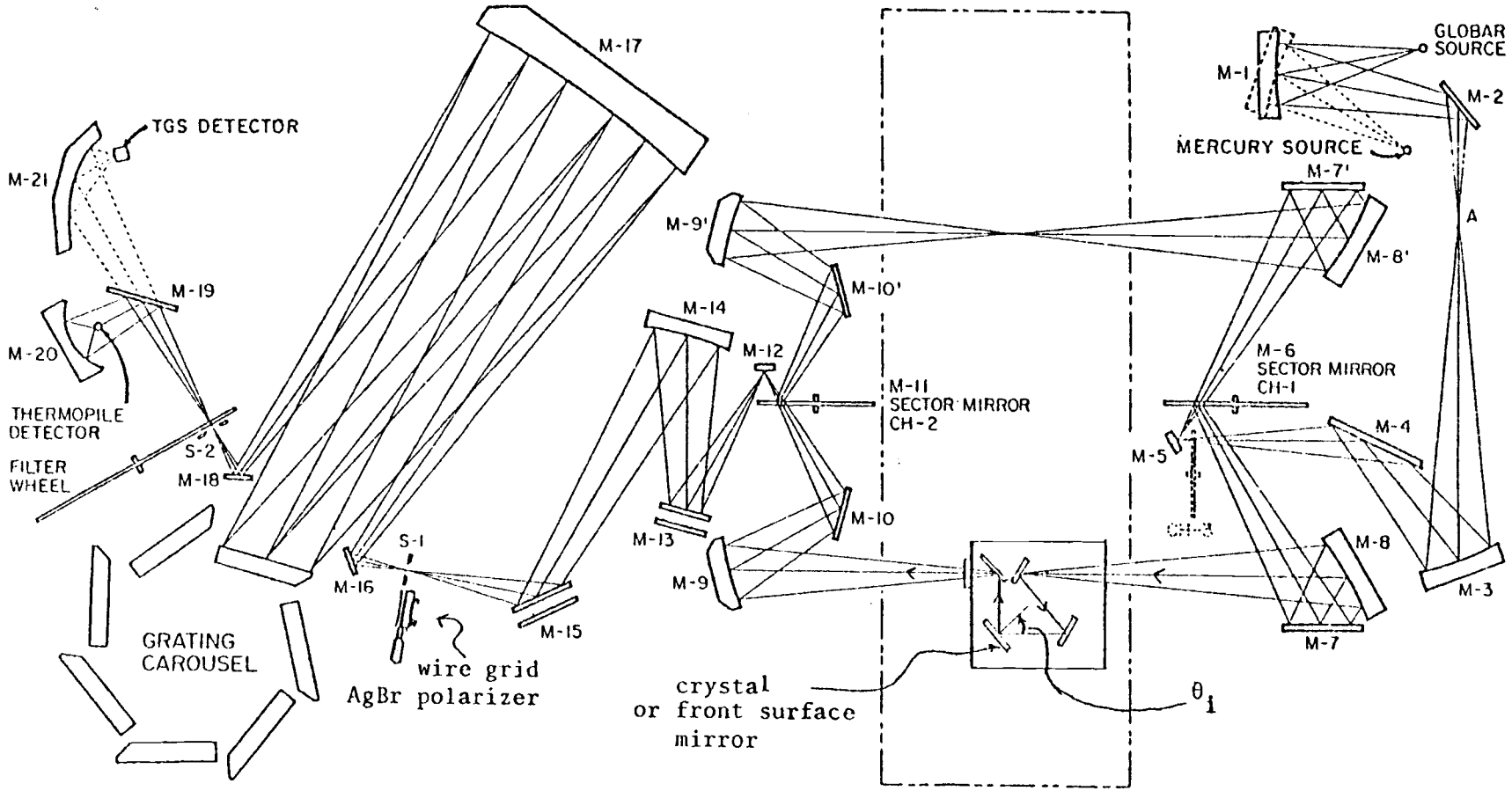

slit width (SSW) of about 1 cm^{-1}. Utilizing an internal silver bromide wire grid polarizer, we discriminated between TE and TM polarized intensities. We recorded the following for each experiment: 1) closed beam (zero level); 2) the (polarized) sample signal; 3) the reflected signal from a front surfaced metal mirror. Being an almost perfect reflector in the infrared region, the mirror provided the 100% reflected signal that in conjunction with the zero measurements allowed the conversion of sample reflection into sample reflectance. The normalization of the spectra was accomplished by hand in the earlier azide studies but was performed on a minicomputer with the transferring of data via paper tape for all later studies.

The incidence angle used in any one experiment was measured by duplicating the path of the ir beam through the beam condenser with a small HeNe laser. Two different methods were used to determine θ_i. In the azide studies, the accepted procedure had been to remove the concave mirror situated after the sample and trace out the path of the laser beam from the sample surface to a convenient point and then, knowing the placement of the sample, the mapped out θ_i was simply measured with a protractor. This method did present problems with respect to reinserting the concave mirror in exactly the same orientation. Therefore, in the later studies it was found to be more reproducible to merely hold a small clear plastic protractor near the

surface of the crystal, or flat mirror, in such a way as to allow some of the laser light to pass through the protractor thus illuminating the incidence angle. The incidence angle for maximum reflection was found to range from 42-50°. Even with the second method of determining θ_i, there is probably still a 10% error in the single value assigned to the center ray of what is really a cone of incident radiation. Since the globar is not a point ir source, one should really convolute the spectrum over a range of angles. From experience, a variation in the angle appears to affect mainly the wings of a TM2 reflection and for TM23 and TE polarized bands, the high frequency (ν_{LL}) side of the band may also be slightly shifted. However, we are most interested in determining the strength of the mode, that is the ν_T-ν_L split, therefore we did not find it necessary to refine θ_i further.

It should be noted, though, that it is a TM3 experiment that is most affected by an error in θ_i. Looking back at equations (27) and (28) one can see that it is necessary to accurately know θ_i to find the correct S_j which in turn modifies ν_T to yield ν_L. Remember that in a TM3 case, the maximum reflection occurs between ν_L and ν_{LL} but that ν_T is still the parameter that is inserted in the reflection equation to calculate R. If the apparent θ_i were lower than the true θ_i, a strength larger in magnitude than the true strength would be needed

to give a good fit to the observed spectrum. Conversely, calculations using a larger θ_i than was really employed in the experiment would cause one to choose a smaller strength to fit the band. An error in θ_i for a TE or TM23 experiment would be less critical for two reasons: 1) the transverse frequency is an experimental observable; 2) only a small fraction of the total maximum reflectivity is angle dependent, i.e. that from ν_L to ν_{LL}.

The frequency scale was calibrated using ammonia in the 800 cm^{-1} region, water in the 1500 cm^{-1} region and carbon dioxide in the 2300 and 600 cm^{-1} ranges. Therefore, the frequencies reported in this work are precise to 1.0 cm^{-1}. The error in the chart recorded intensity scale was determined to be $\sim$5% full scale by testing the transmission through a 47% calibrated screen. However, we did not test the linearity of the error. An error in the intensity would manifest itself in the determination of the damping constant, and like the error in θ_i would have an effect on fitting the wings of a band, rather than the width (strength) of a band. Even though some uncertainties exist, the overall fit achieved for the band width and for the wings is reasonable and the magnitudes of the resultant parameters are consistent for a particular mode under different polarizations at different incidence angles.

The opportunity to check the agreement between a tape recorded spectrum and one of data points selected by hand

was taken using a KHF_2 spectrum. The average difference on a scale of 0 to 1 reflectance was 0.0013 for 109 points. Therefore we believe no significant error is introduced if the spectra are collected and then normalized via paper tape.

IV. BAND ANALYSIS FOR $D_{\infty h}$ MOLECULAR ANIONS

Using the structure information provided by x-ray crystallography in conjunction with the correlation tables, one can find the irreducible representations for the internal modes and lattice modes. The correlation of these modes from free ion to crystal is given in Table 3. At $\vec{k} = 0$, when all molecules in the crystal move in phase, the vibrations allowed by the solid state environment are those admitted by the unit cell symmetry (here D_{4h}). One should then observe six infrared modes: $2A_{2u}$ and $4E_u$. These are evenly divided between the internal and external vibrations. We have dubbed the two E_u lattice modes ν_5 and ν_6. Correlation shows that the E_u far ir modes arise from $T^-(z)$, $T^-(x,y)$, and T^+ (+ and - refers to cation, anion); these three degrees of freedom will become one acoustic mode and two optical modes involving different relative displacements of the cations and anions. We have called the A_{2u} lattice mode ν_4; both anions and cations are active along the z-axis. However, our interest in calculating molecular

Table 3. Correlation table for $D_{\infty h} \rightarrow D_{4h}$.

Molecular Symmetry	Site Symmetry	Factor Group	Modes
$D_{\infty h}$	D_{2h}	D_{4h}	
Σ_g^+	A_g	A_{1g}	ν_1
(ν_1)	B_{1g}	A_{2g}	$R_- T_+$
π_g	B_{3g}	B_{1g}	R_-
(R_{xy})	B_{1u}	B_{2g}	ν_1
Σ_u^+	B_{2u}	E_g	$R_- T_+$
(T_z, ν_3)	B_{3u}	A_{2u}	$\nu_2 \; T_\pm$
π_u	$D_4 \; (K^+)$	B_{1u}	$\nu_2 T_-$
$(\nu_{2x}, \nu_{2y}, T_{xy})$	A_2	E_u	$\nu_2 \nu_3 T'_\pm T''_\pm$
	E		

$$\Gamma^{\text{infrared}}_{\vec{k}=0} = 2A_{2u} + 4E_u$$

dipole derivatives has led us to be principally concerned with the internal modes in the mid-infrared region.

In this region, one should be able to detect the lifting of the degeneracy for the bending mode, ν_2, to allow an in plane (x-y polarized) E_u bend and an out of plane (z polarized) A_{2u} bend. The doubly degenerate antisymmetric stretch ν_3 is also infrared active in the x-y plane with E_u symmetry. Since ν_2 and ν_3 have components of the same symmetry in the factor group, intermode mixing may occur for modes close in frequency.

Figure 4 shows the x,y face of the primitive unit cell for the crystal and identifies K^+ ions as 1 and 2 and anions as 3 and 4. Consideration of this figure along with equations (19) and (20) suggests that TE polarization of the x,y face will select the E_u modes only. TM polarization, case 2, will reveal ν_3 and ν_2 (E_u) that are $\varepsilon_2 = \varepsilon_y = \varepsilon_x$ active and case 3 will admit ν_2 (A_{2u}) which is $\varepsilon_3 = \varepsilon_z$ active. Likewise, for the lattice modes, E_u modes that are x,y active will be observed under TE and TM2 polarization, whereas A_{2u} modes will be TM3 polarized.

In both the KN_3 and KHF_2 studies only an x,y face of the crystal could be studied since an x,z face was too small, less than 1 mm x 20 mm. This edge of the crystal resisted attempts to polish it from a tapered tip (<1 mm) to a smooth surface of adequate area ($\sim$3 mm x 10 mm).

Figure 4. XY face of D_{4h}^{18} crystal with cations 1 and 2, anions 3 and 4, showing $\nu_3(3)$-E_u and $\nu_2(4)$-E_u.

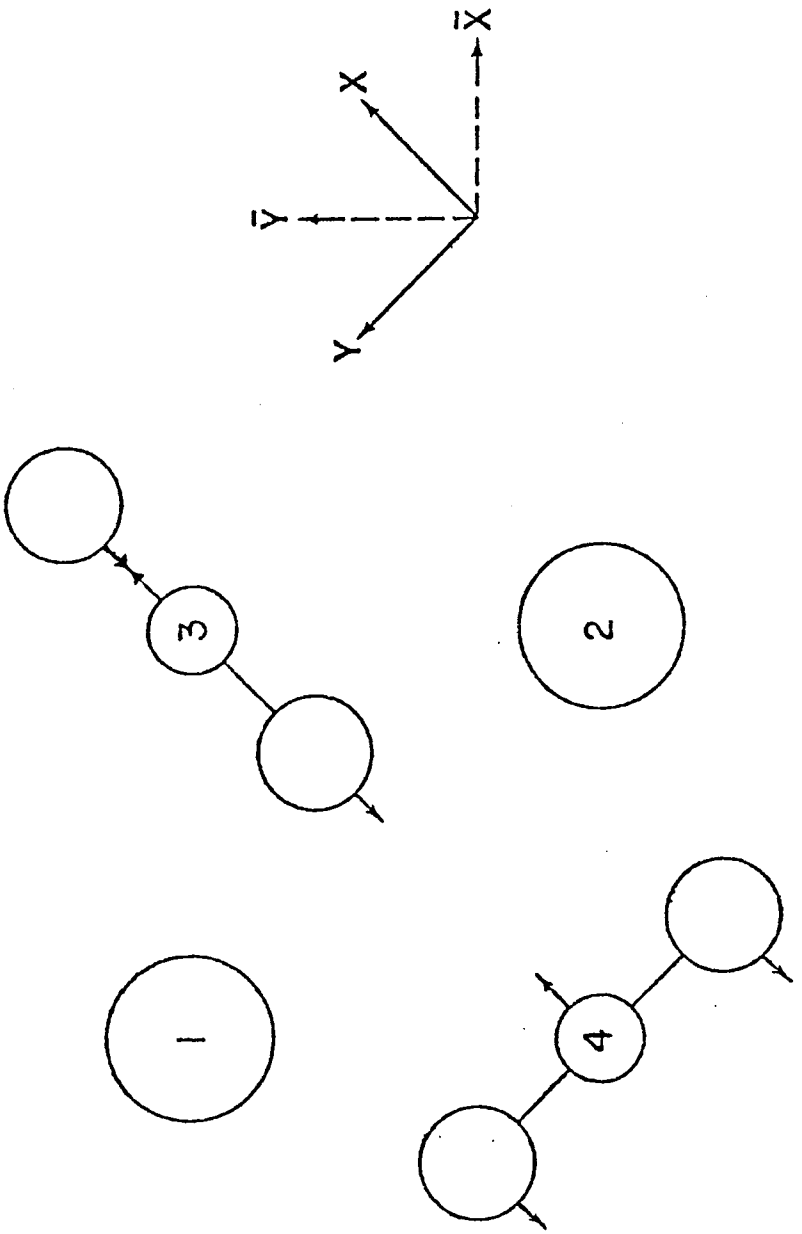
IX
X
IY
Y
3
2
1
4

KN_3 - Potassium Azide

In the case of KN_3, the spectra were chart recorded. The normalized reflectance was calculated at intervals of 4.0, 0.1, and 1.0 cm^{-1} in the ν_3, ν_2 and far ir regions, respectively. Initial estimates of the reflectance parameters were made visually with a graphical Tektronix 4012 computer terminal equipped with a hard copy unit in which we utilized an OS-3 program called GRAFIT. Refinement of the parameters was accomplished by examining a certain range of parameter space corresponding to the adjustable parameters, ν_{jT}, S_j^σ, and γ_j.

The S_j^σ were found in the following way: the E_u modes were divided into three regions, namely, ν_3(I), ν_2(II), and the two mode region of ν_5 and ν_6 (III). In each of these three regions the contributions to the dielectric constant from resonances occurring in the other two regions were neglected. In the lattice mode region III and the TM polarized region II, six parameters were simultaneously adjusted.

The errors consequent upon this separated mode approximation were analyzed by finding the corrections to $\varepsilon^\sigma(\infty)$ to give ε_B^σ as in equation (26). This correction did not exceed 2 or 3% of $\varepsilon^\sigma(\infty)$ for the internal modes. Assuming that the error in S_j^σ is proportional to the error in $\varepsilon^\sigma(\infty)$, we accepted the initial estimates of the parameters

without further refinement, partly since the percent error in $\partial\mu_\sigma/\partial q_j$ is only half that in S_j^σ and also because no account has really been taken of the dispersion in the electronic resonance.

The antisymmetric stretch shown under two polarizations in Figures 5 and 6, is a broad band of some 80 cm^{-1} with a transverse frequency at 2025 cm^{-1} and longitudinal and pseudolongitudinal frequencies of 2086 and 2099 cm^{-1}, respectively. For sixteen separate determinations at angles varying from 43° to 50°, the average strength was found to be 0.162 with an average damping constant of 4.9 cm^{-1} (see Table 4). The typical results shown in these figures correspond to a root mean square error of 3% for 126 points. This error is almost entirely attributable to the obvious discrepancy at the top of the reflectance band. We believe this deviation of experiment from theory is most likely due to a surface that was not polished perfectly flat and/or was not without microscopic pits. It is noteworthy that this azide mode departs from the classical oscillator shape in NaN_3 also (3), which may be indirect evidence for a frequency dependent damping constant. In any event, this deviation affects mainly the evaluation of gamma and has little effect upon the parameter of primary interest, i.e. the strength S for KN_3.

Comparison of Figure 5 with 6 shows several differences between TE and TM2 reflection band shapes which are very

Table 4. Experimental and fitting parameters for KN_3 reflectance.

		$\nu_2(E_u)$			$\nu_2(A_{2u})$			$\nu_3(E_u)$		
θ_i	P[a]	γ_2[b]	ν_{2T}[b]	S_2	γ_2[b]	ν_{2T}[b]	S_2	γ_3[b]	ν_{3T}[b]	S_3
46.5	TE	0.22	649	0.0120				4.0	2029	0.150
	TM	0.25	649	0.0120	0.70	642	0.0137	4.7	2023	0.164
46	TE	0.21	649	0.0128				6.2	2027	0.158
	TM	0.25	649	0.0128	0.50	642	0.0132	5.5	2024	0.166
43	TE	0.18	649	0.0128				4.7	2027	0.164
	TM	0.23	649	0.0128	0.52	642	0.0134	2.5	2024	0.164
43.5	TE	0.25	649	0.0130				4.5[c]	2024[c]	0.169[c]
	TM	0.25	649	0.0129	0.50	642	0.0137	3.6	2024	0.167
45	TE	0.28	649	0.0119				4.7[d]	2026[d]	0.162[d]
	TE	0.21	649	0.0128				4.6	2024	0.168
	TM	0.25	649	0.0119	0.70	642	0.0137	6.0	2025	0.162
	TM	0.25	649	0.0128	0.55	642	0.0137	3.6	2024	0.166
47.5	TE	0.25	649	0.0119				4.7[e]	2027[e]	0.160[e]
	TM	0.25	649	0.0119	0.73	642	0.0137			

[a] "P" is polarization.

[b] Units are cm^{-1}.

[c] RMS error of 2.3%.

[d] RMS error of 3.6%.

[e] RMS error of 4.1%.

Figure 5. TE reflectance in the ν_3 region of KN_3 at room temperature and $\theta_i = 43.5°$; rms error 3%.

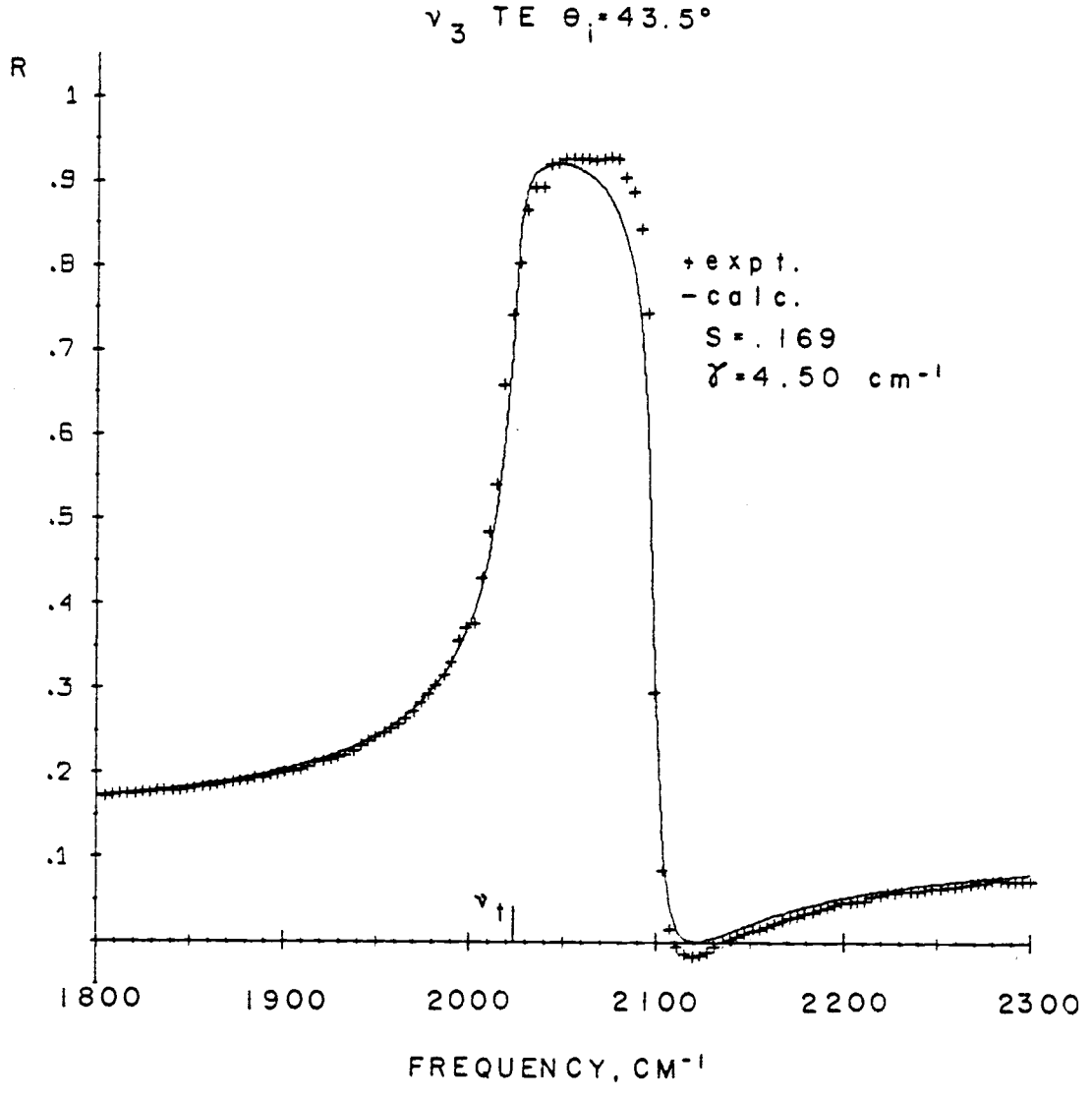
ν_3 TE θ_i=43.5°
R
1
.9
.8
.7
.6
.5
.4
.3
.2
.1
+ expt.
− calc.
S = .169
γ = 4.50 cm^{-1}
ν_t
1800
1900
2000
2100
2200
2300
FREQUENCY, CM^{-1}

Figure 6. TM2 reflectance in the ν_3 region of KN_3 at room temperature and $\theta_i = 45°$; rms error 3%.

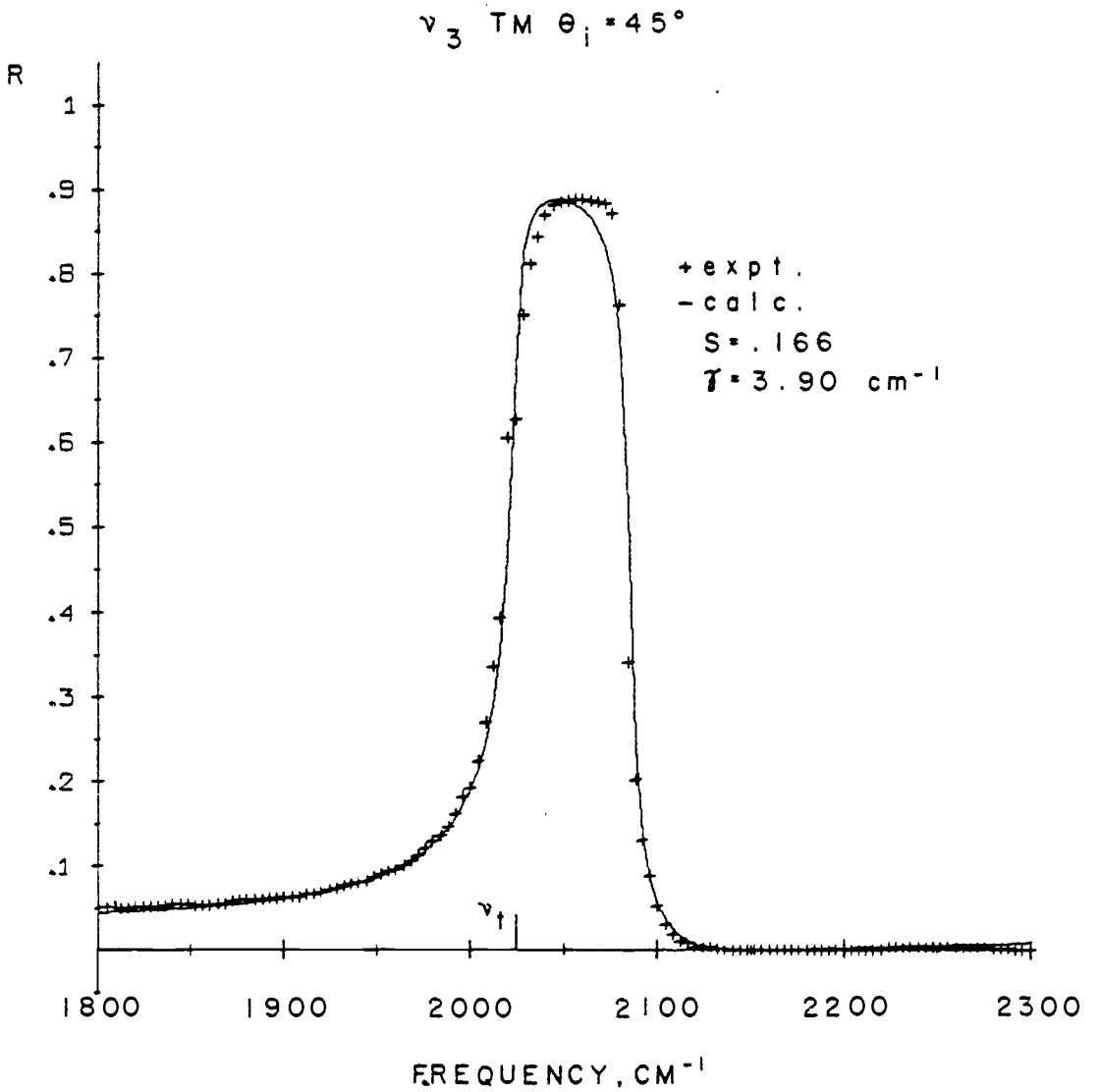
ν_3 TM $\theta_i = 45°$
R
1
.9
.8
.7
.6
.5
.4
.3
.2
.1
+ expt.
− calc.
S = .166
γ = 3.90 cm^{-1}
ν_t
1800
1900
2000
2100
2200
2300
FREQUENCY, CM^{-1}

well reproduced by the model theory. Note that the TM2 spectrum exhibits no conspicuous minimum on the high frequency edge of the band. This behavior in TE is undoubtedly due to the fact that the background reflectance, that is the reflectance in a frequency region with no dispersion, is larger for TE than for TM polarization (see Table 1). For example, at θ_i equal to 45°, ε_x at 2.5 and ε_z at 2.0, R(TE) is 0.11, whereas R(TM) is 0.02. So that even though there is a minimum in the TM2 reflectance it is not as apparent as it is in TE reflectance.

The TM reflectance in the ν_2 region is shown in Figure 7. The nondegenerate, z polarized A_{2u} out of plane bend observed only under TM3 polarization from an x,y face, is shown here occurring at a lower frequency than the corresponding degenerate x,y polarized E_u bend. The average fitting parameters are: $S_{A_{2u}} = 0.0136$, $S_{E_u} = 0.0124$, $\nu_{2T}(A_{2u}) = 642\ cm^{-1}$, $\nu_{2T}(E_u) = 649\ cm^{-1}$, $\gamma_{A_{2u}} = 0.60\ cm^{-1}$, $\gamma_{E_u} = 0.25\ cm^{-1}$. Since the best employable resolution was $1.1\ cm^{-1}$ but the width of the E_u mode is $2\ cm^{-1}$ at half height and that of the A_{2u} mode is less than $1\ cm^{-1}$ at half height, it was necessary to convolute the calculated spectra with a triangular slit function appropriate for a two slit monochromator. However, no data manipulations can change the fact that the resolution was inadequate to determine the width of the A_{2u} reflection. As we shall see in a later section, $S_{A_{2u}}$ is predicted to be twice S_{E_u}; we found

Figure 7. TM2 and TM3 reflectance in the ν_2 region of KN_3 at room temperature and $\theta_i = 46°$, where SSW = 1.1 cm^{-1}.

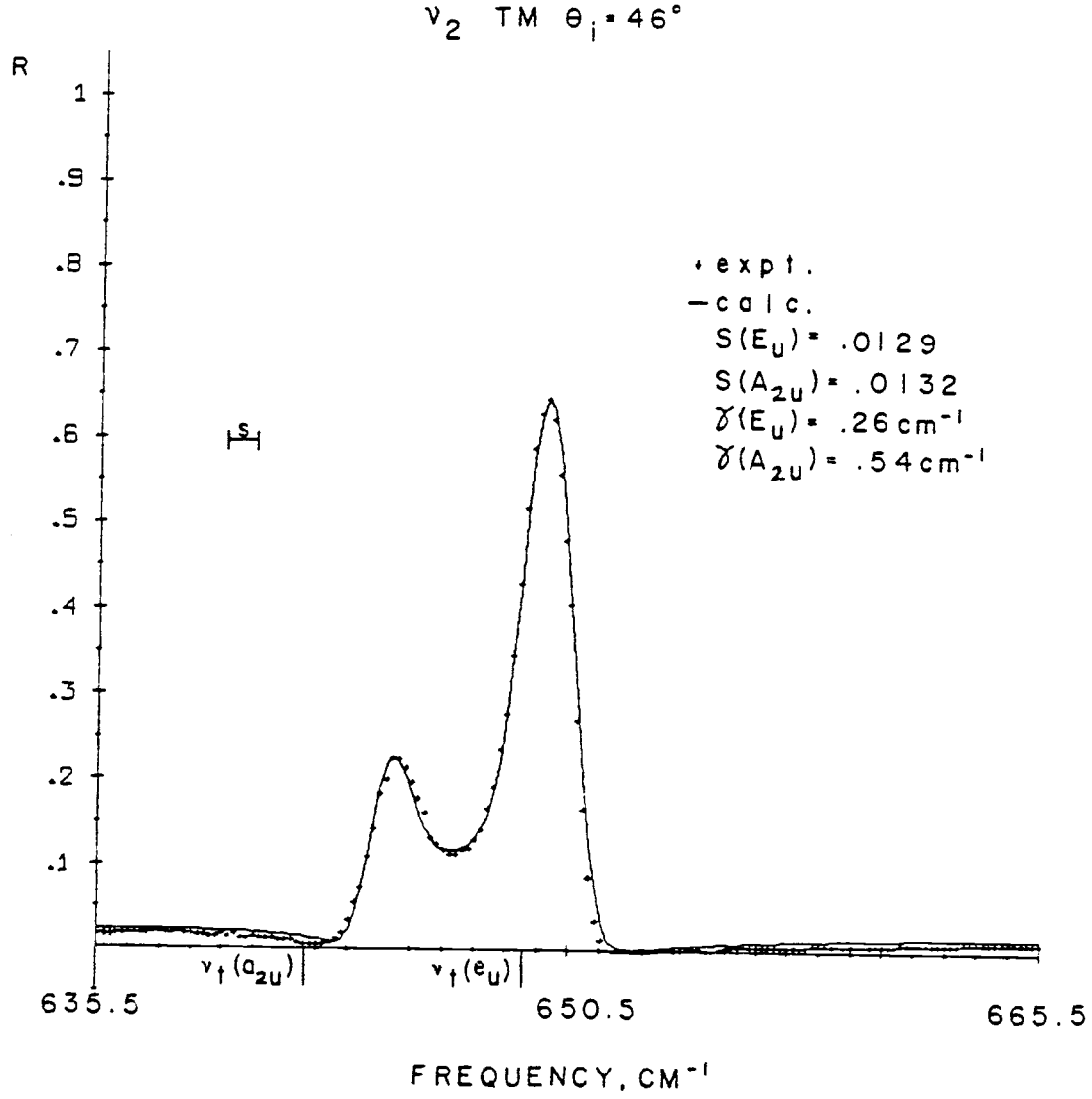
ν_2 TM $\theta_i = 46°$
R
1
.9
.8
.7
.6
.5
.4
.3
.2
.1
S
+ expt.
— calc.
$S(E_u) = .0129$
$S(A_{2u}) = .0132$
$\gamma(E_u) = .26\,cm^{-1}$
$\gamma(A_{2u}) = .54\,cm^{-1}$
$\nu_t(a_{2u})$
$\nu_t(e_u)$
635.5
650.5
665.5
FREQUENCY, CM^{-1}

them to be almost equal. Remembering that in these azide studies a less reproducible method was used to determine θ_i than was used in later studies, suggests that there may be a larger error in the value assigned θ_i here than in subsequent experiments. Since we could only study this mode from an x,y face, it is impossible to say whether the error is in θ_i or in the theoretical effective field for the z direction in the crystal. As we have already said, a variation in θ_i does affect the strength for the TM3 polarization. It is, however, encouraging that the TE experiment for ν_2 (E_u) yields parameters very similar to those from the TM2 experiments: $S_{E_u} = 0.0125$, $\nu_{2T}(E_u) = 649\ cm^{-1}$, and $\gamma_{E_u} = 0.23\ cm^{-1}$. A typical experiment is shown in Figure 8. In the further analysis of dipole derivatives we have adopted an average of the TE and TM2 data to describe ν_2 in N_3^-.

An attempt was made to measure the far infrared modes for KN_3 for the purpose of determining their contribution to the background dielectric constant in the internal mode region. Unfortunately, only the E_u modes shown in Figure 9 could be identified and fitted. In this region, 230-90 cm^{-1}, we were severely limited by decreased S/N. Perhaps the most obvious discrepancy between theory and experiment shown here is that the experimental reflectance dips much lower between the modes than would be predicted. This sort of behavior can be detected in another case we will look at

Figure 8. TE reflectance in the ν_2 region of KN_3 at room temperature and $\theta_i = 46°$ and SSW = 1.1 cm^{-1}.

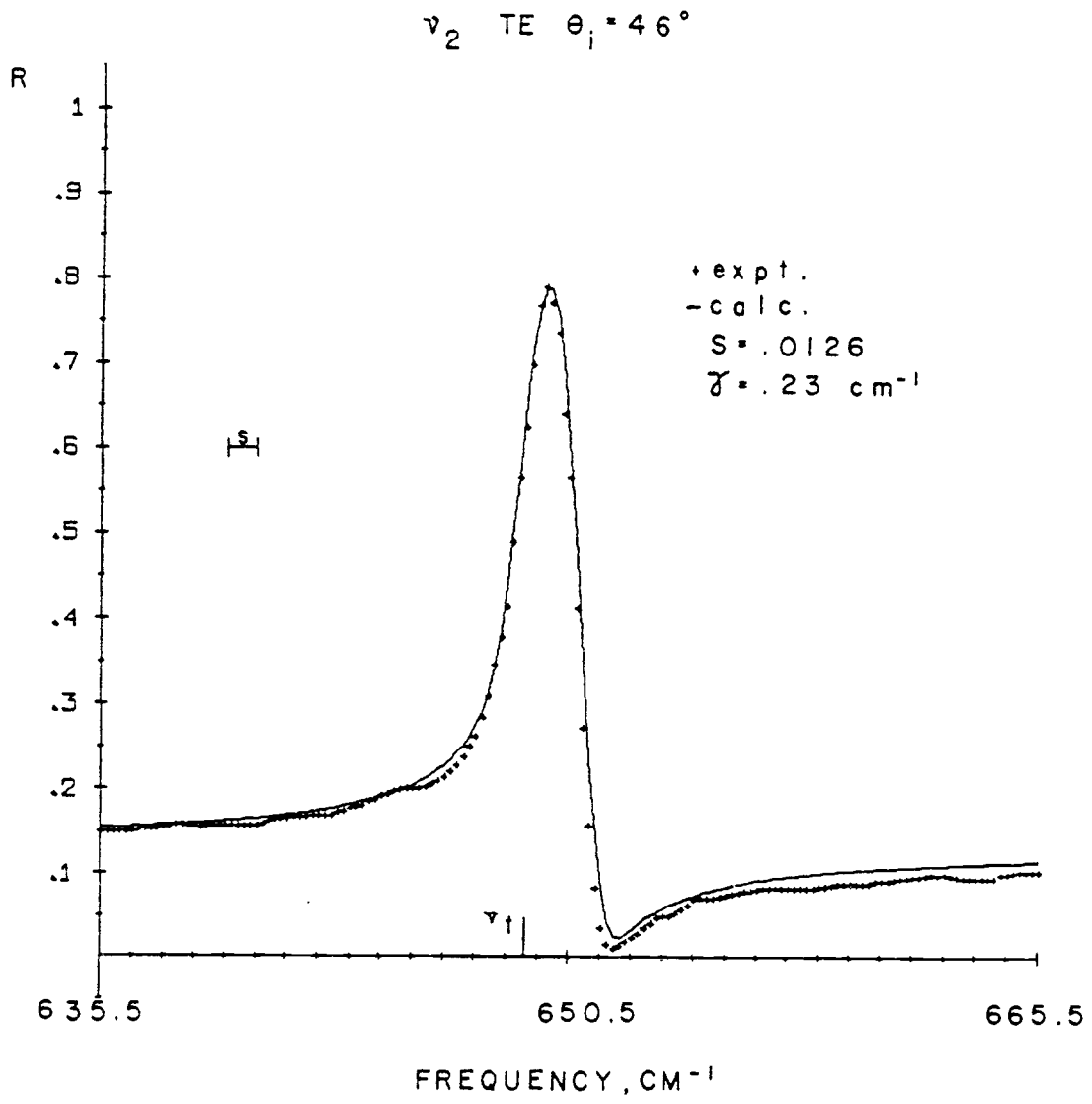
ν_2 TE $\theta_i = 46°$
R
1
.9
.8
.7
.6
.5
.4
.3
.2
.1
S
ν_t
+ expt.
- calc.
S = .0126
γ = .23 cm^{-1}
635.5
650.5
665.5
FREQUENCY, CM^{-1}

Figure 9. Far infrared reflectance in the lattice mode region for KN_3 at room temperature, $\theta_i = 43°$, TE, TM polarizations (A); calculated TE (B) for $S_6 = 2.1$, $\gamma_6 = 10.0\ cm^{-1}$, $\nu_{6T} = 130.0\ cm^{-1}$ and $S_5 = 0.45$, $\gamma_5 = 35.0\ cm^{-1}$, $\nu_{5T} = 165.0\ cm^{-1}$.

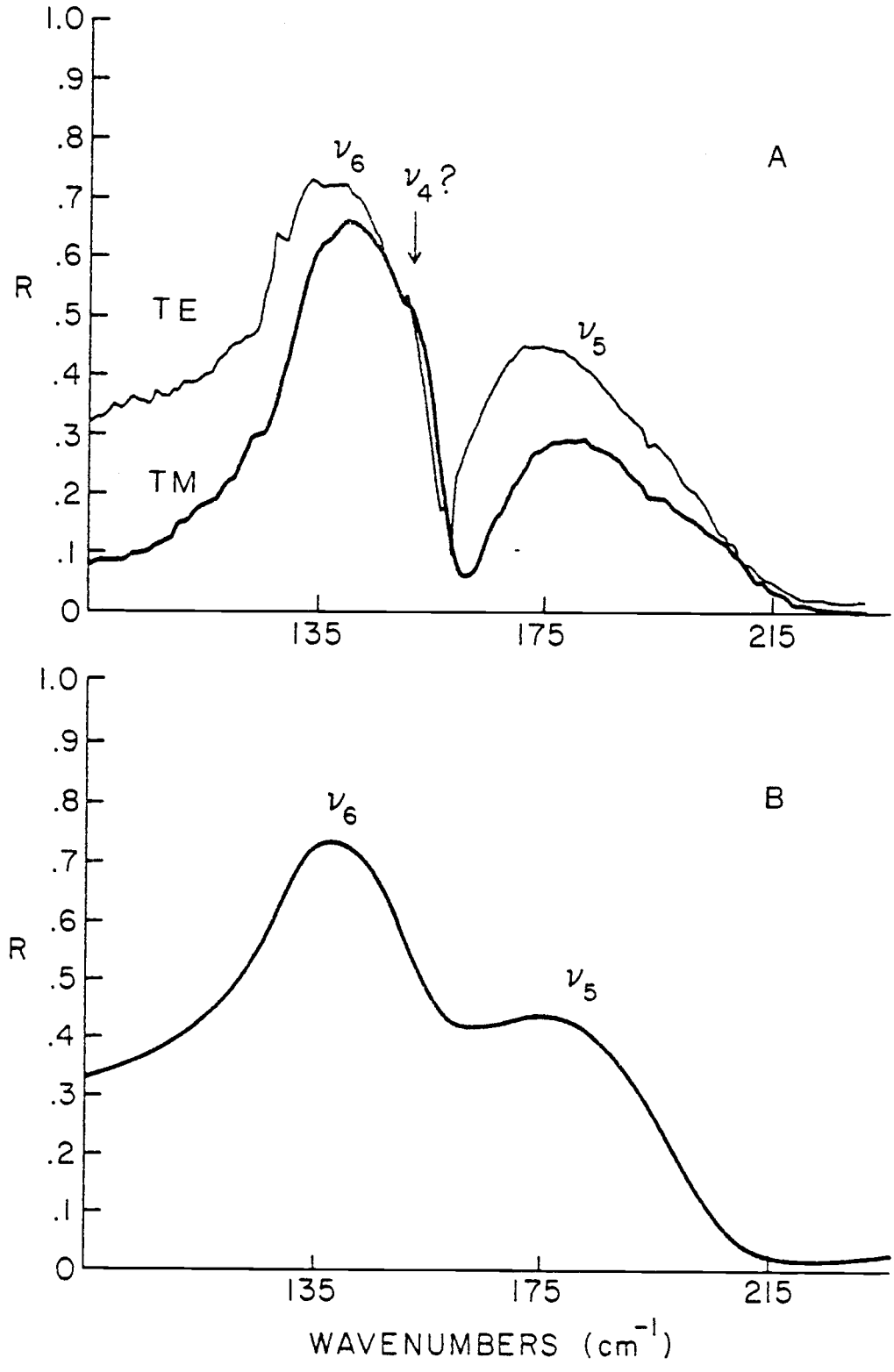
1.0
.9
.8
.7
.6
.5
.4
.3
.2
.1
0
R
TE
TM
ν_6
ν_4 ?
ν_5
A
135
175
215
B
WAVENUMBERS (cm^{-1})

(vide post Figure 10). The difference at this point in the spectrum could be minimized by choosing a smaller damping constant, which would, however, change the fit at the tops of the bands. Luckily, the strengths are not appreciably affected by a change in the damping. This phenomenon may be due to one or more things: 1) a not-so-perfect crystal surface; 2) there may be water absorptions, especially in this region of the infrared, that would interfere with the reflectance from both the mirrored surface and the crystal. The Perkin-Elmer 180 does have very large cell compartments and a long optical bench, so that even though we purge the instrument continually with dry air, some water is bound to be present.

Compared with the internal modes, external modes have large strengths. ν_5 at 165 cm^{-1} has a strength of 0.45 and ν_6 at 130 cm^{-1} has an even larger strength on the order of 2.0. An estimated strength and transverse frequency for the would be A_{2u} mode was made by simply assuming it was not resolved from the low frequency side of ν_5; no fitting procedure was used. The 1% or so error in $\partial\mu/\partial q$ due to omitting the contribution of the lattice modes to the background dielectric constant is within our expectation in light of all other errors introduced by experiment and approximations in the theory.

As a point of interest, we did observe the production of color centers in the azide crystal after it was exposed

to the mercury source lamp conventionally used below 500 cm^{-1}. A purplish gray hue appeared on the crystal upon exposure to the focused beam. Many small rounded pits developed on the surface. This darkly colored spot changed to a faded yellow-orange spot upon additional exposure to the infrared in the ν_2 region. The reflectivity in the ν_2 and ν_3 regions was checked and the intensities were found to be diminished by about 30%. This was probably a consequence of the roughened surface. No new features were observed.

The grayish spot we observed could have been metallic potassium deposited within the crystal. A process is described by Gray and Waddington (23) for this production of metal. Excitons are produced by a certain energy of incident radiation and these are trapped in bimolecular combinations of the surface cation vacancies. Pairs of excitons may then decompose to form N_2 and F centers:

$$N_3^- + h\nu \rightarrow N_3^{-*}$$

$$N_3^{-*} + \text{thermal energy} \rightarrow N_3 + e^-$$

$$2N_3 \rightarrow 3N_2 + Q \ .$$

In addition, when KN_3 is irradiated at room temperature an R' center is said to arise from aggregated F centers.

When an R' center is heated to around 60°C, the R' centers dissociate and neutralize K^+ ion to form the metallic K.

KHF_2 - Potassium Bifluoride

Representative experimental and theoretical reflectance spectra for TE and TM polarizations of KHF_2 are shown in Figure 10 over the frequency range from 1060 to 1750 cm^{-1}. The data for this crystal were acquired digitally and then reduced to normalized reflectance using a PDP-11 computer. With the aid of plotting routines, these spectra were outputed without smoothing.

In the bifluoride case, modes two and three are separated by a mere 200 cm^{-1}. This and the fact that ν_3 is about 150 cm^{-1} wide (that is, it will require a large strength to fit it), suggest that the separated mode approximation used in the KN_3 case is not adequate here. Therefore, in the TM spectra, nine parameters were simultaneously adjusted and in the TE spectra, six parameters were interactively adjusted until a reasonable fit was indicated.

A good fit was determined by investigating the σ values generated by certain ranges about each parameter. σ in this case is

$$\left(\frac{1}{N} \sum \left(R_{calc.} - R_{expt'l.}\right)^2\right)^{\frac{1}{2}}$$

Figure 10. TE and TM reflectance of KHF_2 at room temperature in the fundamental region. +++ = observed; ——— = calculated.

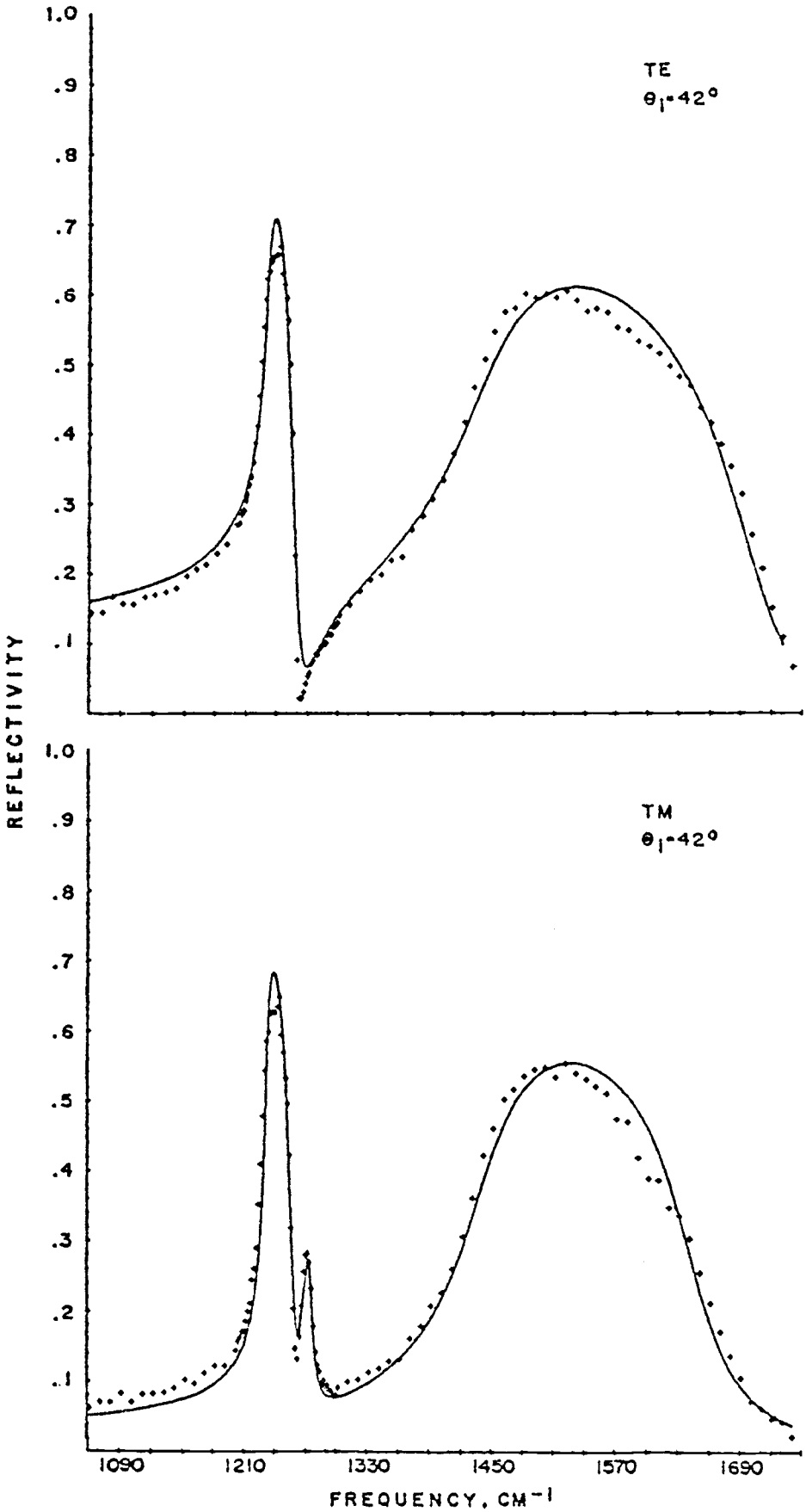
TE
θ_1=42°
TM
θ_1=42°
REFLECTIVITY
1.0
.9
.8
.7
.6
.5
.4
.3
.2
.1
1090
1210
1330
1450
1570
1690
FREQUENCY, CM^{-1}

where N is the number of data points. The use of a mini computer to calculate σ allowed hundreds of combinations of parameters to be searched for those yielding the lowest values. For example, in the 42° TE experiment, using 65 points for the ν_2 region from 1060 to 1300 cm^{-1} and 45 points for the ν_3 region from 1300 to 1750 cm^{-1}, values were generated by varying six parameters. For $\nu_2(E_u)$ the strength was varied from 0.140 to 0.195, the transverse frequency from 1225 to 1233 cm^{-1}, and the damping constant from 2 to 13 cm^{-1}; while for ν_3 (E_u), S_3 was searched from 0.40 to 1.0, ν_{3T} from 1430 to 1445 cm^{-1}, and γ_3 from 25 to 100 cm^{-1}. In the corresponding TM experiment an additional three parameters were needed. The strength of the ν_2 (A_{2u}) mode was adjusted from 0.03 to 0.13, the transverse frequency from 1225 to 1235 cm^{-1}, and the damping constant from 2.5 to 5.5 cm^{-1}. These variations caused the σ values to change from 30% to 3%. For the TE spectrum, the parameters shown in Table 5 lead to an RMS deviation of 2.8% between experiment and theory; the corresponding deviation in TM using a slightly different parameter set was 3.02%.

We did convolute the calculated spectra for KHF_2 using the previously described triangular slit function. We were fortunate here that the band width to resolution ratio was around five to one compared to one to one in the poorly resolved azide case. This lends greater credibility

to the bifluoride numbers than we had for ν_2 (A_{2u}) in KN_3. Unfortunately, there is still a disagreement between the predicted two to one ratio for S_2 $(A_{2u}):S_2$ (E_u) and the experimentally determined relation of approximately one to two! However, KHF_2 has a complicating feature. The frequency for ν_3 (E_u) is close to that for ν_2 (E_u) and being of the same symmetry, these modes can mix together, perturbing their respective strengths. As we shall see in the next section, we have used the parameters for ν_2 (A_{2u}) to characterize the dipole derivative for the bending mode. As for mode 3, the parameters listed in Table 5 are used to describe a lower limit for the dipole derivative for the antisymmetric stretch.

Table 5. Experimental and fitting parameters for reflectance of KHF_2.

			ν_2 (E_u)			ν_2(A_{2u})			ν_3 (E_u)		
θ_i	P[a]	σ (%)	γ_2^d	ν_{2T}^d	$S_2^{(x)}$	γ_2^d	ν_{2T}^d	$S_2^{(z)}$	γ_3^d	ν_{3T}^d	$S_3^{(x)}$
42	TE	2.81	8.37	1232	0.152				83.4	1442	0.491
42	TM	3.02	5.30	1231	0.169	4.62	1235	0.0865	65.8	1438	0.494
43	TE[c]	3.70	9.10	1233	0.140				91.9	1442	0.491
43	TM[c]	2.36	6.80	1230	0.176	5.1	1234	0.0867	74.0	1437	0.494
45	TE[b,c]	4.85	12.9	1232	0.152				104.7	1441	0.480
45	TM	3.14	7.30	1231	0.169	4.62	1235	0.0865	83.8	1438	0.494
46	TE[b]	4.29	9.87	1232	0.152				95.4	1442	0.491
46	TM[b]	3.39	6.30	1231	0.169	6.62	1235	0.0865	74.8	1438	0.494

[a] "P" means polarization.

[b] Experimental reflectance multiplied by constant factor before fitting.

[c] All six or nine parameters simultaneously adjusted; otherwise a partially restrained set was used to generate theoretical reflectance where S_k and ν_{kT} were set to 42° values.

[d] Units of cm^{-1}.

V. DIPOLE DERIVATIVES FOR $D_{\infty h}$ ANIONS

To determine $\partial\mu_\sigma/\partial q_k$ (now abbreviated as μ_k^σ), once the dielectric parameters have been decided upon, one needs to either locate in the literature or calculate the dipole wave sums and also to define the electronic polarizability values. These are then used to calculate the effective field $\underset{\sim}{B}$ (see equation (16)). All of the matrices are factored according to the crystal structure. $\underset{\sim}{D}^{\sigma\sigma}_{mm'}$, ($\sigma$=x,y,z) are diagonal in crystals of at least orthorhombic symmetry. In addition, if the crystal axes coincide with the molecular axes of the dipole sites, $\underset{\sim}{\alpha}$ is diagonal, making $\underset{\sim}{B}^{\sigma\sigma}_{mm'}$ also diagonal. This reduces all matrices involved to order NxN where N is the number of entities in the primitive unit cell. For example, for KN_3 and KHF_2, $\underset{\sim}{D}$, $\underset{\sim}{\alpha}$, $\underset{\sim}{B}$ are 4x4 matrices.

The $\underset{\sim}{D}$ matrices and anion polarizabilities for KHF_2 were evaluated by Cooke (2). He used the planewise summation method for determining the dipole wave sums. For KN_3, it was necessary to deduce the polarizabilities and $\underset{\sim}{D}$ sums. Since KN_3 and KHF_2 have identical crystal symmetries, we simply scaled the KHF_2 $\underset{\sim}{D}$ matrices in the ratio of the unit cell volumes: $v_{KHF_2}/v_{KN_3} = 0.836$. A repetitive procedure for finding $\alpha_\perp$ and $\alpha_{||}$ (described previously in the theory section) was used where α_+ and $\varepsilon_\sigma(\infty)$ were taken from the literature. For example, since

Table 6. $\underset{\sim}{D}$ and $\underset{\sim}{\bar{B}}$ elements for KN_3 and KHF_2.

	KN_3	KHF_2
$D_{mm}^{(x)}$	0.03190	0.03818
$D_{12}^{(x)} = D_{34}^{(x)}$	0.01804	0.01804
$D_{13}^{(x)} = D_{14}^{(x)} = D_{23}^{(x)} = D_{24}^{(x)}$	0.03851	0.04609
$D_{mm}^{(z)}$	0.03213	0.03845
$D_{12}^{(z)} = D_{34}^{(z)}$	0.06579	0.07874
$D_{13}^{(z)} = D_{14}^{(z)} = D_{23}^{(z)} = D_{24}^{(z)}$	0.01892	0.02264
$\bar{B}_{11}^{(x)}$	1.09861	1.1349
$\bar{B}_{21}^{(x)}$	0.57303	0.1144
$\bar{B}_{13}^{(x)}$	0.00481	0.0051
$\bar{B}_{23}^{(x)}$	0.05772	0.0248
$\bar{B}_{33}^{(x)}$	1.10040	1.0379
$\bar{B}_{11}^{(z)}$	1.119131	1.2485
$\bar{B}_{21}^{(z)}$	0.16056	0.0659

$\alpha_\perp$ and α_+ are associated with the z active modes (see equation (47)), one can assume a starting value for $\alpha_\perp$ and use equation (16) to calculate $\underset{\sim}{\beta}$. Upon substitution in equation (17) a calculated $\varepsilon_z(\infty)$ can be compared to the experimentally determined $\varepsilon_z(\infty)$. Once $\alpha_\perp$ is assured, $\alpha_{||}$ can be similarly calculated upon the $\varepsilon_x(\infty)$ determination. The $\underset{\sim}{D}$ matrix elements and $\underset{\sim}{\bar{\beta}}$ elements are listed in Table 6; polarizabilities have been given in Table 2.

The $\underset{\sim}{D}$ matrices calculated by Cooke were conveniently found in an $\bar{x}\bar{y}$ Cartesian frame oriented as shown in Figure 4. The analysis of the intensities, on the other hand is more conveniently conducted with reference to an axis system x,y which differs from $\bar{x},\bar{y}$ by a rotation of 45° around the z axis. Since $D_{mm'}$ is diagonal and $D^{(x)}_{mm'} = D^{(y)}_{mm'}$, such a rotation has no effect upon the $\underset{\sim}{D}$ elements, but it must be noted that $\underset{\sim}{\alpha}$, although diagonal, takes the following form in the x,y axis system:

$$\underset{\sim}{\alpha}^{(x)} = \begin{bmatrix} \alpha_+ & 0 & 0 & 0 \\ 0 & \alpha_+ & 0 & 0 \\ 0 & 0 & \alpha_{||} & 0 \\ 0 & 0 & 0 & \alpha_\perp \end{bmatrix}; \quad \underset{\sim}{\alpha}^{(y)} = \begin{bmatrix} \alpha_+ & 0 & 0 & 0 \\ 0 & \alpha_+ & 0 & 0 \\ 0 & 0 & \alpha_\perp & 0 \\ 0 & 0 & 0 & \alpha_{||} \end{bmatrix};$$

$$\underset{\sim}{\alpha}^{(z)} = \begin{bmatrix} \alpha_+ & 0 & 0 & 0 \\ 0 & \alpha_+ & 0 & 0 \\ 0 & 0 & \alpha_\perp & 0 \\ 0 & 0 & 0 & \alpha_\perp \end{bmatrix}. \qquad (47)$$

In addition, it is advantageous to subject the $\underset{\sim}{E}-\alpha\underset{\sim}{D}$ matrix to a further symmetrizing transformation before inverting it to find $\underset{\sim}{B}$. The equivalence of the potassium ions, m = 1,2, and of the anions, m=3,4, implies four linear combinations of dipole vector components which belong to the following symmetry species of D_{4h}:

$$\bar{\mu}_{k',\text{crystal}} = \begin{bmatrix} \bar{\mu}_1 \\ \bar{\mu}_2 \\ \bar{\mu}_3 \\ \bar{\mu}_4 \end{bmatrix} = 2^{-\frac{1}{2}} \begin{bmatrix} \mu_3^z + \mu_4^z \\ \mu_1^z + \mu_2^z \\ \mu_3^z - \mu_4^z \\ \mu_1^z - \mu_2^z \end{bmatrix} \begin{matrix} A_{2u} \\ A_{2u} \\ B_{1u} \\ A_{2g} \end{matrix} . \qquad (48)$$

Therefore, the transformation $\underset{\sim}{U}(\underset{\sim}{E}-\alpha\underset{\sim}{D})\underset{\sim}{U}^{-1}$ will factor the matrix of interest into a 2x2 and two 1x1 blocks, where

$$\underset{\sim}{U} = \frac{1}{\sqrt{2}} \begin{bmatrix} 0 & 0 & 1 & \bar{1} \\ 1 & 1 & 0 & 0 \\ 0 & 0 & 1 & \bar{1} \\ 1 & \bar{1} & 0 & 0 \end{bmatrix} \quad \text{and} \quad \underset{\sim}{U}^{-1} = \frac{1}{\sqrt{2}} \begin{bmatrix} 0 & 1 & 0 & 1 \\ 0 & 1 & 0 & \bar{1} \\ 1 & 0 & 1 & 0 \\ 1 & 0 & \bar{1} & 0 \end{bmatrix}, \qquad (49)$$

since $\underset{\sim}{U}$ is orthogonal. If we designate the matrices in the symmetrized basis by putting bars over them, we have

$$\bar{\underset{\sim}{B}} = [\underset{\sim}{U}(\underset{\sim}{E}-\alpha\underset{\sim}{D})\underset{\sim}{U}^{-1}]^{-1} = \underset{\sim}{U}\underset{\sim}{B}\underset{\sim}{U}^{-1}$$

which factors into the same blocks as does $\bar{\underset{\sim}{B}}^{-1}$. Now the strength as given earlier in equation (23) is seen to

involve the matrix vector product $\underset{\sim}{B}\mu$ and since $\underset{\sim}{B}\mu = \underset{\sim}{U}^{-1}\bar{\underset{\sim}{B}}\bar{\mu}$, equation (23) can be rewritten as

$$S_j^{\sigma}\nu_{jT}^2 = \frac{1}{c^2\pi v}\left[\sum_{m,k,k'} U_{mk}^{-1}\,\bar{B}_{kk'}\,\frac{\partial\bar{\mu}_{k'}}{\partial Q}\right]^2 \quad . \tag{50}$$

From the form of $\underset{\sim}{U}^{-1}$ given above, and from the fact that the only nonvanishing $\partial\bar{\mu}_{k'}/\partial Q$ in the z direction is that for which $k'=1$, we see that

$$S_2^z\nu_{2T}^2 = \frac{1}{c^2\pi v}\left[2^{\frac{1}{2}}(\bar{B}_{11}^z + \bar{B}_{21}^z)\,\mu_2^z\right]^2 \quad , \tag{51}$$

where we have replaced the barred crystal dipole derivative with the unbarred molecular dipole derivative. The crystal normal coordinate (large Q) is taken as

$$Q_2^z = 2^{-\frac{1}{2}}\{q_2^z(3) + q_2^z(4)\}$$

which has the meaning that in the z direction of the crystal, the crystal normal coordinate is a normalized linear combination of the molecular normal coordinate on molecule number (3) plus that on molecule number (4). Also,

$$\frac{\partial\bar{\mu}_1}{\partial Q_2} = \frac{\partial\mu^z}{\partial q_2} \quad .$$

This result is applicable to the A_{2u}, z polarized mode.

For modes whose dipoles have components in the x or y crystal directions, transformation with the same $\underset{\sim}{U}$ matrix yields the following symmetry species:

$$\bar{\mu}_{k',\text{crystal}} = \begin{bmatrix} \bar{\mu}_1 \\ \bar{\mu}_2 \\ \bar{\mu}_3 \\ \bar{\mu}_4 \end{bmatrix} = 2^{-\frac{1}{2}} \begin{bmatrix} \mu_3^x + \mu_4^x & E_u \\ \mu_1^x + \mu_2^x & E_u \\ \mu_3^x - \mu_4^x & E_u \\ \mu_1^x - \mu_2^x & E_g \end{bmatrix} . \qquad (52)$$

Thus in this case, one can only expect factoring into a 3x3 and a 1x1. Since the sums $\sum_{m,k} \underset{\sim}{U}^{-1}_{m,k}$ vanish for $k=3,4$ and since the only nonvanishing x oriented molecular derivatives are μ_3^x for $q_3^x(3)$ and μ_4^x for $q_2^x(4)$, the strength expressions reduce to the following. For the bending mode:

$$S_2^x \nu_{2T}^2 = \frac{1}{c^2 \pi v} \left[(\bar{B}_{11} + \bar{B}_{21} - \bar{B}_{13} - \bar{B}_{23}) \frac{\partial \mu^x(4)}{\partial q_2} \right]^2 \qquad (53)$$

while for the stretching mode:

$$S_3^x \nu_{3T}^2 = \frac{1}{c^2 \pi v} \left[(\bar{B}_{11} + \bar{B}_{21} + \bar{B}_{13} + \bar{B}_{23}) \frac{\partial \mu^x(3)}{\partial q_3} \right]^2 . \qquad (54)$$

We have chosen to work with the $\bar{x}$ block of $\underset{\sim}{\bar{B}}$ and

$$\bar{\mu}_1^x = -\bar{\mu}_3^x = 2^{-\frac{1}{2}} \frac{\partial \mu^x(x)}{\partial q_2^x(4)} \quad \text{or} \quad 2^{-\frac{1}{2}} \frac{\partial \mu^x(3)}{\partial q_3^x(3)} .$$

In the limit of vanishing polarizabilities, $\underset{\sim}{B}$ becomes a diagonal unit matrix, so that comparison of equation (51) with (53) shows that the strength of the A_{2u} bending mode is expected to be twice that of the E_u bending mode. This is easy to visualize on a unit cell basis. Both anions

participate in the A_{2u} bending motion, whereas there is only one active anion under a specific polarization (x or y) for the E_u mode.

Molecular dipole derivatives have been calculated for the $D_{\infty h}$ anions using equations (51), (53), and (54). These dipole derivatives are with respect to the normal coordinate but in our later analysis of effective charges and charge fluxes, it is more convenient to consider these derivatives with respect to dimensionless symmetry coordinates. To convert from $\partial\mu/\partial q_k$ to $\partial\mu/\partial S_k$, we will need to know the $\underset{\sim}{L}^{-1}$ matrix. In the harmonic approximation, the $\underset{\sim}{L}^{-1}$ is very simple for linear triatomic molecules because it is determined solely by the $\underset{\sim}{G}$ matrix, no force constant treatment is required. One can then write the dipole derivatives with respect to symmetry coordinates in elementary units of charge (e) as

$$\partial\mu/\partial S_k = (G_{kk})^{-\frac{1}{2}}\partial\mu/\partial q_k \qquad (55)$$

where

$$G_{22} = 2\mu_B + 4\mu_A$$

$$G_{33} = \mu_B + 2\mu_A \ .$$

The μ's are reciprocal masses of the respective atoms in AB_2. The dipole derivatives for these anions in the potassium crystals and the previously studied sodium forms are

listed in Table 7. We have used the conversion $1d/\mathring{A} = 0.2082\ e$ with $\partial\mu/\partial q$ in units of $esu \cdot g^{-\frac{1}{2}}$.

A molecular dipole derivative for a particular molecular anion should be constant throughout all the crystallographic forms that the anion can exist in. The $\underset{\sim}{B}$ matrix hopefully guarantees this! However, the multitude of interactions that occur between anions and cations in a crystalline environment may be more than just dipolar couplings. The influence of lone pair-lone pair, lone pair-dipole, dipole-multipole interactions between different anions or of intra and inter molecular hydrogen bonding on the dipole derivatives is not quantitatively known at this time. Although these effects certainly express themselves in the measured value of the high frequency dielectric and therefore influence the selection of $\underset{\sim}{\alpha}_{anion}$, thus penetrating into the evaluation of $\underset{\sim}{B}$, they are not directly included in the theory for the effective field. Also, the $\underset{\sim}{D}$ sums, and hence $\underset{\sim}{B}$, are evaluated in the point dipole approximation which is probably not a good assumption for these non spherical anions. A test of how well $\underset{\sim}{B}$ does describe the anion's solid state surroundings so as to allow us to extract a molecular property from a crystal response, is afforded by comparing mutual $\partial\mu^{\sigma}/\partial q_k$ values (abbreviated μ_k^{σ}) between the potassium salts studied herein and the sodium salts studied previously (2, 3, 24).

Table 7. $\pm\partial\mu/\partial q$, $\partial\mu/\partial S$ for KN_3, NaN_3, KHF_2, $NaHF_2$.

	k	$\pm\partial\mu/\partial q_k$ (esu·g$^{-\frac{1}{2}}$)	$\pm\partial\mu/\partial S_k$ (e)
KN_3	2 (E_u)	30.8	0.126
	3 (E_u)	320	1.86
NaN_3	2 (E_u)	30.1[c]	0.123
	3 (A_{2u})	423[a]	2.45
KHF_2	2 (A_{2u})	111.5	0.148
	2 (E_u)	225	0.299
	3 (E_u)	439	0.825
$NaHF_2$	2 (E_u)	112[b]	0.149
	3 (A_{2u})	--	--

[a]See reference (3).

[b]See reference (2).

[c]Calculated with data from reference (3) with acknowledgement of error in previously published S_{ala1} value (reference (17)): -0.144433 should be -.114433.

For the $D_{\infty h}$ anions, the magnitude of μ_2 in azide ion seems to be well accounted for by a dipolar coupling scheme. Refering to Table 7, one can see that the current determination of μ_2^x and μ_2^y for KN_3 agrees very well with that value reported earlier for $\mu_2 NaN_3$: 30.8 compared to 30.1 esu $g^{-\frac{1}{2}}$, respectively. Bifluoride ion, on the other hand, does not behave so predictably in the crystalline state.

Consulting Table 7 once again, one can see that μ_2^x and μ_2^y for KHF_2 do not agree with μ_2^z KHF_2 or μ_2 $NaHF_2$, which both seem to demand a smaller value for the (same) molecular dipole derivative. One explanation for this apparent discrepancy is the possibility of intermolecular hydrogen bonding mediating a mixing of infrared intensities for the two E_u modes. Looking back to Figure 4, one will agree that when anion 3 executes a stretching motion and anion 4 a bending motion, a hydrogen bond could be produced between the two anions. Since the frequency difference $\nu_{3T}-\nu_{2T}$ is only on the order of 200 cm^{-1}, and ν_3 is a mode of large strength ($S_3 = 0.42$), the weaker bending mode, say $S_2 = 0.09$, can gain some strength to become $S_2 = 0.16$ at ν_3's expense. Hence we find μ_2^z to be smaller than μ_2^x and can use it to describe the unmixed μ_2^0 for HF_2^-. One way to support this hypothesis is to determine the empirical coupling constant

for the two modes and see how well it compares to one calculated from dipolar coupling theory.

The vibrational secular determinant can be written as

$$\begin{bmatrix} \lambda_2^0 - \lambda & K \\ K & \lambda_3^0 - \lambda \end{bmatrix} = 0 \qquad (56)$$

where λ is $4\pi^2 c^2 \tilde{\nu}^2$ and

$$K = -\tfrac{1}{2}[(DB)_{34} + (DB)_{43}]\ \mu_2^0 \mu_3^0 \ . \qquad (57)$$

The μ_k^0 values are the unperturbed dipole derivatives and we have used: $\mu_2^0 = 112$, $\mu_2 = 225$, $\mu_3^0 = 481$ and $\mu_3 = 440$ esu $g^{-\frac{1}{2}}$. The coefficients of the orthogonal transformation are found to be

$$\begin{aligned} \mu_2 &= 0.9704\ \mu_2^0 + 0.2415\ \mu_3^0 \\ \mu_3 &= -0.2415\ \mu_2^0 + 0.9704\ \mu_3^0 \ . \end{aligned} \qquad (58)$$

These mixing coefficients, however, further imply via the secular equations that a semi-empirical value for the coupling constant is

$$K = -1.389 \times 10^5\ cm^{-2}$$

whereas the direct use of equation (57) yields the value $K = -0.415 \times 10^5\ cm^{-2}$. Even though the dipolar model is not quantitatively correct, some intermolecular coupling

mechanism, which could be designated loosely as "hydrogen bonding" significantly perturbs the μ_2^0 value in the E_u species and the correct unperturbed values are closer to 110 for μ_2^0 and $480 > \mu_3^0 > 440$ esu·g$^{-\frac{1}{2}}$.

So far in our analysis we have assumed that all modes are harmonic modes and have calculated μ_k accordingly (see equation (23)). For a mode that is suspected to be anharmonic, it would be nice to be able to use the complete relationship as expressed in equation (21), to calculate μ_k. ν_3 in HF_2^- is a mode which has been suggested to be highly anharmonic with diverging rather than converging energy levels. This belief seems to stem from the observation of a mode in the spectrum at 5099 cm^{-1} (25, 26). If this is interpreted as $3\nu_3$, it is nearly 800 cm^{-1} higher than three times the fundamental (1440 cm^{-1}). But as has been alluded to earlier (Chapter 2, page 11), the intensity profile of an overtone in the solid state is usually a map of the joint density of states. Since little is known about the $\vec{k}$ dependence of ν_3, it may be premature to reach conclusions about the anharmonicity. Also, one might think that the great breadth of the KHF_2 reflection in the ν_3 region is due to a progression of transitions like $v = 0 \rightarrow 1$, $1 \rightarrow 2$, $2 \rightarrow 3$, etc. However, studies of HF_2^- isolated in alkali halide matrices (27, 38) do not show any unusual breadth, nor are separate peaks identifiable. The frequencies do exhibit quite a large sensitivity to

the host matrix, and have been reported as 1599 (NaBr), 1570 (KCl), 1527 (KBr), and 1478 (KI), all in cm^{-1}. Both the fact that these numbers are significantly higher than the transverse mode frequency in KHF_2 (1440 cm^{-1}) and the variation with host are in qualitative accord with a harmonic oscillator model involving a very large value of μ_3. Further, the excited states even for the harmonic oscillator would have Boltzmann factors much too small to contribute to the observed spectrum at room temperature; in the quartic case the levels are even higher. From these observations, it is unlikely that we are dealing with some transition other than $v = 0 \rightarrow 1$.

Since Chan, Stelman, and Thompson (29) have given the transition moments for any mixture of the two oscillator models, we can consider what the magnitude of difference is between the harmonic versus quartic description of ν_3 in KHF_2. The strength equation (21) was given as

$$S^{\sigma}_{jk\ \omega^2_{kT}} = \frac{4\pi}{v} \frac{2\omega_{kT}}{\hbar} \left| B\ \mu_k \langle 0|Q|1\rangle \right|^2 . \qquad (21)$$

In reference (29) the transition integral is reported in terms of a dimensionless coordinate X, and the above equation becomes (in cm^{-1})

$$S\nu^2_{kT} = \frac{1}{c^2 \pi v} \left| B\ \mu_k \right|^2 \left(\frac{R}{4}\right) |\langle 0|X|1\rangle|^2 . \qquad (59)$$

The last two terms of this expression are given as a function of a parameter α, by Chan, et al., such that when $\alpha = 0$, these two terms are unity (harmonic approximation), and when $\alpha = 1$, these terms amount to 1.33 (quartic approximation). For the complete range then, $0 \leq \alpha \leq 1$, the correction to μ_k varies by at most 15%. But as we have expressed in the previous paragraph, we believe the experimental evidence really suggests that HF_2^- behaves as a quadratic not a quartic oscillator. Therefore, we adopt a value of 440 esu $g^{-\frac{1}{2}}$ for μ_3 in KHF_2, keeping in mind that the quartic anharmonicity could decrease the μ_3 value by the factor $(1.33)^{-\frac{1}{2}} = 0.87$ in the extreme though unlikely limit of a pure quartic oscillator.

Unfortunately we were not successful in our attempts to grow a single crystal of $NaHF_2$ and so we have no data with which to compare our KHF_2 results. However, we are lucky to have two independent determinations for μ_3 in NaN_3 as comparisons for our KN_3 value.

One study of μ_3 NaN_3 was done using only TM3 polarization for an $\underline{X}\,\underline{Y}$ face (3), while the second was accomplished through TE polarization on the $\underline{Z}\,\underline{Y}$ face (24). As we have discussed previously (see Chapter 3, page 43), some restraint may be warranted in admitting that a TM3 experiment alone could define μ_3 since this arrangement is particularly sensitive to any error in measuring θ_i. In this case, however, the TE

determination of μ_3 in NaN_3 supports the TM3 measurement. Thus, we find a μ_3 value for KN_3 ~25% smaller than that found for the same mode in NaN_3.

An explanation for this difference is offered by closer examination of the ν_3 reflectivity in the NaN_3 crystal.[1/] The ν_3 band in the sodium case was observed to have structure on its high frequency side. This structure then presents a dilemma as to whether or not it should be included as part of the ν_3 strength when the band is fitted. Fredrickson and Decius (3) decided to include the structure and thus $S_3(NaN_3)$ may have been overestimated, hence leading to a larger $\partial\mu/\partial q_3$ value than would otherwise be obtained.

On the other hand, in view of the assumptions made in the theory, namely those of harmonic oscillator and point dipole, a 25% difference between the two values for $\partial\mu/\partial q_3$ in N_3^- may not be unreasonable. In any event, we have chosen at this time, not to attempt refinement of Fredrickson and Decius' value for ν_3 NaN_3 nor to pursue any corrections to the theory that might otherwise help explain this discrepancy but simply accept that for N_3^- $320 \leq \mu_3 \leq 420$ esu $g^{-\frac{1}{2}}$.

[1/] See Figure 5, in reference (3).

VI. BAND ANALYSIS FOR D_{3h} MOLECULAR ANIONS

Calcite ($CaCO_3$) and sodium nitrate share a similar crystal structure, $D_{3d}^6 - R\bar{3}c$ with D_{3h} anions occupying D_3 sites (1). The correlation of vibrational modes of the free ion to those of the ion in the crystal is given in Table 8, and the modes are diagrammed in Figure 11. ν_2 is an out of plane bend, ν_3 is essentially an in-plane stretch, and ν_4 can be described as an in-plane bend. ν_1, the symmetric stretch, is not infrared active. Since both ν_3 and ν_4 are E_u modes, intermode mixing of symmetry coordinates occurs.

An experimental schematic in Figure 12 identifies the crystal axes and incidence planes and can be used to illustrate which modes are active under a particular polarization. In part (a) of Figure 12, one sees that for a YZ crystal face, modes 3 and 4 alone appear for TE polarization. The incidence plane is XZ and the $\vec{E}$ vector is parallel to the Y axis. If instead TM polarization is used, the $\vec{E}$ vector will have components in the X and Z directions, so that all three infrared active fundamentals are observable. If the incidence plane is changed to XY as in part (b) of Figure 12, ν_2 appears under TE polarization, ν_3 and ν_4 under TM polarization.

Since the three fundamental (internal) modes are quite widely separated from one another and from the lattice

Table 8. Correlation table D_{3h} to D_{3d}.

Molecular Symmetry D_{3h}	Site Symmetry D_3 (AB_3^{n-})	Factor Group D_{3d}	Mode[a]
A_1' (ν_1)	A_1	A_{1g}	ν_1
A_2' (R_z^-)	A_2	A_{2g}	ν_2, T_z^-, R_z^-
$E'(\nu_3, \nu_4, T_{x,y}^-)$	E	E_g	$\nu_3, \nu_4, T_{x,y}^-, R_{xy}^-$
		A_{1u}	ν_1, T_z^+
$A_2''(\nu_2, T_z)$	$S_6(M^{n+})$	A_{2u}	$\nu_2, T_z^-, R_z^-, T_z^+$
E'' $(R_{x,y}^-)$		E_u	$\nu_3, \nu_4, T_{x,y}^-, R_{x,y}^-, 2T_{x,y}^+$
	$A_u(T_z^+)$		
	$E_u(T_{x,y}^+)$		

$$\Gamma_{ir} = 3A_{2u} + 5E_u$$

[a] Optical plus acoustic modes.

Figure 11. Vibrational modes for D_{3h} anions.

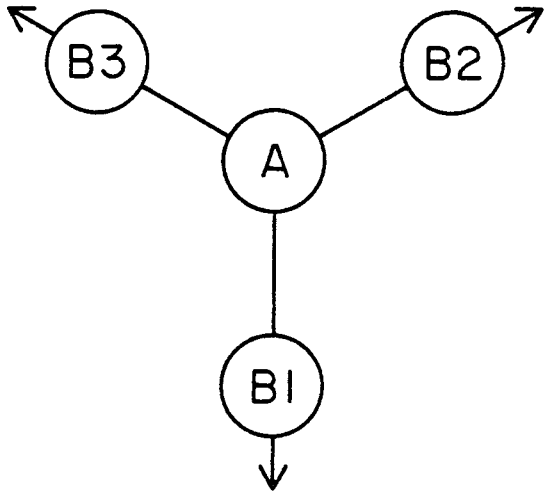

$\nu_1(A_1')$

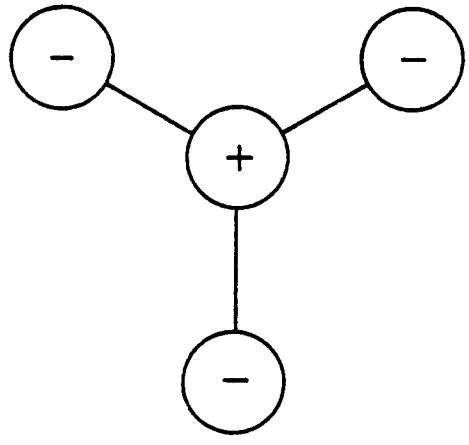

$\nu_2(A_2'')$

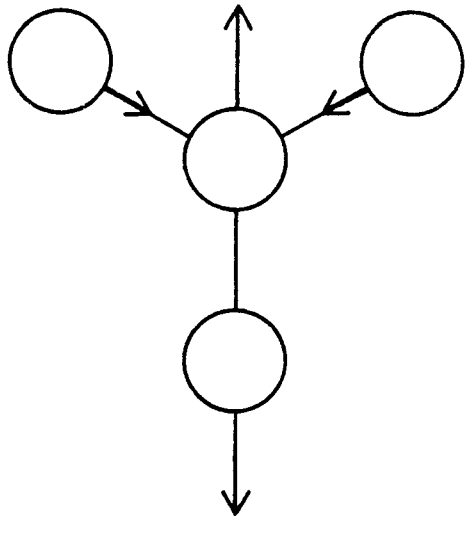

$\nu_3^y(E')$

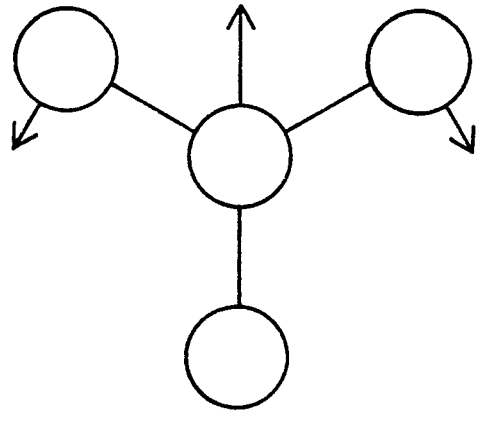

$\nu_4^y(E')$

Figure 12. Experimental perspectives for a D_{3d}^{6} crystal cut along the major axes. A) XZ incidence plane; B) XY incidence plane.

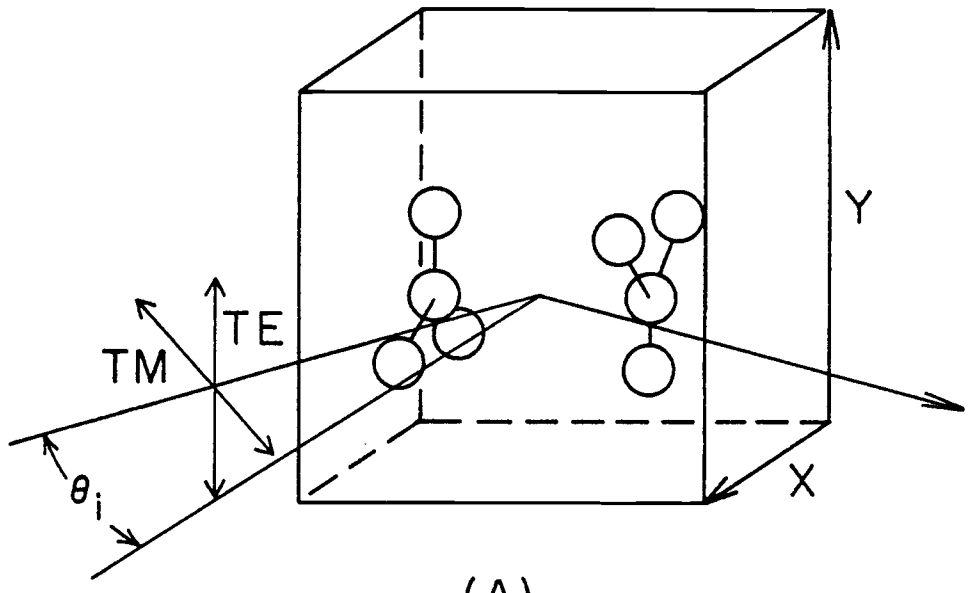

(A)

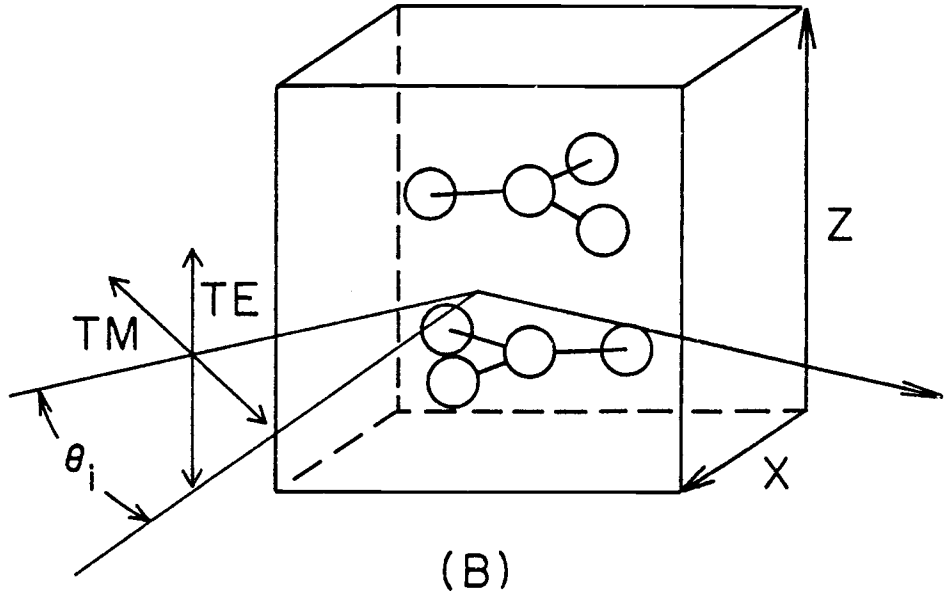

(B)

modes, the separated mode approximation[2/] should be valid. Thus, ε_B^σ (equation (26)) can be used to represent the background dielectric constant, one value for each mode, and it can be used in the fitting procedure. Implementing this approximation does require that one know at least rough values for the strength and transverse frequency of each mode (including the lattice modes) or that one use a process of iteration starting with $\varepsilon_B^\sigma = \varepsilon^\sigma(\infty)$. In either case, good convergence is to be expected. Table 9 shows the values of the background dielectric constants employed in this work, based upon the dielectric constants at optical frequencies and earlier estimates of the strengths and frequencies of the lattice modes (7).

With the background dielectric constant thus fixed, we were then able to adjust the three characteristic parameters for each band so as to minimize the deviation between experiment and theory. With unrestrained variation of these three parameters typical rms errors in the reflectivity were 2-4%. Such errors could in some cases be further reduced by adjustments of the incidence angle θ_i by a few degrees. Moreover, somewhat different angle adjustments were found to optimize the fit in experiments on the same band in different polarizations. Also, the unconstrained variation of the three parameters yielded slightly different parameters

---

[2/] Refer to page 22.

Table 9. Background dielectric constants (ε_B) at $\nu \sim \nu_2$, ν_3, ν_4.

	$CaCO_3$		$NaNO_3$	
	σ = X,Y	σ = Z	σ = X,Y	σ = Z
$\infty(\varepsilon_\infty)$	2.749	2.208	2.519	1.785
ν_3	2.626	2.062	2.464	1.744
ν_2	3.367	1.959	2.987	1.711
ν_4	3.032	2.091	2.912	1.773

for the same band in different polarizations. For example, TM3 seemingly required a ν_{jT} value a few wavenumbers lower than TE in some cases. Since none of these discrepancies affected the strength $S_j^{(\sigma)}$ by more than 2% (and hence $\partial\mu/\partial q$ by as much as 1%), we report average values in Table 10.

In Figure 13 (a-c) we illustrate for the ν_3 mode of $NaNO_3$ the experimental and theoretical reflectance using a partially constrained parameter set with $S_3 = 0.425$, $\nu_{3T} = 1354$ cm^{-1}, γ_3 taking values from 5.0 to 8.4 cm^{-1}. This set of figures further serves to illustrate the limiting mode frequencies ν_T, ν_L and ν_{LL}. For $NaNO_3$, the observations were made on the YZ face, so that with an XZ incidence plane TE and TM3 polarization were possible for this mode (see also Figures 12(a)), while for an XY incidence plane, TM23 was observed (Figure 12(b)). The agreement between theory and experiment is impressive so far as the general shape of the bands is concerned. The theory accounts for the striking differences in the shapes of TE, TM23, and TM3. The one notable discrepancy is the narrow dip in the reflectance at about 1448 cm^{-1}; this has been attributed (14) to a sharp maximum in the damping constant at the frequency $2\nu_4$. This dip appears in both the TE and TM23 spectra, but not in TM3 where the high intensity region lies above $\nu_L = 1466$ cm^{-1}. Aside from this well understood discrepancy, the

Table 10. Dielectric parameters for ν_2, ν_3, ν_4 in $NaNO_3$ and calcite.

Mode	Face	Polarzn	θ_i, deg	ν_T, cm^{-1}	ν_L, cm^{-1}	S[a]	γ	σ,%
$NaNO_3$								
ν_2	YZ	TE	45-49	834.1	839.1	0.0209 ± 0.0003	1.4	1.0
	YZ	TM2	41-46	834.0	839.2	0.0213 ± 0.0001	1.5	0.6
	average			834.1	839.2	0.0211 ± 0.0003		
ν_3	YZ	TE	46.5	1354.0	1465.6	0.423 ± 0.003	6.0	2.8
	YZ	TM23	46-49	1354.0	1465.5	0.423 ± 0.003	4.9	2.4
	YZ	TM3	41-46	1354.0	1465.4	0.422 ± 0.001	5.2	3.6
	average			1354.0	1465.5	0.423 ± 0.002		
ν_4	YZ	TE	∿45	725		(0.8-4) x 10^{-4}	<2.8	(see text)
$CaCO_3$								
ν_2	YZ	TE	44-46	869.7	887.2	0.0796 ± 0.0020	1.5	2.2
	YZ	TM2	43-50	869.8	887.6	0.0811 ± 0.0014	2.0	2.2
	XY	TM3	50	869.8	887.2	0.0792	1.6	1.3
	average			869.8	887.4	0.0803 ± 0.0017		
ν_3	XY	TE	46-48	1409	1552	0.56	13	4.3
	XY	TM2	46-48	1407	1551	0.565	11	4.0
	average			1408	1551.5	0.56 ± 0.004		
ν_4	XY	TE	46-48	712.05	713.1	0.00875	1.9	2.7
	XY	TM2	46-48	711.7	713.3	0.01400	2.5	0.7
	average			711.9	713.2	0.0114 ± 0.0030		

[a] ± average range of parameter.

Figure 13. Reflectance of ν_3 mode from a YZ face of $NaNO_3$ at $\theta_i = 46.5°$: A) incidence plane XZ, $\vec{E}$ // Y (TE); reflectance limits ν_T and ν_{LL}; B) incidence plane XY, $\vec{E}$ in incidence plane (TM23); reflectance limits ν_T and ν_{LL}; C) incidence plane XZ, $\vec{E}$ in incidence plane (TM3); reflectance limits ν_L and ν_{LL}. ··· = observed; ———— = calculated.

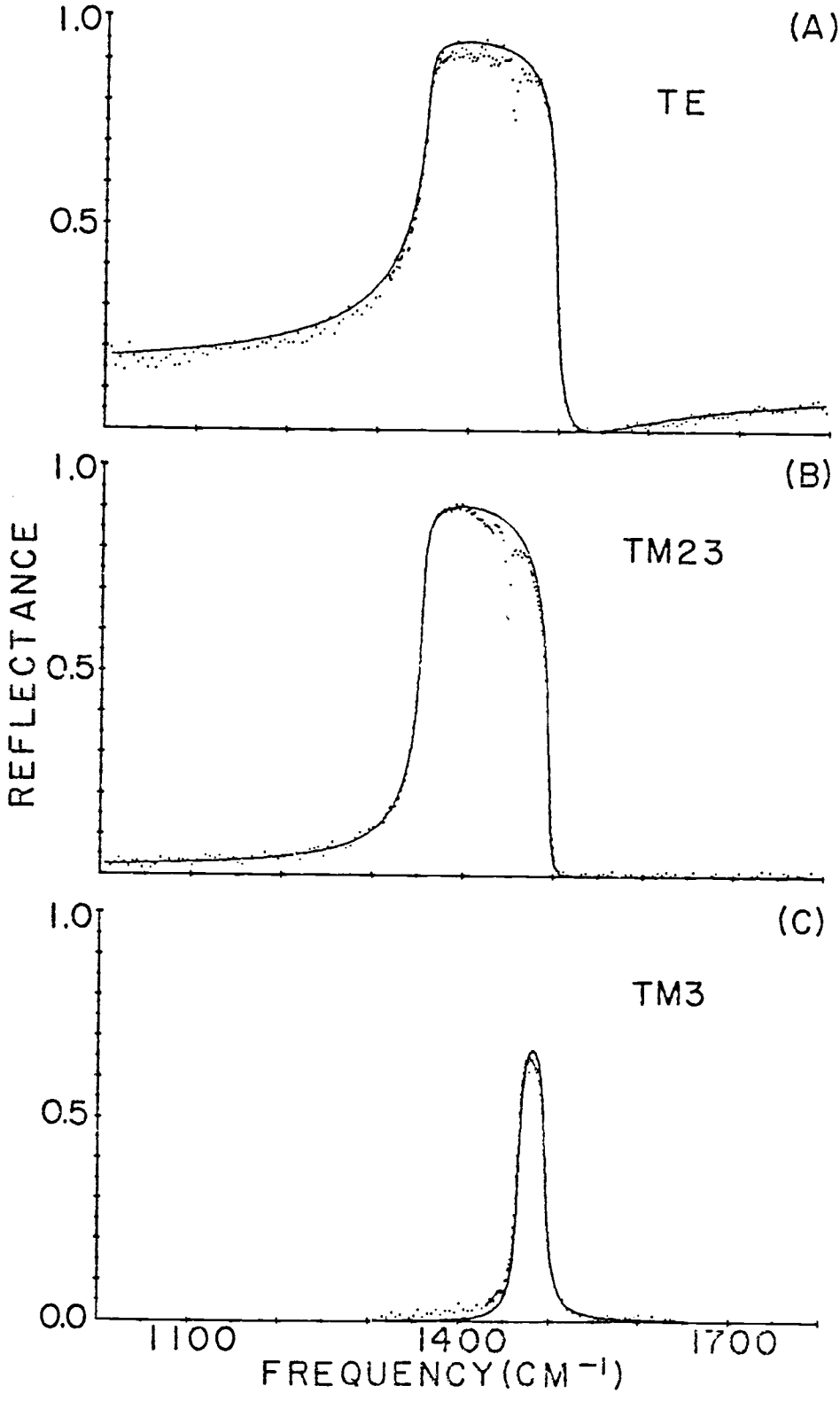
1.0
0.5
(A)
TE
1.0
0.5
(B)
TM23
REFLECTANCE
1.0
0.5
0.0
(C)
TM3
1100
1400
1700
FREQUENCY(CM⁻¹)

approximation of a frequency independent damping constant is remarkably successful. It may also be noted in Figure 13(c) that the experimental points on the low frequency side of the band lie considerably above the theoretical curve. This we attribute to alignment imperfection or polarization leakage, since this is a region in which a 90° rotation of the polarizer yields very high reflectivity.

The polarized ν_2 mode for $NaNO_3$ is shown in Figure 14(a,b) along with the theoretically generated curves. For the XY incidence plane, a TE spectrum is produced and for the XZ incidence plane, a TM2 spectrum is observed. The agreement between parameters used here is very good: $S_2 = 0.0212,\ 0.0213$; $\nu_{2T} = 834.1,\ 834.0\ cm^{-1}$; $\gamma_2 = 1.38,\ 1.43\ cm^{-1}$. All in all, a well behaved mode! The ν_2 mode in calcite serves here to illustrate the relationship between TE, TM2, and TM3 reflection spectra (Figure 15(a-c)). In addition to the two incidence planes used in the nitrate study, we were also able to observe a TM3 polarized calcite ν_2 from the XY face. Again, the theory is impressively successful in accounting for the characteristically different shapes and frequency limits of these differently polarized experiments. In contrast to Figure 13(c), Figure 15(c) also in TM3 polarization does not show an experimental reflectance significantly larger than the theoretical value on the low frequency side of the band. This is to be expected since neither polarization leakage

Figure 14. Reflectance in ν_2 region from a YZ face of $NaNO_3$ at $\theta_i = 46.5°$: A) incidence plane XY, $\vec{E}$ // Z (TE); rms error = 0.75% for 150 points; B) incidence plane XZ, $\vec{E}$ in incidence plane (TM2); rms error = 1.03% for 195 points. ··· = observed; ——— = calculated.

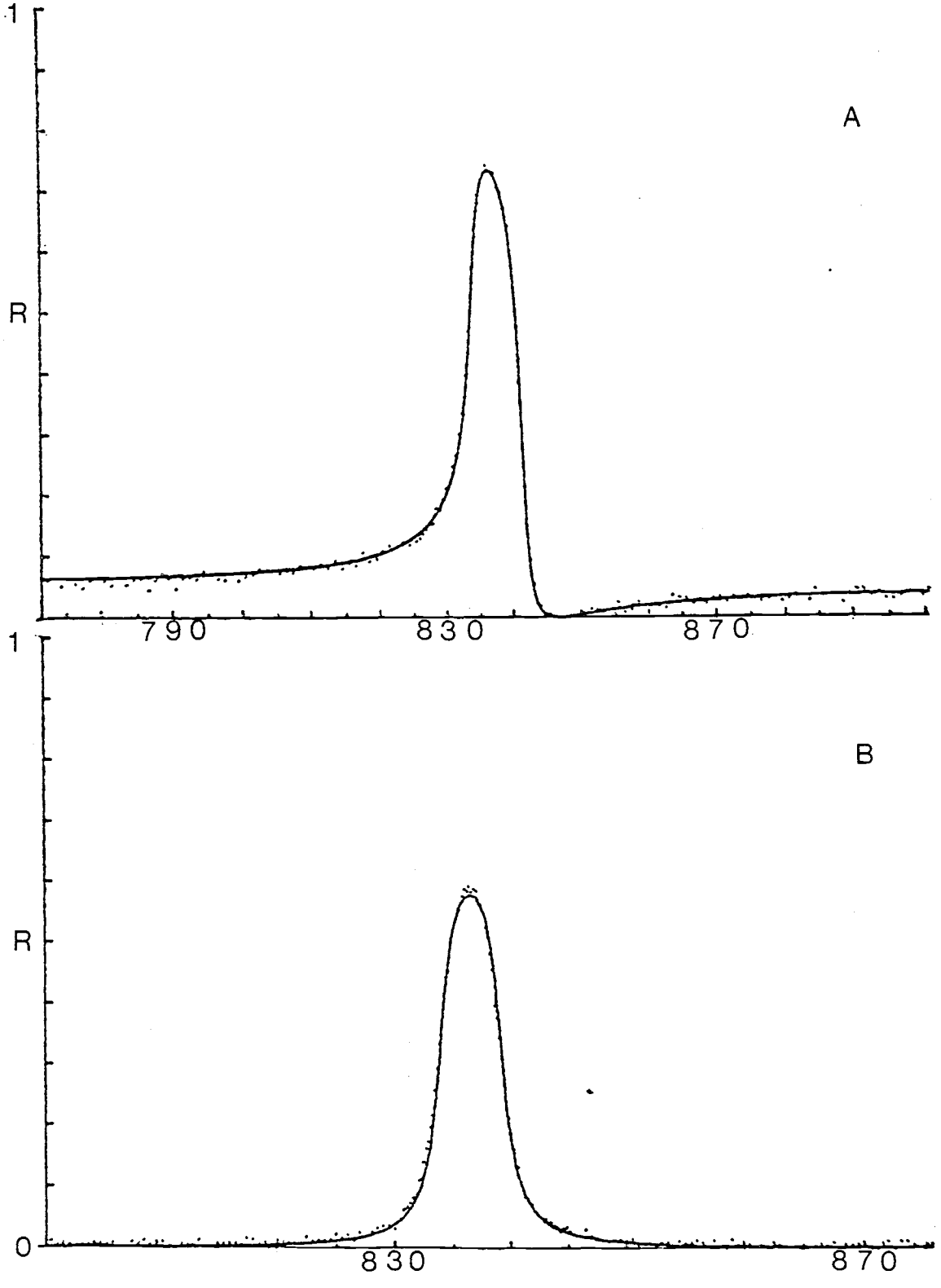
1
R
A
790
830
870
1
B
R
0
830
870
WAVENUMBERS, CM^{-1}

Figure 15. Reflectance of the ν_2 mode of $CaCO_3$ at $\theta_i \simeq 45°$: A) crystal face YZ, incidence plane XY, $\vec{E}$ // Z (TE); reflectance limits ν_T and ν_{LL}; B) crystal face YZ, incidence plane XZ, $\vec{E}$ in incidence plane (TM2); reflectance limits ν_T and ν_L; C) crystal face XY, incidence plane YZ, electric vector in incidence plane (TM3); reflectance limits ν_L and ν_{LL}.
··· = observed; ——— = calculated.

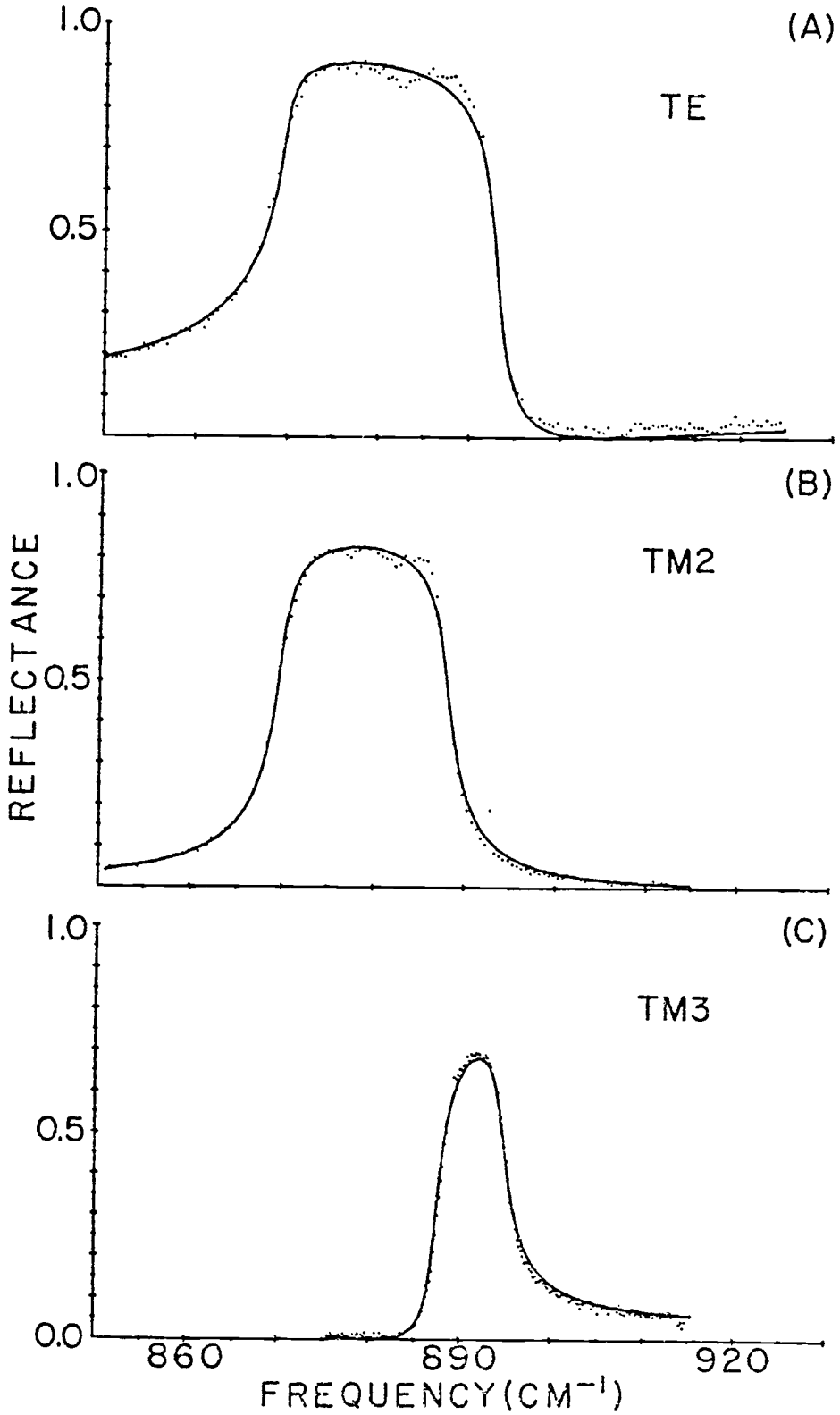
1.0
0.5
(A)
TE
1.0
0.5
(B)
TM2
REFLECTANCE
1.0
0.5
0.0
(C)
TM3
860
890
920
FREQUENCY(CM⁻¹)

Figure 16. Reflectance of the ν_3 mode of $CaCO_3$ at $\theta_i \sim 46°$ from XY crystal face, YZ incidence plane: A) TE polarization, rms error = 4.2%; B) TM2 polarization, rms error = 3.7%. ··· = observed; ——— = calculated.

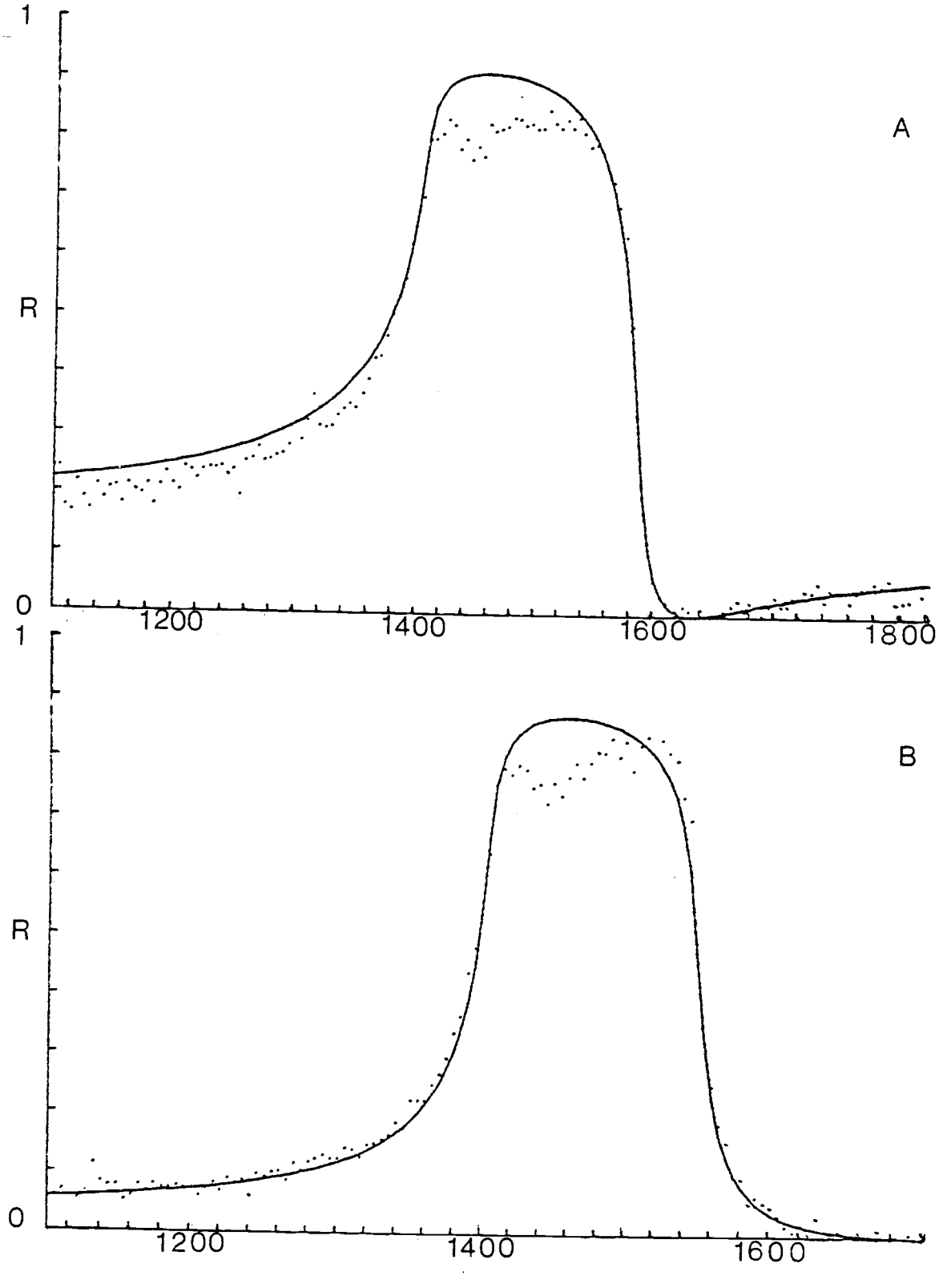
1
R
0
1200
1400
1600
1800
A
1
R
0
1200
1400
1600
B
WAVENUMBERS, CM^{-1}

nor misalignment can contribute to the reflectance in this configuration.

An additional comment on the ν_2 calcite spectra is called for. There is an apparent dip at about 882.5 cm^{-1} in the TE and TM2 polarized spectra. This dip is most probably due to the same phenomenon as has been ascribed to the dip at 1448 cm^{-1} in ν_3 of $NaNO_3$. That is, there is an increase in the density of modes for some overtone, combination, or difference vibration. In this case at least one member of the combination would seem to be a lattice mode and, therefore, the mode would be expected to be widely dispersed ($\vec{k}$ dependent).

ν_3-$CaCO_3$ was observed from the XY face in both TE and TM2 polarization as exemplified by Figure 16(a,b). The degree of overall fit here is a bit less desirable than previously found, and in general the TE polarized mode required a ν_{3T} a few wavenumbers larger than that for TM2 polarization. Noticing that there is a rather large difference between theory and experiment over the "forbidden" gap in frequencies ($\nu_T - \nu_L$), one might first suspect the polish on the crystal to be less than adequate. A frequency dependence in γ may be at work here, although two few data points were taken to substantiate a dip at say $2\nu_4$ ($\sim$1426 cm^{-1}) in either polarization. Again, we stress the fact that γ does not affect our calculation of $\partial\mu/\partial q$, the strength does and one can see that the

strength and transverse frequencies obtained for the two polarizations agree very well.

For calcite we were able to observe the ν_4 (E_u) in plane bending mode from the XY face. A typical fit for this mode of weak intensity is illustrated in Figure 17(a, b), in which 180 data points were taken over the 90 cm^{-1} region. Each spectrum shown here is an average of four successively recorded runs. It was hoped that this procedure would help increase the signal/noise ratio, which was on the order of 2.5 for any one run under TE polarization and 3.0 for TM polarization. However, the calculated reflectivity in the wings for a TE curve remained high compared to experiment. Resolution employed was around 0.8 cm^{-1} and this band is around 3 cm^{-1} wide at half height. Convolution of the calculated spectrum was tried with the result that it mainly influenced the selection of the damping constant, leaving the strength and transverse frequency unchanged. Convolution was therefore not considered crucial to fitting this band and the examples shown here are without convolution.

It may be significant that a similar deviation to that between experiment and theory for ν_4-TE was noted for the low frequency side of the ν_3-TE band in $CaCO_3$. This difference also accompanied a lowered signal/noise ratio. The frequency regions affected had one thing in common: both occurred at the beginning of a grating range in the

Figure 17. Reflectance of the ν_4 mode of $CaCO_3$ at θ_i = 47.5° from XY crystal face, YZ incidence plane: A) TE; B) TM2; each plot is an average of four consecutive scans. ··· = observed; ——— = calculated.

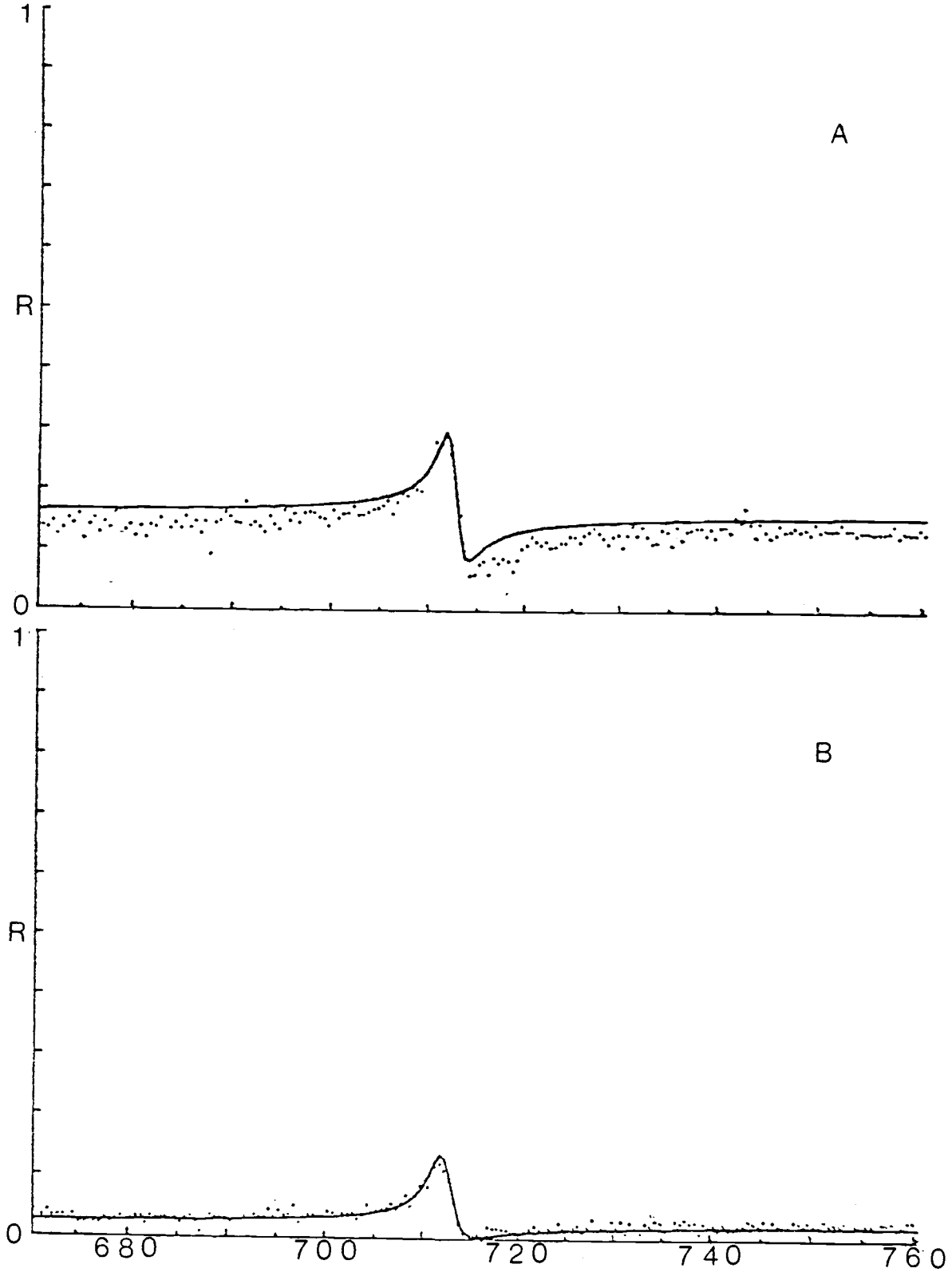
1
R
0
A
1
R
0
B
680
700
720
740
760
WAVENUMBERS, CM^{-1}

spectrometer. At the beginning and end of a grating, resolution drops off. This might explain why TE polarization ($\vec{E}$ vector perpendicular to the grooves on the grating) is more affected here than TM polarization ($\vec{E}$ vector parallel to the grooves). TE is simply more distorted than TM in the wings of a grating. Since in both ν_2 and ν_3, TM2 polarization yields a reasonably good fit by theory, one is led to believe there is some experimental problem in the TE observations. To characterize the dipole derivative for each of these modes, we have simply averaged the parameters and acknowledge there is some error in γ_j.

The ν_4 band of $NaNO_3$ requires special discussion. It appears as a slight fluctuation in the reflectivity around a background value of approximately 0.13. In order to achieve a S/N ratio on the order of 400, a slit width of approximately 1.5-2 cm^{-1} was required; under these conditions, in the direction of increasing frequency the reflectivity rose to a maximum at 723.6 ± 0.3 cm^{-1} and then fell to a minimum at 726.5 ± 0.4 cm^{-1}. The total excursion in reflectivity between maximum and minimum was about 0.7%.

For weak bands such as this one, the TE reflectance as calculated using equations (19) and (26) shows that the frequency separation of maximum and minimum is approximately equal to γ, and that the transverse frequency occurs approximately at the inflection point. Our observations

would thus seem to imply a γ value of 2.9 cm^{-1} and a transverse frequency of 725 cm^{-1}. Since this analysis neglects convolution, we made a theoretical reflectance calculation using $\gamma = 2.0$ cm^{-1} and found that a strength value of the order of 4×10^{-4} would reproduce the observed excursion in the reflectance.

It should here also be mentioned that the reflectivity scans in this region invariably exhibited a weak minimum at 720.3 cm^{-1} superimposed upon the reflection curve. We suspected that this was due to a well known carbon dioxide band appearing as an absorption in the double beam mode owing to the extended optical path required by our reflection optics. This suspicion was confirmed (a) by making a single beam scan of the reference path, and (b) by recording the reflection of a KBr crystal in this region for the double beam mode. Incidentally, in contrast to the other bands for which metal mirror ($R \sim 1.0$) was used as a reflection standard, we estimated the reflection scales for ν_4 $NaNO_3$ using KBr as a standard at $\theta_i = 45°$; the reflectance of KBr at 725 cm^{-1} is 0.096.

It is also possible to estimate the dielectric parameters of the ν_4 mode in $NaNO_3$ by reference to the transmission spectrum given by Matossi and Hohler (5) for a crystal of 0.014 cm thickness. If one simply equates their observed transmission[3/] with

[3/] See equation (5-5-1), reference (15) for transmission through a slab.

$$T = e^{-\alpha \ell} \qquad (60)$$

i.e. neglects reflection and interference effects, it is possible to deduce values of $\gamma = 2.8\ cm^{-1}$ and $S = 0.8 \times 10^{-4}$, by noting the values of α, the absorption coefficient, at the maximum and the width of the absorption, say, at one-tenth the maximum absorbance. Again, the effect of finite resolution has simply been neglected. We are thus left with a rather wide uncertainty in the strength of this very weak band, but have not thought it necessary at this point to undertake a superior measurement.

VII. DIPOLE DERIVATIVES FOR D_{3h} ANIONS

As in the D_{4h} equations, $\underset{\sim}{D}$, $\underset{\sim}{B}$, and $\underset{\sim}{\alpha}$ for the D_{3d} crystals are reduced to 4 x 4 matrices; there are two cations and two anions in the dynamical primitive unit cell. The evaluation of the $\underset{\sim}{D}$ sums[4/] for $NaNO_3$ and $CaCO_3$ was reported by Frech and Decius (20). The polarizabilities are also given in this reference. It is then a straightforward procedure to find $\underset{\sim}{B}$ and $\partial\mu/\partial q_k$. $\underset{\sim}{B}^{\sigma}$ the effective field is of course expressed as: $\underset{\sim}{B} = [\underset{\sim}{E} - \underset{\sim}{\alpha}\,\underset{\sim}{D}]^{-1}$. $\underset{\sim}{D}$ is characterized by three types of interactions: those between similar ionic species, those between different ionic species, and those between ions of the same kind but of different orientation. $\underset{\sim}{B}^{z}$ involves only the cation polarizability (α_+) and the polarizability of the anion along the main symmetry axis of the anion ($\alpha_{\parallel}$). $B^{x,y}$ relates to α_+ and $\alpha_{\perp}$. As in the D_{4h} system, we can again employ symmetry factoring of $\underset{\sim}{B}$ to produce $\underset{\sim}{\bar{B}}$, a matrix which is more easily inverted. $\underset{\sim}{\bar{B}}^{x,y}$ is then composed of a 1 x 1 and a 3 x 3 matrix; $\underset{\sim}{\bar{B}}^{z}$ of two 1 x 1's and one 2 x 2.

If these crystals were cubic in structure, one could use the Lorentz-Lorenz field approximation for in the limit of a cubic field,

---

[4/] $\underset{\sim}{D}$ in this reference is called $-\underset{\sim}{S}$.

$$\sum_{m} B_{mm'} = \frac{\varepsilon_\infty + 2}{3} \qquad (61)$$

so that equation (22) becomes

$$S\nu_{jT}^2 = \frac{1}{c^2 \pi v} 2\left[\frac{\varepsilon_\infty + 2}{3} \frac{\partial \mu}{\partial q_j}\right]^2 . \qquad (62)$$

As shown in Table 11, even the Lorentz-Lorenz field approximation lies within 2% of the values obtained from lattice dipole sums in $NaNO_3$ and within 1% in calcite. However, we have used the effective field model developed earlier (equation (23)) to calculate $\partial\mu/\partial q_k$ for these anions.

In Table 12 we present the values of $\partial\mu/\partial q_2$, $\partial\mu/\partial q_3$, and $\partial\mu/\partial q_4$ for the carbonate and nitrate ions as obtained from the present work and for comparison, from previously reported dielectric strengths (7) or from estimates of the ν_T and ν_L frequencies (6, 32). Table 12 also includes the gas phase values for BF_3. One can see that the agreement between the values found in the present work and those determined through different types of analyses compare quite nicely.

Next, we wish to express these $\partial\mu/\partial q_k$ values as more fundamental $\partial\mu/\partial S_k$ values. This change from molecular normal coordinates to molecular symmetry coordinates requires the $\tilde{L}^{-1}$ matrix (see equation (34)). For ν_2 this transformation is simply

Table 11. Effective field values for $NaNO_3$ and $CaCO_3$.

α_+, Å^3	$\alpha_{\parallel}$, Å^3	$\alpha_{\perp}$, Å^3	V, Å^3	$\varepsilon_z(\infty)$	$\varepsilon_{x,y}(\infty)$	B_Z	$B_{X,Y}$
$NaNO_3$							
0.41	2.67		124.8	1.785		1.815	
0.292	2.76					1.823	
Lorentz-Lorenz field						1.784	
0.41		4.65			2.519		2.091
0.292		4.79					2.085
Lorentz-Lorenz field							2.130
$CaCO_3$							
1.1	3.18		121.9	2.208		1.989	
0.792	3.42					2.015	
Lorentz-Lorenz field						1.984	
1.1		4.21			2.749		2.226
0.792		4.57					2.211
Lorentz-Lorenz field							2.239

Table 12. Molecular dipole derivatives in $CaCO_3$, $NaNO_3$, and BF_3 [in units of esu($g^{-\frac{1}{2}}$)].

		$\pm\partial\mu/\partial q_2$	$\pm\partial\mu/\partial q_3$	$\pm\partial\mu/\partial q_4$
$^{12}CO_3^{2-}$	($CaCO_3$)	72.3[a]	278[a]	20[a]
		76[b]	277[b]	19[b]
			281[c]	
		80[d]	282[d]	
	($MgCO_3$)	88[b]	253[b]	40[b]
			276[c]	
$^{14}NO_3^-$	($NaNO_3$)	39.5[a]	250[a]	2-5[a,f]
		41[b]	241[b]	
			236[c]	
			217[d]	
	($LiNO_3$)		231[c]	
$^{11}BF_3$		102[e]	227[e]	39[e]

[a]Present work.
[b]Calculated from data of reference (7).
[c]See reference (32).
[d]See reference (6).
[e]See reference (31).
[f]See text.

$$\frac{\partial \mu}{\partial S_2} = (G_{22})^{-\frac{1}{2}} \frac{\partial \mu}{\partial q_2} \tag{63}$$

where $G_{22} = 3\mu_A + \mu_B$, μ being the reciprocal mass. The situation for modes 3 and 4 is a bit more complex. Both of these modes have E' molecular symmetry and therefore each symmetry coordinate must be expressed as a linear combination of the two normal coordinates:

$$\begin{aligned} \frac{\partial \mu}{\partial S_3} &= \underset{\sim}{L}^{-1}_{33} \frac{\partial \mu}{\partial q_3} + \underset{\sim}{L}^{-1}_{34} \frac{\partial \mu}{\partial q_4} \\ \frac{\partial \mu}{\partial S_4} &= \underset{\sim}{L}^{-1}_{43} \frac{\partial \mu}{\partial q_3} + \underset{\sim}{L}^{-1}_{44} \frac{\partial \mu}{\partial q_4} \quad . \end{aligned} \tag{64}$$

The $\underset{\sim}{L}^{-1}$ matrix may be determined provided one knows a sufficient number of fundamental frequencies and can identify the $\underset{\sim}{G}$ matrix and $\underset{\sim}{F}$ matrix:[5/]

$$(\underset{\sim}{F}\ \underset{\sim}{G} - \underset{\sim}{E}\ \lambda_k)(\underset{\sim}{L}^{-1})^{\dagger}_k = 0 \tag{65}$$

where $\lambda_k = 4\pi^2 c^2 \tilde{\nu}_k$ and $\underset{\sim}{E}$ is a unit matrix.

Although we do not know the force constants for carbonate and nitrate, we can perhaps gain some insight into the possible solutions to equation (65) by inspecting the force constants used by McKean (31) for the analysis of the infrared intensities in the isoelectronic molecule BF_3.

[5/] See reference (21), equation 12, p. 74.

Figure 18. Dipole derivatives (symmetry coordinates), $\partial\mu/\partial S_k$, for A) $^{11}BF_3$, B) CO_3^{2-} in calcite, and C) NO_3^- in $NaNO_3$ versus F_{34}. The symbols 3(+,∓) and 4(-,±) designate, respectively, $\partial\mu/\partial S_3$ and $\partial\mu/\partial S_4$, where we have indicated the sign choice of $\partial\mu/\partial q_3$ and $\partial\mu/\partial q_4$. The lines (-·-·) indicate values of $\partial\mu/\partial S_4$ (in-plane bend) deduced from $\partial\mu/\partial S_2$ (out-of-plane bend) shown as 2(+), assuming negligible flux. The small letters indicate reported values for F_{34}: (a) reference (31) = -0.25; (b) reference (33) = -0.81; (c) reference (34) = -0.31 mdyn/Å. Note that sign choices differ from those shown in Figure (3) of reference (9).

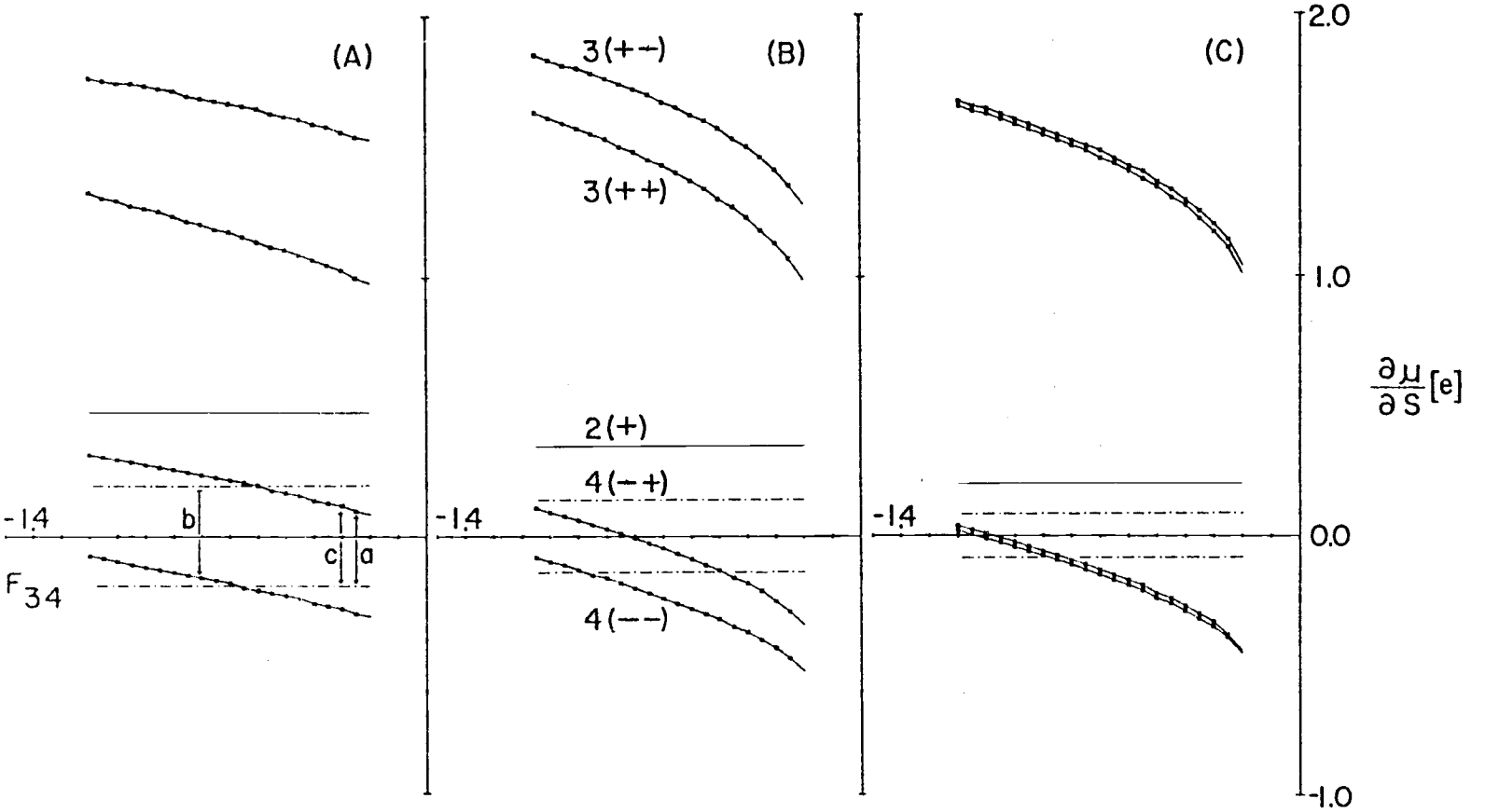
(A)
(B)
(C)
3(+−)
3(++)
2(+)
4(−+)
4(−−)
-1.4
-1.4
-1.4
b
c
a
F_{34}
2.0
1.0
0.0
-1.0
$\frac{\partial \mu}{\partial S}$[e]

McKean (31) utilized a normal coordinate transformation based upon a choice of force constants which reproduced the ν_3 and ν_4 frequencies (with anharmonicity corrections) of the isotopic species $^{10}BF_3$ and $^{11}BF_3$. This procedure is not very certain in fixing the interaction force constant, F_{34}. More recent work has been directed to the resolution of this problem through a study of the Coriolis coupling constant. Levin and Abramowitz (33) reported a Coriolis constant of 0.7 based upon the band contour at relatively low resolution. More recently, Duncan (34) found a Coriolis constant of 0.81 ($^{10}BF_3$) at relatively high resolution. The values of F_{34} which best fit the observed frequencies, together with the Coriolis constant in the latter two cases were: -0.25 (21), -0.81 (33), or -0.31 ± 0.025 (34).

We have investigated the sensitivity of the $\partial\mu/\partial S_k$ values to various assumed magnitudes of F_{34}. The other potential constants were chosen to fit the observed ν_3 = 1453.8 and ν_4 = 480.1 cm^{-1} in $^{11}BF_3$. The $\tilde{L}^{-1}$ matrix was next determined and finally the values of $\partial\mu/\partial S_3$ and $\partial\mu/\partial S_4$ were calculated. The results are exhibited in Figure 18A which illustrates the following points.

Firstly, although $\partial\mu/\partial S_3$ varies by about 10% over the range of the F_{34} values, the variation in the dipole derivatives for the weaker mode, $\partial\mu/\partial S_4$, is much larger, at least two fold. Secondly, if we fix the equilibrium

charges so that no flux is allowed for the bending modes, our vibrational description becomes equivalent to the bond dipole model and from equations (47) and (49), one would expect

$$(\partial\mu/\partial S_4)/(\partial\mu/\partial S_2) = (2^{\frac{1}{2}}/6)/3^{-\frac{1}{2}} = 0.4082 \ . \qquad (66)$$

Therefore, if $\partial\mu/\partial S_2 = 0.48e$, the expected value of $\partial\mu/\partial S_4$ is 0.196 e for the BF_3 case. Although the data here do not support a fixed charge model for mode 4 for any of the three reported F_{34} values, in the absence of a really definitive determination of the potential function, the extent of deviation of the bending mode intensities from a fixed charge model must remain in some doubt. Thirdly, in view of the above points, it does not seem feasible to determine the flux term for mode 4, which is the measure of the departure of this mode from the bond dipole (fixed equilibrium charge) model. This is especially true in connection with our studies of the nitrate and carbonate ions, for which the Coriolis data are not available to reinforce the determination of the potential function.

The data for carbonate and nitrate ions are treated similarly in Figure 18b,c. Again, one sees that just as for boron trifluoride, the dipole derivative $\partial\mu/\partial S_4$ cannot be determined with any certainty until the potential constant F_{34} is fixed. Nevertheless, in calcite a

solution for $\partial\mu/\partial S_4$ in which the flux term vanishes would require what we regard as a rather unlikely value of F_{34} (-1.15 md/Å) and this is also the case for the nitrate ion ($F_{34} \sim$ -1.2 md/Å). In the absence of information concerning nitrate and carbonate interaction force constants, we have arbitrarily adopted the same value for these two anions as was found for BF_3, F_{34} = -0.31 md/Å. Looking at Figure 18 one can see that at an F_{34} of -0.31 md/Å, the difference between a $\partial\mu/\partial S_4$ with no flux (fixed charge model) and one with flux is greatest for the multiply bonded systems, which is reasonable, and also that $\partial\mu/\partial S_4$ for both carbonate and nitrate may have a very similar amount of flux.

The selection of a representative molecular frequency for these crystals also posed a problem. The assumption that the only intermolecular coupling is dipolar is not well born out by a comparison of the transverse, longitudinal, and Raman frequencies in these crystals (35). The arbitrary assumption that was made, namely that the uncoupled frequency lies at about two-thirds the distance from ν_T to ν_L probably produces a value within 1% of the uncoupled frequency, and such a number was used in the normal coordinate calculations for carbonate and nitrate.

The pertinent frequencies, $\underset{\sim}{F}$ and $\underset{\sim}{G}$ matrix elements, along with $\underset{\sim}{L}^{-1}$ elements for CO_3^{2-}, NO_3^-, and BF_3 are listed in Table 13. The $\partial\mu/\partial S_K$ values are listed in

Table 13. $\underset{\sim}{G}$, $\underset{\sim}{F}$, $\underset{\sim}{L}^{-1}$ elements for CO_3^{2-}, NO_3^-, and BF_3.

	$^{12}CO_3^{2-}$	NO_3^-	$^{11}BF_3$
ν_3	1504	1428	1453.8
ν_4	712.8	725	480.1
G_{22}	0.3125	0.2768	0.3251
G_{33}	0.18752	0.16964	0.18888
G_{44}	0.56256	0.50892	0.56665
G_{34}	0.21651	0.18554	0.23599
F_{34}	-0.31	-0.31	-0.31
F_{33}	5.92	5.88	6.53
$\underset{\sim}{L}^{-1}_{33}$	1.72	1.78	2.12
$\underset{\sim}{L}^{-1}_{43}$	0.449	0.501	0.133
$\underset{\sim}{L}^{-1}_{34}$	-2.58	-2.57	-2.54
$\underset{\sim}{L}^{-1}_{44}$	1.73	1.74	1.91

Table 14 for these tetraatomic molecules. Here we have indicated solutions for the sign choices of $-\partial\mu/\partial q_3 \mp \partial\mu/\partial q_4$ for reasons we will explain later. One should, however, note that, from Table 13, $\tilde{L}^{-1}_{34}$ is a relatively small negative number (~ -0.4) compared to the other transformation elements, which are on the order of +2. Looking back to the equations in (64), this means $\partial\mu/\partial S_3$ and $\partial\mu/\partial S_4$ will be negative for this combination of signs for $\partial\mu/\partial q_3$ and $\partial\mu/\partial q_4$, since the magnitude of $\partial\mu/\partial q_3 >> \partial\mu/\partial q_4$. Only one half of the solutions for $\partial\mu/\partial S_3$ and $\partial\mu/\partial S_4$ have been illustrated in Figure 18: $+\partial\mu/\partial q_3 \mp \partial\mu/\partial q_4$ and $-\partial\mu/\partial q_3 \pm \partial\mu/\partial q_4$.

Table 14. Dipole derivatives with respect to symmetry coordinates for CO_3^{2-}, NO_3^-, and BF_3.

	$\partial\mu/\partial S_2$	$\partial\mu/\partial S_3$	$\partial\mu/\partial S_4$[a]
CO_3^{2-}	±0.621e	-1.14e	-0.43e
		-1.42e	-0.25e
			∓0.25e[b]
NO_3^-	±0.383e	-1.18e	-0.35e
		-1.21e	-0.33e
			∓0.16e[b]
BF_3	±0.842e	-1.03e	-0.28e
		-1.56e	+0.12e
			±0.20e[b]

[a] Sign choice - $\partial\mu/\partial q_3 \mp \partial\mu/\partial q_4$.

[b] Fixed charge value based on theory: $\partial\mu/\partial S_4 = \partial\mu/\partial S_2$ x (0.4082).

VIII. INTERPRETATION OF DIPOLE DERIVATIVES IN TERMS OF THE EC-CF MODEL

The equilibrium charge-charge flux or EC-CF model, discussed in the theory section, can be used in rationalizing the dipole derivatives in terms of fundamental charges within the molecular anions. The word "rationalize" implies a process based on empirical testing and categorizing. When the intensities of molecular vibrations are being rationalized, molecular symmetry plays a very important role. Since we are considering dynamic, molecular vibrations in the limit of their equilibria, the use of geometrical constraints based on knowing the equilibrium symmetry coordinates allows one to set up a reference frame for the definition of a positively or negatively directed dipole derivative. By studying isoelectronic and isosymmetric molecules, one hopes to substantiate the EC-CF theory and thus be able to report both the signs as well as the magnitudes of dipole derivatives. In turn, one can define equilibrium effective charges for the atoms in the molecule and also can quantitate electronic flux between the atoms. Ultimately if one could characterize the infrared behavior of many molecules, one would gain insight into, and perhaps be able to actually calculate, the transition dipole matrix (see equation (21)) by simply recording and analyzing an infrared reflection from a single crystal.

There are, of course, other ways of calculating so-called "effective charges." One way is to measure the quadrupolar splitting via NMR and extract the effective charges. These charges are derived from the second moment of the charge distribution, unlike vibrational moments ($\mu = qr$). In addition, whereas an interaction between a quadrupolar nucleus and an electric quadrient at the nucleus is described by a point charge model, the vibrational interaction with an electric field is a dynamic one. Another method is to record the x-ray photoelectron spectrum (XPES). In this case, one can measure the energy it takes to ionize certain core electrons in each environmentally different atom and relate this to the effective charge at the atom. However, this result relies on an oversimplification, namely that this selective ionization occurs as an isolated incident, with no relaxation effects (Koopman's theorem). A third way to obtain effective charge information is to calculate it using electronic wavefunctions. More of these calculated values are becoming available and effective charges were published for HF_2^- as long ago as 1962 (36). Besides being very costly, this method is plagued by a need to make decisions as to which basis functions adequately describe the bonding in the system; a slight change in basis functions may make the difference between assigning a positive or negative sign to the effective charge. This sort of calculated charge

therefore can be contrived as well as more indicative of the point charge model.

In interpreting the current EC-CF analysis, we shall assume that the sign and approximate magnitude of the flux terms are related to the dissociation of the molecule. Provided we know the outcome of dissociation, we then gain reliable insight into how the charges on the atoms are distributed in the dissociated fragments, which may be ions or neutral molecules. We also must relate the sign of a symmetry coordinate to a dissociation process. Following our sign convention,[6/] we have for the $D_{\infty h}$ anions,

$$(B_1 - A - B_2)^{-\zeta} \xrightarrow{+S_3^x} B_1^{-\zeta} + A - B_2$$

and for the D_{3h} case,

Here ζ is the overall net charge on the molecule.

With these definitions in hand, we are ready to consider some specific values for the effective equilibrium charges and charge fluxes for N_3^-, HF_2^-, CO_3^{2-}, and NO_3^-. The magnitudes and sign choices for the ζ_α's and

---

[6/] Refer to page 29.

$\partial\zeta_\alpha/\partial S_k$'s (abbreviated $\zeta_\alpha^{(k)}$) are compiled in Table 15 for $D_{\infty h}$ anions; Table 16 for D_{3h} anions. In figuring these values, we have used equations (45), (46) [$D_{\infty h}$], and equations (47)-(49) [D_{3h}].

$D_{\infty h}$ Anions

In the azide and bifluoride cases we are presented with four choices for the sign and magnitude of these effective charges and charge fluxes. One hopefully can decide which combination best describes the molecular ion by utilizing one's general chemical intuition. For example, in the bifluoride study, one is suspicious of solutions III and IV, since they would attribute equal charges to all atoms in HF_2^-: hydrogen and both fluorines would carry charges of -0.33e. A more plausible solution would be I or II where ζ_H = +0.27e and ζ_F = -0.635e.

If the HF_2^- molecular ion were naively regarded as a superposition of the structures F^- ... H-F and F-H ... F^-, using the effective charges for hydrogen fluoride (8), ζ_H = +0.4e, ζ_F = -0.4e, would yield ζ_H = +0.4e and ζ_F = -0.7e in the bifluoride ion. Some redistribution is to be expected, but the solutions I and II would appear to yield reasonable effective charges.

If one accepts this ζ set, the question remains as to how to distinguish between the two possible solutions

Table 15. EC-CF values for some $D_{\infty h}$ anions.

	$\partial\mu/\partial S_2$(e)	$\partial\mu/\partial S_3$(e)	ζ_A(e)	ζ_B(e)	b(e/A)
N_3^- (K^+)					
I	-0.126	1.86	-0.586	-0.207	-1.24
II	-0.126	-1.86	-0.586	-0.207	+1.24
III	0.126	1.86	-0.081	-0.459	-1.03
IV	0.126	-1.86	-0.081	-0.459	+1.03
HF_2^- (K^+)					
I	0.15	0.82	0.27	-0.625	-0.37
II	0.15	-0.82	0.27	-0.635	+0.62
III	-0.15	0.82	-0.33	-0.335	-0.62
IV	-0.15	-0.82	-0.33	-0.335	+0.37

Table 16. EC-CF values for some D_{3h} anions.

	$\partial\mu/\partial S_2$(e)	$\partial\mu/\partial S_3$(e)	$\partial\mu/\partial S_4$(e)	ζ_A(e)	ζ_B(e)	b(e/Å)	c(e/Å)
CO_3^{2-}							
I	+0.621 (-0.621)	-1.42	--	+0.20 (-1.00)	-0.73 (-0.33)	-1.04[a]	--
II	+0.621	-1.14	--	+0.20	-0.73	-0.86[b]	--
III	+0.621	--	-0.25	+0.20	-0.73	--	-0.43[a]
IV	+0.621	--	-0.43	+0.20	-0.73	--	-0.54[b]
NO_3^-							
I	+0.383 (-0.383)	-1.21	--	+0.12 (-0.58)	-0.37 (-0.14)	-0.89[a]	--
II	+0.383	-1.18	--	+0.12	-0.37	-0.87[b]	--
III	+0.383	--	-0.33	+0.12	-0.37	--	-0.40[a]
IV	+0.383	--	-0.35	+0.12	-0.37	--	-0.42[b]
BF_3							
I	+0.842	-1.56	--	+1.46	-0.49	-1.36[a,c]	--
II	+0.842	-1.03	--	+1.46	-0.49	-1.03[b,c]	--
III	+0.842	--	+0.12	+1.46	-0.49	--	-0.14[a]
IV	+0.842	--	-0.28	+1.46	-0.49	--	-0.40[b]

[a] Choice of signs of $\partial\mu/\partial q_3$ and $\partial\mu/\partial q_4$ at F_{34} = -0.31 is (-,+)(corrected from ref. 9).
[b] Choice of signs of $\partial\mu/\partial q_3$ and $\partial\mu/\partial q_4$ at F_{34} = -0.31 is (-,-)(corrected from ref. 9).
[c] $r^{(o)}$ for BF_3 is 1.29 Å.

with $b(I) = -0.37e/\mathring{A}$ and $b(II) = +0.62e/\mathring{A}$. A positive value of S_3 represents a displacement in the direction of dissociation (vide supra). Such a dissociation requires ζ_{F1} to decrease towards -1e and ζ_{F2} to increase towards -0.4e. Such a change is consistent with a negative $b = 2^{-\frac{1}{2}}\partial(\zeta_{F1} - \zeta_{F2})/\partial S_3$, and on this ground we adopt solution (I).

We can compare our ζ_H value of +0.27e to some calculated charges for ζ_H in bifluoride. Many researchers have published values for the gross charge on H in HF_2^- as determined by SCF-LCAO-MO calculations. The values are unfortunately as varied as the basis sets used. From the work of E. Clementi and A. D. McLean (36), ζ_A ranges from +0.18e to -0.05e; from Bessis and Bratozs (39) $\zeta_H = +0.14e$; from Sanderson (40) $\zeta_H = -0.44e$! However, as we have said, a dynamic effective charge determined via the EC-CF analysis cannot be expected to coincide with a calculated (static) atomic charge.

As for the azide ion, if one considers elementary bonding schemes one learns in freshmen chemistry, azide ion can be represented as: $^{-}N = \overset{+}{N} = N^{-}$. From Table 15, solutions III and IV appear plausible since they would have ζ_A^o more positive than ζ_B^o. Of these two choices, III is consistent with a negative charge flux for a positive phase S_3. That is, upon dissociation along the X axis, $\partial(\zeta_{B1} - \zeta_{B2})/\partial S_3$ would be expected to be negative.

$$N_{B1}\ (-.46e) = N_A\ (-.08e) = N_{B2}\ (-.46e) \xrightarrow{+S_3^x} N_{B1}\ (-1.0e) + N_A\ (0.0e) \equiv N_{B2}\ (0.0e).$$

It should be noted that neither of these solutions for ζ_A and ζ_B is close to the charges reported by Campbell and Coogan (41) who measured the contribution to the second moment of a ^{23}Na nuclear resonance in NaN_3 by quadrupolar splitting. Using a point charge model they found $\zeta_A = +0.714e$ and $\zeta_B = -0.857e$. These charges are in quite good agreement with charges deduced from a point charge model of the molecular quadrupole moment as calculated by Gora and Kemmey (42) who used SCF-MO molecular electronic wavefunctions, of which the best included $\underline{d}$ functions in the basis set.

D_{3h} Anions

In addition to the effective charge calculations, we report the flux terms b and c in Table 16 for CO_3^{2-} and NO_3^- ions, keeping in mind that we really do not have an accurate value for F_{34}. Upon examination of the resonant bonding structures proposed for these molecules by Pauling (29):

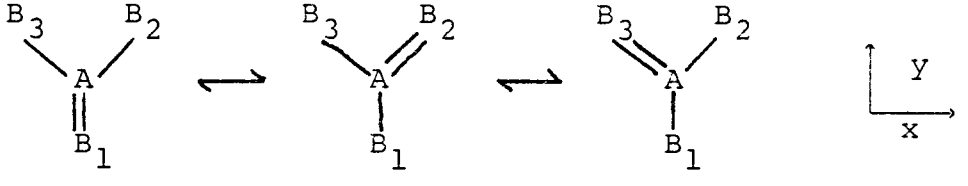

in the limit of dissociation we can expect

$$\xrightarrow{+S_3^Y} \quad B_3 - A - B_2 \quad + \quad B_1^{-\zeta}$$

That is a positive value of S_{3y} accentuates structures in which atom B1 becomes more negative and atoms B2 and B3 become more positive, so that from equation (50) the flux term is expected to be negative in sign. Combining equations (47) and (48), we find that

$$b = 6^{-\frac{1}{2}} \left(2 \frac{\partial \mu}{\partial S_3} - 2^{\frac{1}{2}} \frac{\partial \mu}{\partial S_2}\right)/r^{(0)}$$

and further since the magnitude of $\partial\mu/\partial S_3$ exceeds that of $\partial\mu/\partial S_2$, only negative solutions for $\partial\mu/\partial S_3$ will lead to negative b. One is reminded that we did use a sign choice of $-\partial\mu/\partial q_3 \mp \partial\mu/\partial q_4$ to calculate $\partial\mu/\partial S_3$ as shown in Table 14, thus we have listed only the negative values for $\partial\mu/\partial S_3$.

Correspondingly, the expression for the charge flux parameter in mode 4, c, is from equations (47) and (49):

$$c = 3^{-\frac{1}{2}} \left(2^{\frac{1}{2}} \partial\mu/\partial S_4 - \partial\mu/\partial S_2\right)/r^{(0)} \quad .$$

We do have available one bit of information that seems to support our resultant signs for the effective charges and

charge fluxes in the carbonate ion. Referring to information given in reference (3), the gas phase values of CO_2 for $\partial\mu/\partial S_3$ and $\partial\mu/\partial S_2$ are 1.73e and 0.26e. These yield effective charges of $\zeta_C = 0.52e$ and $\zeta_O = -0.26\,e$. If one accepts the dissociation limit argument, then a negative flux for mode 3, where the flux parameter given in equation (50) as

$$b = 6^{-\frac{1}{2}} \frac{\partial(2\zeta_{B1} - \zeta_{B2} - \zeta_{B3})}{\partial S_3} ,$$

seems reasonable from these values, i.e.

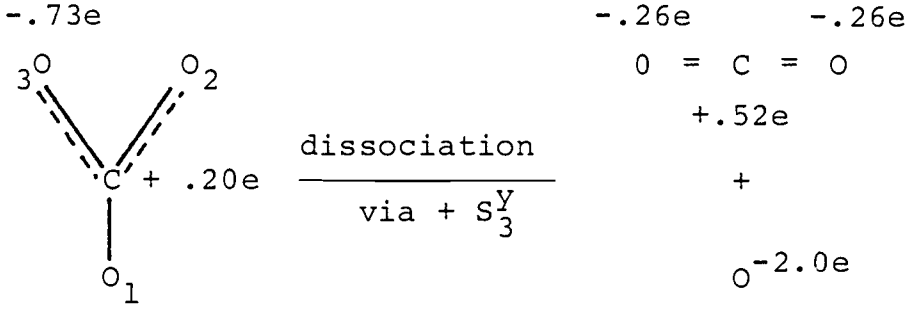

Upon dissociation, ζ_{B1}, would be expected to become more negative, ζ_{B2} and ζ_{B3} more positive. The calculated effective charges agree.

Another comparison to be made between the effective equilibrium charges on the three D_{3h} molecules analyzed here, is that these charges follow the general trends in electronegativity of the central atom: $\zeta_B^0 > \zeta_C^0 > \zeta_N$.

REFERENCES

1. Ralph W. G. Wyckoff, "Crystal Structures," Interscience, New York, 1964, Vol. 2, page 277 (D_{4h}^{18} crystals), page 359 (D_{3d}^{6} crystals).

2. R. D. Cooke, Doctoral thesis, Oregon State University, 1973, "Infrared Reflections and Raman Spectra of Sodium and Potassium Bifluoride."

3. L. R. Fredrickson and J. C. Decius, J. Chem. Phys., 63, 2727 (1975).

4. J. C. Decius, J. Mol. Spectrosc., 57, 348 (1975).

5. F. Matosi and V. Hohler, Z. Naturforsch. A, 22, 1516 (1967).

6. C. Haas and D. F. Hornig, J. Chem. Phys., 26, 707 (1957).

7. K. H. Hellwege, W. Lesch, M. Plihal, and G. Schaack, Z. Phys., 232, 61 (1970).

8. J. C. Decius and C. Pastorek, J. Chem. Phys., 68, 1715 (1978).

9. C. Pastorek and J. C. Decius, J. Phys. Chem., 83, 1379 (1979).

10. R. F. Wallis and A. A. Maradudin, Phys. Rev., 125, 1277 (1962).

11. A. A. Maradudin and R. F. Wallis, Phys. Rev., 123, 777 (1961).

12. M. Plihal, Phys. Status Solidi B, 58, 315 (1973).

13. O. P. Maksimov, V. S. Horelik, and M. M. Sushchinskii, FizTverd. Tela, 17, 2827 (1975). [Sov. Phys. Solid State, 17, 1892 (1976)].

14. H. Nichols and R. Frech, J. Chem. Phys., 68, 4983 (1978).

15. J. C. Decius and R. M. Hexter, "Molecular Vibrations in Crystals," McGraw-Hill, New York, 1977.

16. R. D. Cooke, C. Pastorek, R. E. Carlson, and J. C. Decius, J. Chem. Phys., 69, 5 (1978).

17. R. Frech and J. C. Decius, J. Chem. Phys., 51, 5315 (1969).

18. J. Tessman, A. Kahn, and W. Shockley, Phys. Rev., 92, 890 (1953).

19. J. Pirenne and E. Kartheuser, Physica 30, 2005 (1964).

20. J. C. Decius, R. Frech, and P. Bruesch, J. Chem. Phys., 58, 4056 (1973).

21. E. B. Wilson, Jr., J. C. Decius, P. C. Cross, "Molecular Vibrations," McGraw-Hill, New York, 1955.

22. R. S. Mulliken, J. Chem. Phys., 23, 1833 (1955).

23. B. C. Evans, A. D. Yoffe, and D. Gray, Chem. Rev., 59, 515 (1959); P. Gray, Quarterly Reviews, 17, 441 (1963).

24. R. Frech (private communication).

25. K. S. Pitzer and E. F. Westrum, J. Chem. Phys., 15, 526 (1947).

26. G. L. Cote and H. W. Thompson, Proc. of Soc. London Sec. A, 210, 206 (1951).

27. J. A. A. Ketelaar, C. Haas, J. van der Elsken, J. Chem. Phys., 24, 624 (1956).

28. J. A. Salthouse and J. C. Waddington, J. Chem. Phys., 48, 5274 (1968).

29. S. I. Chan, D. Stelman, and L. E. Thompson, J. Chem. Phys., 41, 2828 (1964).

30. L. Pauling, "The Nature of the Chemical Bond," 3rd ed., Cornell University Press, Ithaca, 1973.

31. D. C. McKean, J. Chem. Phys., 24, 1002 (1956).

32. R. Frech and J. C. Decius, J. Chem. Phys., 54, 2374, (1971).

33. T. W. Levin and S. Abramowitz, J. Chem. Phys., 43, 4213 (1965).

34. J. L. Duncan, J. Mol. Spectrosc., 22, 247 (1967).

35. J. C. Decius, J. Chem. Phys., 49, 1387 (1968); R. Frech and J. C. Decius, ibid, 51, 1536 (1969).

36. E. Clementi and A. D. McLean, J. Chem. Phys., 36, 745 (1962).

37. R. W. Dreyfuss, P. W. Levy, Proc. Roy. Soc. (London), A246, 233 (1958).

38. M. Born and K. Huang, "Dynamical Theory of Crystal Lattices," Claven Press, Oxford, 1954.

39. G. Bessis and S. Bratoz, J. Chem, Phys., 57, 769 (1960).

40. R. T. Sanderson, J. Chem. Phys., 23, 217 (1955).

41. I. D. Campbell and C. K. Coogan, J. Chem. Phys., 44, 2075 (1966).

42. T. Gora and P. J. Kemmey, J. Chem. Phys., 57, 3579 (1972).

APPENDICES

APPENDIX A. THE "FORBIDDEN" FREQUENCY GAP

The motions responsible for phonon dispersion are completely described by wavevectors ($\vec{k}$) in the first Brillouin zone (BZ); outside of the first BZ, the descriptions of the modes are redundant. The boundaries of the first BZ are, of course,[a] at $\vec{k} = \pi/2a$, where a is the lattice constant, thus, $\vec{k}$ (phonon) will be on the order of $10^8 cm^{-1}$. For a typical infrared photon, $\vec{k} \sim 10^3 cm^{-1}$. Since wavevectors of the photon and phonon modes are conserved upon their interaction, the dispersion in the phonon wavevector is the dispersion near the BZ center, or $\vec{k} \sim 0$. The transitions that occur between states then have $\Delta\vec{k} \sim 0$. Since the ground state has $\vec{k} = 0$, the excited state must be for $\vec{k} \approx 0$. The infrared frequency region is therefore the long-wavelength region and entire planes of molecules in the crystal move in phase. Ideal dispersion of a polariton, or the coupled photon-phonon wave in a crystal for radiation incident normal to the surface, is diagrammed as

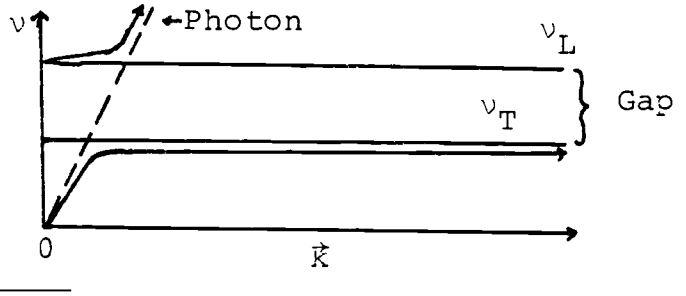

[a] For single cubic crystals.

By the very nature of three dimensional space, the molecules locked in the crystal structure have three degrees of freedom in which to move in phase: a doubly degenerate transverse degree (perpendicular to wave propagation) and a non-degenerate, longitudinal degree (parallel to wave propagation). In the above figure, the degeneracy of the transverse degree is broken down into a low frequency component (shown) and a high frequency component. At the transverse frequency, ν_T, resonance occurs between the photons and molecules exercising a transverse degree of freedom. There is a frequency gap between ν_T and ν_L, the longitudinal frequency, where a wave (without damping) cannot propagate. Here the dielectric constant is complex. Resonance again occurs at ν_L when the molecules exercise a degree of freedom parallel to the propagation of the photon wave.

At oblique incidence the above story is perturbed a bit, except for the TM2 polarized case, which does display maximum reflectance between ν_T and ν_L. The off axis polarized experiments, e.g. TM3, TM23, TE, extend maximum reflectance past ν_L to some pseudo-longitudinal frequency, ν_{LL}, that depends on the angle the incident radiation makes with the normal to the crystal face. TM3 polarized spectra are the most different from normal incidence reflection spectra since, ε_3 is imaginary from ν_L to ν_{LL}. In this

case, only dipoles active parallel to the propagation direction can couple with the incoming radiation.

APPENDIX B. DEVELOPMENT OF THE DIPOLE DERIVATIVES IN TERMS OF EC-CF PARAMETERS FOR THE D_{3h} ANIONS.

The symmetry coordinates for the D_{3h} molecular anions which were diagrammed in Figure 11 can be described in terms of angle bends and bond stretches as

$$S_{1y} = 3^{-\frac{1}{2}} (\Delta r_1 + \Delta r_2 + \Delta r_3) \qquad (A_1')$$

$$S_{2z} = 3^{-\frac{1}{2}} r^{(0)} (\Delta\phi_1 + \Delta\phi_2 + \Delta\phi_3) \qquad (A_2'')$$

$$S_{3y} = 6^{-\frac{1}{2}} (2\Delta r_1 - \Delta r_2 - \Delta r_3) \qquad (E')$$

$$S_{4y} = 6^{-\frac{1}{2}} r^{(0)} (2\Delta\phi_1 - \Delta\phi_2 - \Delta\phi_3) \qquad (E') \ .$$

According to J. C. Decius (4), the dipole derivative in a z direction, which is also the symmetry axis in the crystal, can be expressed simply in terms of S_2, the out-of-plane bend, which has no charge flux associated with it:

$$\frac{\partial \mu^z}{\partial S_2} = 3^{-\frac{1}{2}} (\zeta_A^{(0)} - \frac{m_A}{M} \zeta_m) \ .$$

Thus all the effective charges can be determined from the out-of-plane bending mode intensity. To write down expressions for $\partial\mu^y/\partial S_3$ and $\partial\mu^y/\partial S_4$ that have, in addition to effective charge terms, flux terms, one first must find how the various atoms in the molecule transform under the symmetry operations of D_{3h}, i.e.

$$\Gamma(\zeta_A) \rightarrow A_1'$$

$$\Gamma(\zeta_B) \rightarrow A_1' + E' \quad .$$

This means that the charge on atom A can change during the totally symmetric stretching vibration (A_1'). Also, the charge on the B atoms can change during the totally symmetric stretch and the doubly degenerate (E') vibrations, namely ν_3 and ν_4. A flux parameter can then be assigned for each coincidence between the atomic irreducible representations and the symmetry coordinates. These coincidences are shown in Table 17 where small case letters are used to symbolize the charge flux parameters. In order to conserve the dipole, any charge flux on atom A must be balanced by normalized and oppositely directed charge flux on all B atoms. Since S_1 is not infrared active, we will be concerned only with charge flux parameters $\underline{b}$ and $\underline{c}$ which we have previously described in equations (50) and (51)

$$b = 6^{-\frac{1}{2}} \frac{\partial(2\zeta_{B1} - \zeta_{B2} - \zeta_{B3})}{\partial S_3}$$

and

$$c = 6^{-\frac{1}{2}} \frac{\partial(2\zeta_{B1} - \zeta_{B2} - \zeta_{B3})}{\partial S_4} \quad .$$

As for the equilibrium effective charge contribution to the varying dipole, we have from equation (30),

Table 17. Coincidence in symmetry between $\Gamma(\zeta_\alpha)$ and S_k for D_{3h}, AB_3 molecules.[a]

	$A(A_1')$	$B(A_1')$	$B(E')$
$S_1(A_1')$	a	$-3^{-\frac{1}{2}}a$	-
$S_2(A_2'')$	-	-	-
$S_3(E')$	-	-	b
$S_4(E')$	-	-	c

[a]Reproduced from reference (4).

$$\Delta_1\mu_y = \zeta_A^{(0)}\ \Delta y_A + \zeta_{B1}^{(0)}\ \Delta y_{B1} + \zeta_{B2}^{(0)}\ \Delta y_{B2}$$

$$+ \zeta_{B3}^{(0)} \Delta\ y_{B3}$$

or, since $\zeta_A^{(0)} + 3\zeta_B^{(0)} = \zeta_m$, where ζ_m is the overall molecular charge,

$$\Delta_1\mu_y = \zeta_A^{(0)}\,[\Delta y_A - \tfrac{1}{3}(\Delta y_{B1} + \Delta y_{B2} + \Delta y_{B3})]$$

$$+ \tfrac{1}{3}\,\zeta_m[\Delta y_{B1} + \Delta y_{B2} + \Delta y_{B3}]\ ,$$

assuming $\zeta_{B1}^{(0)} = \zeta_{B2}^{(0)} = \zeta_{B3}^{(0)}$. Since these molecular ions are charged, consideration of conservation of linear momentum about Y will yield the additional condition that

$$Y = 0 = M^{-1}[m_A\ \Delta y_A + m_B(\Delta y_{B1} + \Delta y_{B2} + \Delta y_{B3})].$$

Definition of S_3^Y and S_4^Y in terms of the Cartesian displacements results in

$$S_3^Y = 6^{-\frac{1}{2}}[3\Delta y_A - 2\Delta y_{B1} - \tfrac{1}{2}(\Delta y_{B2} + \Delta y_{B3})$$

$$- \frac{3^{\frac{1}{2}}}{2}\ (\Delta x_{B2} - \Delta x_{B3})]$$

and

$$S_4^Y = 3\cdot 6^{-\frac{1}{2}}[3\ \Delta y_A - \frac{3^{\frac{1}{2}}}{2}\ (\Delta y_{B2} + \Delta y_{B3})$$

$$+ \tfrac{1}{2}(\Delta x_{B2} - \Delta x_{B3})].$$

Taking an appropriate linear combination of the two, eliminates the x coordinate dependence:

$$\sqrt{6}\ S_3 + \sqrt{2}\ S_4 = 6\Delta y_A - 2(\Delta y_{B1} + \Delta y_{B2} + \Delta y_{B3}) \ .$$

We have then the fixed charge contribution to the changing dipole, or

$$\Delta_1 \mu_y = \frac{1}{6}\{\zeta_A^0 - (\frac{m_A}{M})\ \zeta_m\}\{\sqrt{6}\ S_3 + \sqrt{2}\ S_4\} \ .$$

The charge flux contribution to the changing dipole in the y direction is from equation (31):

$$\Delta_2 \mu_y = \sum_\alpha \zeta_\alpha^{(3)}\ y_\alpha^{(0)}\ S_3 + \sum_\alpha \zeta_\alpha^{(4)}\ y_\alpha^{(0)}\ S_4$$

$$= \frac{r^{(0)}}{2}\ [\frac{\partial(2\zeta_{B1} - \zeta_{B2} - \zeta_{B3})}{\partial S_3}]\ S_3$$

$$= \frac{r^{(0)}}{2}\ [\frac{\partial(2\zeta_{B1} - \zeta_{B2} - \zeta_{B3})}{\partial S_4}]\ S_4$$

where $r^{(0)}$ is the equilibrium bond length and incorporating the charge flux parameters this reduces to

$$\Delta_2 \mu_y = \frac{6^{\frac{1}{2}}}{2}\ \{br^{(0)}\ S_3 + cr^{(0)}\ S_4\}$$

Finally, taking derivatives,

$$\frac{\partial \mu_y}{\partial S_3} = \Delta_1 \mu_y^{(3)} + \Delta_2 \mu_y^{(3)}$$

and

$$\frac{\partial \mu_y}{\partial s_4} = \Delta_1 \mu_y^{(4)} + \Delta_2 \mu_y^{(4)}$$

or equations (48) and (49), respectively.